2 Flight Vehicle Equations

Eric T. Falangas
Flixan Engineering Services
Web Site: Flixan.com
Email: info@flixan.com

Background

In aerospace vehicle development one of the central features is the simulation model of the vehicle dynamics. This model is a mathematical representation of its expected behavior and dynamic response to the controls and gust disturbances. This math model allows the stability and control engineer to develop control laws that allow a human pilot or an autopilot to maneuver the vehicle and to perform its mission. The math model also forms the basis for simulators used to train a pilot and to develop the skills needed to operate the vehicle. To be able to predict the resulting motion of a vehicle it is necessary to understand the physics of how forces cause objects to move. This field of study is called *dynamics* and is a college-level course. Dynamics also examines the behavior of structures under the effects of external forces and torques. Equations of motion describe how the vehicle will move in response to applied forces. For example, simple equations describe how a rocket will accelerate when a constant thrust is provided by the rocket's engine. More difficult equations describe how the sloshing of fuel in a rocket's fuel tank will cause the rocket's structure to vibrate or throw the rocket off-course. Another type of modeling would be to predict, in a mathematical equation, how an aircraft will respond to hitting an updraft in the atmosphere, or how the aircraft will respond to the deflection of various control surfaces at different airspeeds. These equations are *differential* equations, in which the rate of change of some quantity is described as being dependent upon other quantities and their rates of change. The set of mathematical equations that describe these motions are collectively called a *math model* or *simulation model* of the vehicle, and they can range in complexity from a single equation to a complex set of equations. Complex vehicle models are, for convenience, broken down into *subsystem models* that deal with different sets of dynamics.

This section describes the equations of motion that can be used to describe the dynamic characteristics of different types of flight vehicles, such as: rockets, launch vehicles, re-entry vehicles, airplanes, gliders, and spacecraft, inside or outside of atmosphere. They can be used to model generic flight vehicles, such as: an aircraft or a Space Shuttle from lift-off to re-entry. The equations describe how a dynamically complex vehicle model will behave in response to a combination of applied forces and torques, and they are presented in two forms: (a) the non-linear large angle equations suitable for 6-dof time-domain simulations, and (b) the linearized equations that describe small variations of a vehicle from its nominal trim position. The Flixan flight vehicle modeling program uses the linear equations to create state-space systems, mainly for flight control analysis. The coefficients of the linearized equations are functions of vehicle parameters at fixed flight conditions, *"time-slices"* for rockets, Mach and alpha for aircraft. The parameters include: mass properties, aerodynamic coefficients, trajectory data, slosh parameters, and structural modes. The vehicle data are obtained from 6-dof simulations, wind tunnel data or CFD models, mass properties, fuel slosh models, and finite element structural models (such as Nastran).

Linear vehicle models are used to analyze short period dynamic behavior of flight vehicle in terms of stability, robustness against uncertainties, and system performance in response to commands and to wind gusts disturbances. Launch vehicles are usually controlled by small deflections of the TVC engines (δ_e) with respect to their trim positions. Trim positions are the gimbal angles required to balance the aero moments. Engine throttling can also be used in some cases to control the vehicle by varying its engines thrust by from its nominal thrust (T_e), that is, ($T_e \pm \delta Th$). Entry vehicles, gliders, and aircraft are controlled by deflecting the control surfaces ($\pm\delta_{cs}$) from their nominal trim angle (Δ_{cs}) positions. The inputs to the dynamic models are: control surface and engine deflections, thrust variations or throttle inputs, and wind-gust velocity in (feet/sec). In spacecraft we also have reaction wheel and CMG torques but those are described in a different section. In Flixan the thrust variation

2

inputs are normalized by dividing the thrust variation input with the nominal engine thrusts. This normalization is defined as throttle control ($\delta Th/T_e$). Wind-gust inputs are disturbances defined as variations in wind velocity. The direction of the gust relative to the vehicle is fixed and defined in the input data. The vehicle outputs are: attitude, rates, accelerations, angles of attack and sideslip (α, β), and vane sensors that measure (α, β) with flexibility at specific locations. The sensor specifications, such as: body or stability rates, Euler or rate integral attitudes, accelerometer types, etc. are defined in the vehicle data. The Flixan program creates the dynamic models in state-space form which is a well-known mathematical representation used in modern control applications, such as, singular value/ robustness analysis, LQG, and H-infinity control design methodologies.

One apparent limitation of linear modeling is that its state-variables describe only variations relative to their nominal values. It captures, however, the dynamic characteristics of the vehicle for small dispersions relative to its trimmed flight condition and this is acceptable for flight control design, performance evaluation and stability analysis. Six-dof equations are often used to simulate the entire non-linear behavior of the vehicle trajectory but they usually include only the rigid-body motion, they are very complex and they cannot be used for control design and control analysis. Both types of equations are used from different groups of people for flight vehicle design, to address different issues. The linearized model is valid if its parameters remain fairly close to the target trajectory and the trim condition defined from the 6-dof simulation. The control system which is designed based on a linear model must be able to stabilize the vehicle in this design condition and to provide a certain amount of robustness to parameter uncertainties. It must also have the control authority to correct small departures from the target trajectory caused by wind-gusts.

Control analysis and design is based on linear models at fixed flight conditions with constant coefficients and the control gains are interpolated between design points. The coefficients of the vehicle equations, however, are not fixed but they are time varying and they are functions of the mass properties, aerodynamics, Mach number, alpha, and other parameters which are changing as the vehicle depletes fuel and changes speed and altitude along a trajectory. The common approach in flight control design is to derive control laws using linear models at fixed flight conditions and interpolate the control laws in between. The assumption is that, if the flight control system can provide an acceptable performance, stability margins, and robustness to uncertainties at multiple flight conditions along a trajectory (or Mach versus alpha) this will obviously be a good indication that the vehicle can be successfully guided without deviating from the trajectory due to instability or due to its inability to respond to guidance signals. This assumption is generally acceptable when the variation of vehicle parameters occur at rates significantly lower than the time constants associated with the vehicle dynamics. The "time-slice" model is valid only for relatively short periods of time, (in the order of a few seconds), and the time constant associated with the rate of change of the coefficients is usually large in comparison with the time constants associated with the vehicle short period dynamics. Critical control design and analysis conditions for launch vehicles are at maximum dynamic pressure, lift-off, maximum slosh, before and after staging, and near main engines cut-off. For aircraft, design and analysis is performed for a wide range of Mach versus angle of attack conditions and the gains are interpolated in-between. The linear modeling and control analysis, however, must be completed with a detailed 6-dof non-linear simulation with multiple trajectory dispersion runs, various winds and parameter variations.

Equations of Motion

The rigid-body equations used in the flight vehicle modeling program consist of three rotational (roll, pitch and yaw), and three translational equations along x, y and z axes. The vehicle forces and moments generated in this model are calculated with respect to the body axes system. The reference axes are shown in Figure (2.1a). The x axis is aligned along the fuselage reference line and its direction is positive along the velocity vector. The z axis is positive downwards, and the y axis is defined by the right hand rule, perpendicular to the x and z axes and positive towards the right wing. The Euler angles (φ, θ, ψ) define the vehicle attitude with respect to the inertial reference axes. In a launch vehicle the attitude reference is usually measured with respect to the launch pad with the Euler angles initially at $(0°, 90°, 0°)$ respectively. Coupling between the pitch and lateral axes is also included in the equations of motion. This coupling may occur due to lack of vehicle symmetry, such as, thrust mismatch in the TVC, products of inertia, a non-symmetrical structure, or due to aerodynamic coupling coefficients, such as: $Cm\beta$, $Cn\alpha$, or flying at a constant roll angle and sideslip, etc. The x, y, z coordinates of various vehicle locations are defined in the input data with respect to the vehicle reference axes. These locations include: engine gimbals, control surface hinges, IMU, gyros, accelerometers, slosh masses, the CG and moment reference center (MRC), etc. Figure (2.1) is an example of coordinate axes showing the origin and directions of the reference axes in a typical flight vehicle. In some cases the trajectory model, the mass properties, and the structures model are defined in a different coordinate directions and units and the analysts must perform the proper transformations and unit conversions in the mass properties, aero data, trajectory, and modal data when setting up their database.

Feedback from the IMU, rate gyros, and accelerometers is used to control the vehicle attitude and flight direction. Feedback from the accelerometers or vanes is often used for "*load-relief*" to control the normal and lateral aerodynamic loading on the structure, especially in launch vehicles. Normal acceleration feedback is also used to control the rate of descent in a re-entry vehicle. Variations in altitude and velocity $(\delta V, \delta h)$ are also included in the equations state vector to implement the phugoid dynamics. These states are used for simulating the longitudinal guidance laws in aircraft or re-entry vehicles at high angles of attack, and using speed-brake, variable thrust, or alpha control as means to regulate the speed and altitude. Cross-range velocity is also included in the equations and used for lateral guidance. There are situations, however, where some of states and outputs are not required in the analysis and they can be taken out in order to minimize the state-vector. There are Flixan utilities for post-processing and reducing the vehicle state-space model. For example, the $(\delta V, \delta h)$ states are not useful in a launch vehicle with a fixed thrust and flying at zero (α). The x-acceleration output is also not needed because it cannot be controlled from a TVC input (δ_e). The system modification utilities are used in extracting a smaller system from a bigger system, or for separating a coupled system into a pitch and lateral subsystems. Note that, it is a good practice to reduce the vehicle model by removing the non-contributing state-variables, especially when creating models for control synthesis, because most design algorithms require minimal state-space realizations.

Aerodynamic Models

The aerodynamic coefficients used in the equations are based on complex aerodynamic models. An aerodynamic model describes how the vehicle will respond to forces caused by motion of the vehicle through the atmosphere, and predicts the effects of each different control surface (such as the flaps, rudders, ailerons, etc.) upon the motion of the vehicle. Aerodynamic models are often complex and are usually based on wind-tunnel data, in which the forces and moments exerted on a scaled model are measured at various speeds, flow angles, and with combinations of control surface deflections, until

4

enough data is available to predict the forces and moments that will act on the full-scale vehicle. Increasingly more data is being added by using a technology called Computational Fluid Dynamics (CFD) in which the same forces and moments are predicted in a computer program, using the geometry (shape) of the vehicle in a virtual wind tunnel. The resulting aerodynamic subsystem model will predict what the forces and moments would be as a result of any combination of control surface deflections, thrust settings, and flight conditions. The equations of motion described here use aerodynamic coefficients and derivatives that are extracted from these complex aerodynamic models at steady-state conditions.

Structural Flexibility

Structural flexibility is a very important issue in flight control system design and stability. Flight vehicles are designed with minimum weight objectives and hence in some cases their structures exhibit a considerable amount of flexibility, requiring the development of flexible structure equations to account for motion of various parts of the vehicle in relation to other parts. Long and slender vehicles made of lightweight materials will require some attention to this aspect of modeling. Some parts of the vehicle can develop considerable amounts of displacement and acceleration as a result of excitations and structural flexibility in addition to the displacement and acceleration that arise owing to the rigid body motion. The structural dynamics should be considered as an integral part of the control loop. If the deformation characteristics are ignored, the flight vehicle may not be properly controlled, and in many instances it may exhibit self-excited divergent oscillations that can be destructive. Thus, the control system designer must be aware that divergent structural feedback can occur and must ensure that the flex phenomena are properly modeled and analyzed. Flexibility also limits the control system bandwidth, affects vehicle performance, and often requires filter design in the control system. In launch vehicles the main source of flex mode excitation is the TVC. In aircraft, the acceleration of the vehicle in combination with the aerodynamic forces can excite the structure into flexure oscillations, especially in the wings and the tails. This causes significant aero-elastic phenomena to occur which may have a serious impact on vehicle stability and performance.

The elastic behavior of a vehicle structure can be represented with a superposition of flex modes which are excited by the actuator forces and moments, slosh forces, aerodynamic coupling, and other disturbances. The term "elastic modes" refers to the normalized mode shapes of the flight vehicle in *"free-free"* vibration. The mode shapes and frequencies of the "free-free" vehicle (the modal data) are obtained from a finite element modeling program, such as Nastran. Each bending mode is represented by a second order transfer function with a low damping coefficient (ζ_j), and a resonance frequency (ω_j rad/sec). The modal equation is excited by forces and moments acting on the vehicle structure in different locations, and also by aerodynamic forces (aero-elastic terms). The coefficients of each bending mode are derived from the finite elements model. The modal data for each mode consist of mode frequency (ω_j), the generalized mass $m_g(j)$, and generalized mode shapes (φ), and slopes (σ), (eigenvectors), in different locations on the vehicle (nodes). In most applications 20 to 80 modes is sufficient to get an accurate representation of the structural flexibility. Sometimes as many as 400 modes can be included for flight verification. When a sensor is mounted on the structure, in addition to the rigid-body motion, it also measures a linear combination of modal displacements (η_j) from all flex modes which are observable at that sensor. The elastic modes produce high frequency oscillations superimposed on the the rigid body measurements.

The aero-elastic coupling between the aero-surfaces and flexibility is implemented using two different approaches. The first approach is easier to model but less accurate. It assumes that the structure is

excited only by the aerodynamic forces and torques at the hinges generated by the deflections and accelerations of the aero-surfaces, which are assumed to be rigid, and they couple with the vehicle structure as separate bodies. It requires modal shapes at the aero-surface hinges. The mass properties of the aero-surfaces, gimbaling engines, and slosh masses should not be included in the FEM model because they couple with the vehicle by the forces generated by the pivoting bodies as described in the equations. The second method is more efficient because it uses aero-elastic data created from an aero-elastic model, such as a CFD used for flutter analysis. It captures the dynamic coupling between structural flexibility and the aerodynamic forces and moments created by the vehicle motion due to: (α, β, p, q, r) variations, and also due to the deflection of the aero-surfaces (δ_{as}). In addition to the modal data it requires two additional sets of coefficients: the *"Generalized Aero Force Derivatives"* (GAFD) data and the "Inertial Coupling coefficients" or *"h-parameters"*. The second approach includes also equations and GAFD coefficients that calculate the moment variations at the aero-surface hinges caused by the vehicle motion, flexibility, and surface deflections. The "Inertial Coupling Coefficients" define the dynamic coupling between structural flexibility and the engine or control surface angular accelerations. The finite-elements model in this case must include the control surfaces or the engines rigidly attached at the hinges. The surfaces are released in the equations via the h-parameters. Both approaches require a Nastran model that is "free-free".

Propellant Sloshing

The dynamic behavior of propellant sloshing inside the tanks is a very important issue in launch vehicle stability and design. Sloshing is defined as the periodic motion of the free surface of a liquid in a partially filled tank or container. Typical fuels and oxidizers used in launch vehicles are liquid oxygen (H_2O), liquid hydrogen (LH_2), peroxide (H_2O_2), hydrazine, etc. Slosh frequencies depend on the tank size and acceleration, and they typically range between 2.5 to 6 (rad/sec). Slosh frequencies are usually lower than structural resonances but they are sometimes near the control system bandwidth and may create problems. Most of the time they are passively phase-stable but sometimes they may require lead-lag phase compensation. Propellant sloshing is induced by variations in normal and lateral accelerations due to maneuvering, thrust variations, wind gusts, etc. If the liquid is allowed to slosh freely, the uncontrolled oscillations can produce disturbance forces that cause additional accelerations on the vehicle. These oscillations are at low frequency and sometimes close to the control system bandwidth. They are sensed and responded to by the flight control system, forming a closed-loop that may degrade performance or lead to an instability. It is also possible for the slosh resonances to interact with flexibility and to cause even further deterioration in stability and to excite oscillations.

In general, fuel sloshing is an undesirable effect on the vehicle, not only in terms of potential instability and attitude oscillations but it can also cause other problems and hardware malfunctions. The most commonly used mechanical solution for dampening slosh instabilities is to include mechanical baffles in the interior of the tank. There are situations, however, where slosh instabilities may be tolerable. For example, if the duration of the instability is relatively short or if the slosh mass is small in comparison with the total vehicle mass creating a small disturbance or a limit-cycle. In reality, the amplitude of the slosh mass oscillation inside a tank will not grow forever, but it is limited by the radius of the tank. In fact studies show that when the slosh mass amplitude reaches approximately 3/4 of the tank radius the fuel wave brakes, splashing the liquid inside the tank and the oscillations start building up again from low amplitudes. When slosh instabilities occur, engineering intuition is required to determine the severity of the problem. One has to consider what would the impact be on the vehicle if the slosh mass is allowed to limit-cycle at 3/4 tank radius. It may be acceptable if the mass is small.

The liquid motion can be analyzed using pendulum or spring mass analogy models. The sloshing propellant is often approximated with an oscillating spring-mass system with very low damping coefficient. One end of the spring is attached at a point in the tank centerline below the surface and the other end of the spring is attached to a mass that represents the sloshing part of the fuel. The slosh mass has two translational degrees of freedom and generates normal and lateral forces on the vehicle (along the z and y axes). It is constrained to oscillate along a plane that is perpendicular to the acceleration vector. The spring mass linear model is acceptable for linear stability analysis, but it is too conservative for larger slosh mass deflections and for time domain simulations because it does not limit the slosh mass deflections, as the pendulum model does. The slosh parameters required to implement the spring-mass slosh model are: the slosh mass (m_s), the slosh frequency (ω_s) in (rad/sec) which is a function of vehicle acceleration, the damping coefficient (ς_s), and the average location of the slosh mass (x_s, y_s, z_s) relative to the vehicle reference frame. The slosh parameters are usually obtained from experiments. Typical values of slosh masses in launch vehicles vary between, 100 to 5000 slugs. The slosh frequencies at 1 (g) vary between: 0.4 to 1(Hz). The slosh frequency is proportional to the square root of the vehicle acceleration. The slosh frequencies in the Flixan data are defined at 1 (g) and they are automatically scaled by the program by multiplying them with the square root of the acceleration in g's. Two frequencies per tank must be entered for the z and the y slosh oscillations separately because they may be different due to tank asymmetry. The slosh damping coefficients (ς_s) are usually very small and they vary from 0.0002 for a tank without baffles to 0.002 for a tank with baffles. They are also defined twice per tank due to asymmetry. The spring mass analogy model is shown in Figure (2.6.1). The slosh masses should not be included in the vehicle mass properties (mass, inertias, and cg calculations). Its effects on the vehicle are defined by the forces which are presented by the equations described in Section (2.6).

Vehicle/ Actuator Dynamic Coupling

The inertia forces introduced by the accelerating motion of gimbaling engines or control surfaces may also cause dynamic instability. The "tail-wags-dog" are reaction forces and moments applied on the vehicle at the gimbals or surface hinges. They are created by the swiveling (accelerations) of the TVC engines or the control surfaces. On a flight vehicle controlled by gimbaling engines, an excitation frequency exists at which the magnitude of the engine inertia reaction force is equal and opposite to the magnitude of the lateral component of thrust, or for a pivoting control surface, the force at the hinge due to the surface inertia is equal to the lateral component of the aero force. Below this so called "tail-wags-dog" (TWD) frequency, the resultant lateral force at the gimbal is predominantly due to thrust being in-phase with the gimbal angle. That is, an increase in gimbal angle results in an increase in lateral force. Above this frequency, the engine inertia forces produce the dominant lateral force which is in-phase with the gimbaling acceleration, or 180° out of phase with the gimbal angle. The TWD introduces a complex pair of zeros in the transfer function "θ(s)/δ(s)". A 180° phase reversal occurs at frequencies greater than the TWD frequency and a system designed without the TWD consideration may perform unsatisfactorily above the TWD frequency. In particular, some of the higher frequency flex modes may be driven into divergent oscillations by this phase reversal if adequate structural damping or filter attenuation is not present. The TWD frequency should, therefore, be higher than the control system bandwidth. Fortunately, the TWD phenomenon provides significant amount of attenuation at around the TWD frequency which helps the flex mode attenuation.

Oscillations due to TWD phenomena have occurred during staging when the engines thrust decays and for a few seconds an active control system exists with very low or zero thrust, causing the TWD frequency to drop considerably. The drop in the control force phase-reversal then drives some flex

modes to instability causing divergent oscillations until the hydraulic pressure in the actuators is depleted and the oscillations cease due to lack of actuation. This type of problem is fixed by phasing-down the control system gains during staging. TWD type of instabilities have also occurred in aircraft exciting control surface oscillations at low speeds or during ground testing when the control system is turned-on. The aero surfaces oscillate at their local natural frequency. These type of problems are usually alleviated by including filters in the control loop and stiffening the backup structure of the control surfaces in combination with detailed control analysis and simulations.

The dynamic coupling between the engines or surfaces, the actuators, and the effector backup structure play a critical role in the control system stability and in effector performance. It often causes "tail-wag-dog" type of oscillatory instabilities if not properly designed. Oscillations may occur due to interactions between actuator dynamics and the supporting structure of the control surface or gimbaling engine. Sometimes all three deformations contribute to instability: actuator flexibility, local and vehicle body deformations. They couple with the actuator servo nonlinearities and cause a local control instability. This type of instability sometimes is not predicted in the pre-flight analysis due to lack of modeling details. A filter is often included either in the control system or in the actuator control loop to eliminate the instability problem.

Another effect that involves the actuator and the effector backup structure and requires proper modeling is the "load-torque", which is an external loading torque at the hinge or gimbal of the effector. When the vehicle accelerates, as a result of maneuvering or due to disturbance forces, the accelerations create an external loading torque that may react against the control torque provided by the actuator. These phenomena are discussed in Section (2.8) and also in the actuator section in Chapter 4. Initially the TWD dynamics and load-torque feedback are not included in the preliminary modeling and analysis phase often due to lack of effector data. They are incorporated later as the design matures. The following parameters, such as: hydraulic fluid compressibility, nozzle or control surface flexibility, backup structure stiffness, Coulomb/ Dahl friction at gimbal, load inertia, play critical role in the control system analysis, and they are usually captured in a separate actuator model, preferably non-linear.

To properly model the tail-wags-dog and load-torque feedback dynamics a dedicated actuator model is required for every control surface hinge or gimbaling engine which is included in the vehicle model. The actuator model is more than just a simple transfer function, but it has two inputs: a deflection δ-command and an external load-torque input. It also has three outputs: engine or surface deflection, rate and acceleration. The actuator inputs and outputs couple with the vehicle model to implement the TWD and load-torque dynamics, as shown in Figure (2.8.1), which is similar to both: aero surfaces and TVC engines. An actuator models similar to those described in Section 4 are used to drive each effector, and they are applicable to both: TVC engines or aero-surfaces, but the actuator parameters may be different. Notice, that when the engines and aero-surfaces are implemented as separate bodies interacting with the vehicle, their masses and moments of inertia should not be included in the vehicle mass, moments of inertia, and CG calculations.

Control Issues

Feedback from the IMU, the rate gyros, the accelerometers, or the vane sensors is used to control the vehicle attitude and flight direction. Feedback from the accelerometers or vanes is often used for "*load-relief*" in order to reduce the normal and lateral aerodynamic loading on the structure, especially in launch vehicles at high dynamic pressures. Normal acceleration feedback is also used to control the

rate of descent in a re-entry vehicle. The equations also include variations in altitude and in velocity (δV, δh) outputs which characterize the phugoid dynamics. These variables are used for feedback design and the implementation of longitudinal guidance laws in aircraft or re-entry vehicles flying at high angles of attack, and using speed-brake, variable thrust, or alpha control as means to regulate the speed and altitude. Cross-range velocity is also included in the equations and it is used for lateral guidance. There are situations where some of the states and outputs are not required in the dynamic model and they should be taken out in order to minimize the state-vector. For example, the (δV, δh) states are not useful in a launch vehicle with a fixed thrust and flying at zero (α). The x-acceleration output is also not needed because it cannot be controlled from a TVC input. It is a good practice to reduce the vehicle model by removing the non-contributing state-variables, especially when creating models for control synthesis, because most design algorithms require minimal state-space realizations.

Modeling Issues

When the TWD/ load-torque dynamics are included, the flight vehicle model must be created with the TWD/ load-torque option turned-on. There is a flag in the vehicle input data that turns this option "on". In this case the vehicle model provides "load-torque" outputs and gimbal acceleration inputs for every engine direction and for every control surface. These inputs and outputs couple the vehicle model with the actuators as shown in Figure (2.8.1). The hinge moment and the tail-wag-dog equations for aircraft control surfaces are similar to the load-torques and the tail-wag-dog equations for the TVC engines. The inputs to the vehicle model consist of: surface deflection, rate, and acceleration for every aero-surface. An actuator model, such as the ones described in section 4, can be used to drive each aero-surface. The same actuator models can be used for either, TVC engines or control surfaces. The input parameters are different. The actuator outputs consist of: surface deflections in (radians), rates, and angular accelerations in (rad/sec^2). Notice that, when the TWD option is turned off, the engines and the control surfaces are not treated as externally coupling bodies, and therefore, their masses and moments of inertia should be included the vehicle total mass and moments of inertia calculations. The actuators also do not need the extra inputs and outputs for TWD modeling, and they can be simplified to transfer functions "$\delta(s)/\delta_{com}(s)$".
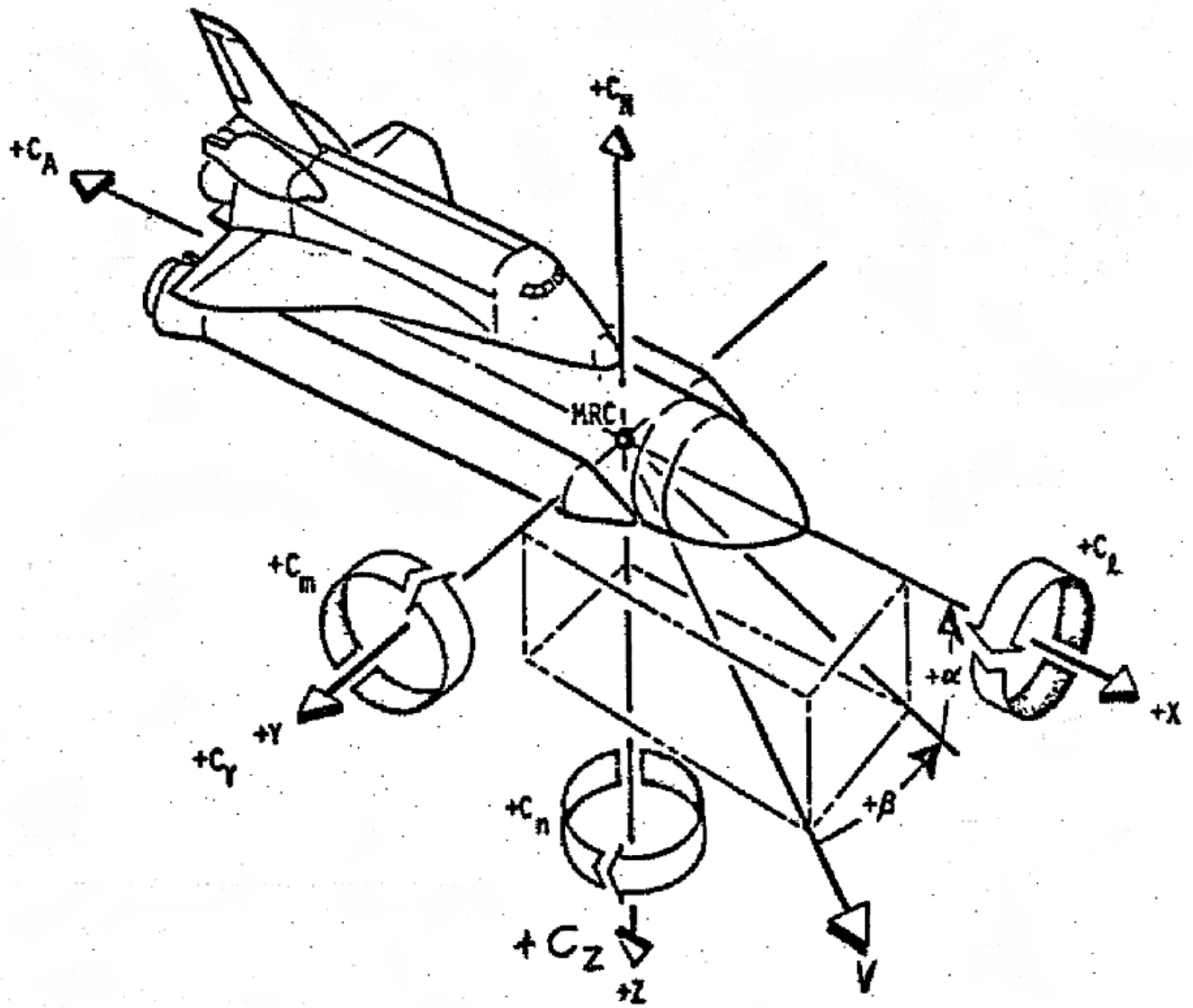
Figure 2.1a Vehicle Axes and Directions of the Aerodynamic Forces and Moments

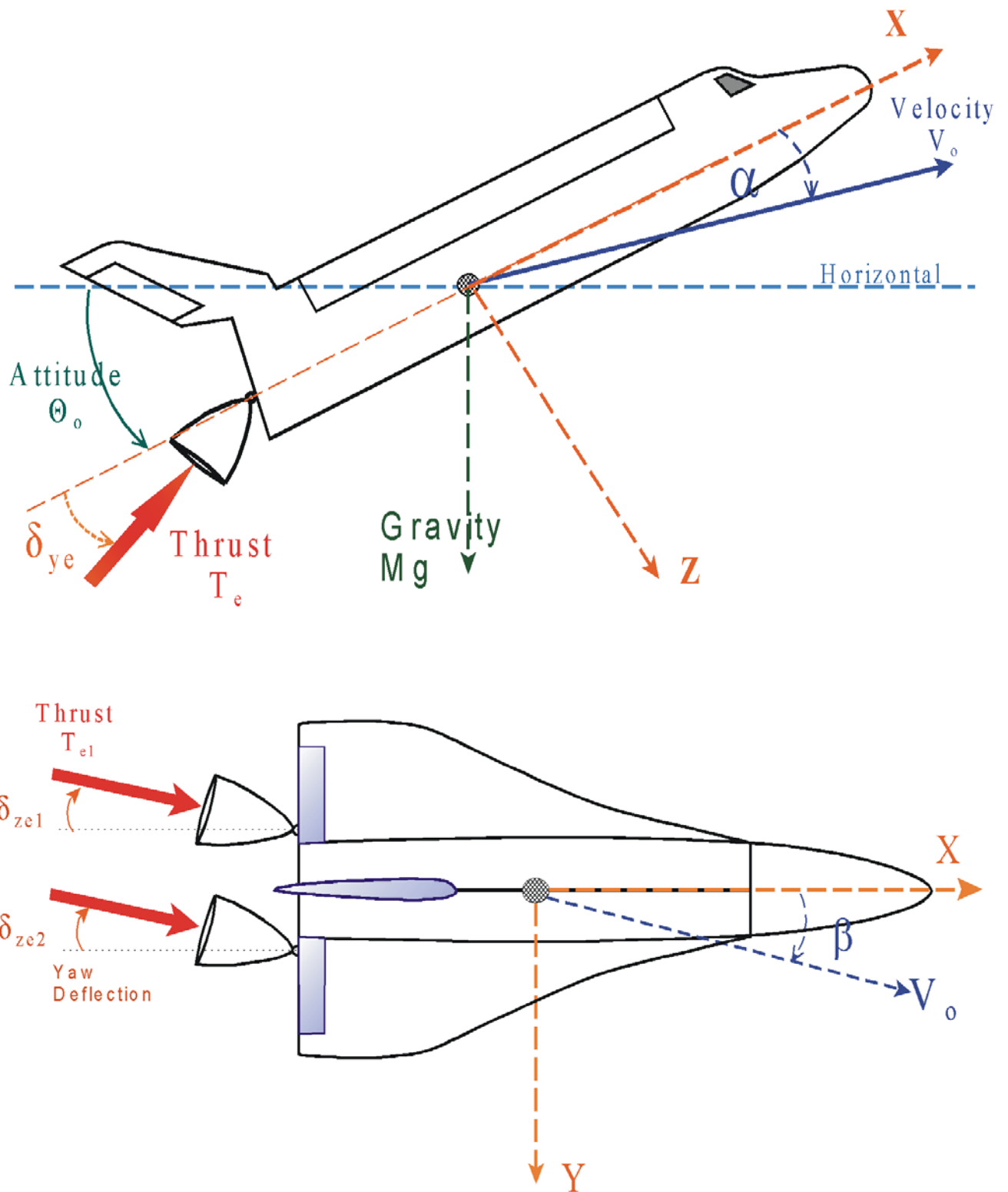**Figure 2.1b Vehicle Axes and Gimbal Directions**

Nomenclature

Symbol	Description
A_x A_y A_z	Sensed vehicle nominal accelerations along x, y and z axes (ft/sec^2)
U_o, V_o, W_o	Nominal vehicle inertial velocities along x, y, and z axes (ft/sec)
P_o, Q_o, R_o	Nominal vehicle rates about x, y, and z axes (rad/sec)
Φ_o Θ_o Ψ_o	Euler Angles (roll, pitch, and yaw) (radians)
u_g v_g w_g	Wind-gust velocity components along vehicle x, y, and z axes (feet/sec)
I_{xx} I_{yy} I_{zz}	Vehicle Moments of Inertia about the vehicle CG (ft-lb-sec^2)
I_{xy} I_{xz} I_{yz}	Vehicle Products Inertia about the vehicle CG (ft-lb-sec^2)
$\delta_{ya}(k)$ $\delta_{za}(k)$	Engine (k) Pitch and Yaw gimbal rotations from trim due to actuator deflections alone (excluding bending) (radians)
$\delta_{ye}(k)$ $\delta_{ze}(k)$	Engine (k) total deflections about y and z axes respectively (due to actuator deflection including bending) (radians)
$\Delta_Y(k)$ $\Delta_Z(k)$	Engine or thruster (k) nozzle pitch and yaw trim angles (elevation and azimuth angles measured from the vehicle -x axis) (radians)
$\delta_{cs}(k)$	Rigid deflection at surface (k) due to actuator rotation (rad)
$\delta_{fcs}(k)$	Total deflection at surface (k) about the hinge (includes rotation due to structure flexibility) (rad)
T_{Lyk} T_{Lzk}	Pitch and Yaw Load-Torques at Engine (k) Gimbal (ft-lb)
$L_{hs(k)}$	Moment Arm from hinge line to control surface CG, $(X_{sk}-X_{sk\ cg})$ (feet)
l_{ek}	Distance from engine gimbal to engine CG, $(X_{ek}-X_{ecgk})$ (feet)
l_{xek} l_{yek} l_{zek}	Distance from vehicle CG to engine (k) gimbal along x, y, and z (feet)
M_v	Mass of the vehicle (Engines and Slosh Masses Excluded) (lb-sec^2/ft)
m_{si}	Slosh Mass (i) (slug)
l_{sxi} l_{syi} l_{szi}	Slosh Mass (i) distance from the vehicle CG (along x, y and z) (feet)
m_{ek}	Mass of Engine (k) (slug)
T_{ek}	Thrust of Engine (k) (lb)
δT_{ek}	Change in Engine (k) thrust from its nominal value (lb)
X_{cg} Y_{cg} Z_{cg}	Location of the Vehicle Center of Gravity (ft)
X_{ek} Y_{ek} Z_{ek}	Location of Engine (k) Gimbal (ft)
X_{gi} Y_{gi} Z_{gi}	Location of Gyro (i) (ft)
X_{ai} Y_{ai} Z_{ai}	Location of Accelerometer (i)(ft)
X_{si} Y_{si} Z_{si}	Location of the Slosh Mass (i) (ft)
ϕ, θ, ψ	Small changes in vehicle attitude from nominal (roll, pitch, yaw) (radians)
p, q, r	Changes in vehicle body rates (radian/sec)
α β	Changes in the angles of attack and sideslip (radians)
$C_{z\alpha}$ $C_{y\beta}$	Normal and Side Force Aero Derivatives due to α and β (1/deg)
$C_{m\alpha}$ $C_{l\beta}$ $C_{n\beta}$	Aerodynamic Moment Derivatives (1/deg)
C_{mq} C_{np} C_{lp}	Aerodynamic Moment Velocity Derivatives (-)
C_{nr} C_{lr}	Aerodynamic Moment Velocity Derivatives (-)
$C_{z\delta si}$ $C_{y\delta si}$	Normal and Side Force Aero Derivatives due to Control Surface Deflections δ_{asi} (1/deg)
$C_{m\delta i}$ $C_{l\delta i}$ $C_{n\delta i}$	Aero Moment Derivatives due to control surface δ_{si} (1/deg)
S_{ref}	Vehicle Reference Area (feet^2)
l_{ch} , l_{sp}	Mean Aerodynamic Chord and Span Vehicle Reference Lengths (feet)
ϕ_{hs} , λ_{hs}	Control Surface Hinge Line Orientation Angles (deg)
Q-bar	Dynamic Pressure (lb/ft^2)

η_j Generalized Modal Displacement of a mode (j) (feet)

$M_g(j)$ Generalized mass for mode (j) (lb-sec^2/ft)

$\varphi_{yek}(j), \varphi_{zek}(j)$ Mode (j) Shapes along y and z axes, at engine (k) gimbal (ft/ft)

$\sigma_{yek}(j), \sigma_{zek}(j)$ Mode (j) Slopes about y and z axes, at engine (k) gimbal (rad/ft)

$\varphi_{ysi}(j), \varphi_{zsi}(j)$ Mode (j) Shapes along y and z at slosh mass (i) location (ft/ft)

$\varphi_{yai}(j), \varphi_{zai}(j)$ Mode (j) Shapes along y and z, at accelerometer (i) (ft/ft)

$\sigma_{hsk}(j)$ Modal slope for mode (j) at surface (k) about the hinge vector (rad/ft)

$\sigma_{ygi}(j), \sigma_{zgi}(j)$ Modal slope for mode (j) about the y and z axes, at gyro (i) location (rad/ft)

$M_{hs}(k)$ Hinge Moment about the hinge vector of surface (k) (ft-lb)

$C_{\eta j\alpha} \ C_{\eta j\beta}$ Generalized modal force stability derivatives of mode (j) with respect to (α, β) (1/radian)

$C_{\eta jp} \ C_{\eta jq} \ C_{\eta jr}$ Generalized modal force stability derivatives of mode (j) with respect to (p, q, and r) (1/rad/sec)

$C_{\eta j \ \delta k}$ Generalized modal force stability derivatives of mode (j) with respect to a control surface (k) deflection (1/rad)

$C_{\eta j \ \eta i}$ Generalized modal force stability derivatives of mode (j) with respect to a generalized modal displacement η_i of mode (i) (1/ft)

$C_{hi \ \alpha} \ C_{hi \ \beta}$ Hinge moment derivative at control surface (i) due to α and β variations respectively (1/rad)

$C_{hi \ \delta k}$ Hinge moment derivative at control surface (i) due to surface (k) deflection (1/rad)

$C_{hi \ \eta j}$ Hinge moment derivative at control surface (i) due to generalized modal displacement η_j of mode (j) (1/ft)

$C_{l\eta j} \ C_{m\eta j} \ C_{n \ \eta j}$ Roll, pitch, and yaw moment derivatives with respect to modal displacement η_j of mode (j) (1/ft)

$C_{Y\eta j} \ C_{Z\eta j}$ Force derivatives along Y and Z axes with respect to modal displacement η_j of mode (j) (1/ft)

N_{aer} Number of Aero Surfaces

N_{mod} Number of Bending Modes

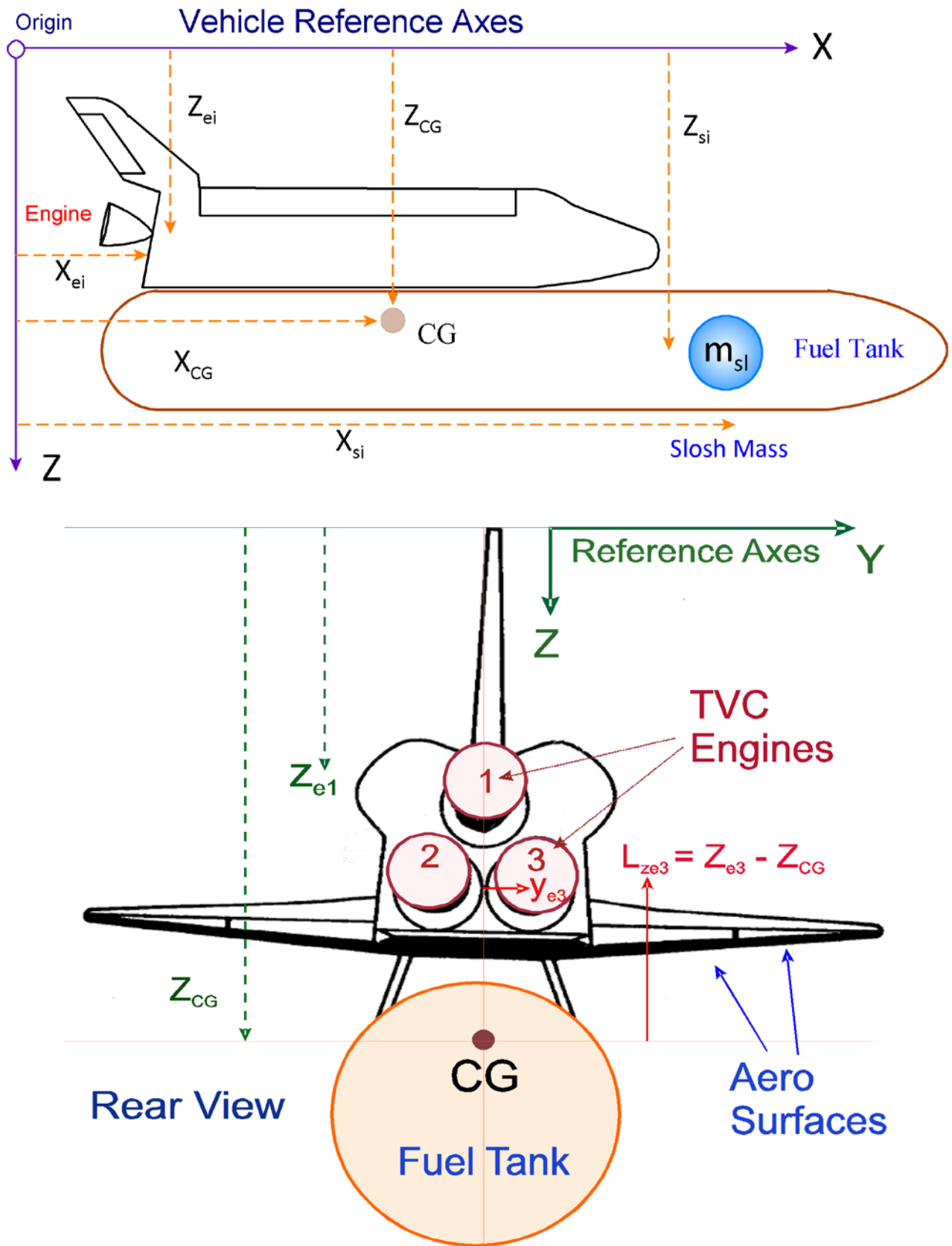N_{eng} Number or Engines

N_{sl} Number of Slosh Masses

Figure 2.2 Flight Vehicle Reference Axes

14

2.1 Force and Acceleration Equations

The combined external forces applied on the vehicle consist of the following types: aerodynamic, engine (TVC) forces, propellant sloshing, wind gust disturbance, and gravity forces. Although slosh is an internal force we treat it as external in this case because it is implemented as separate body that exerts forces on the vehicle.

$$F_X = F_{Xaero} + F_{Xeng} + F_{Xslosh} + F_{Xgrav} + F_{Xgust}$$

$$F_Y = F_{Yaero} + F_{Yeng} + F_{Yslosh} + F_{Ygrav} + F_{Ygust} \qquad (2.1.1)$$

$$F_Z = F_{Zaero} + F_{Zeng} + F_{Zslosh} + F_{Zgrav} + F_{Zgust}$$

The vehicle acceleration measured at the CG is the result of all forces, either external or internal, with the exception of gravity and centripetal forces. That is because accelerometers do not "feel" the gravity force. The accelerations measured by an accelerometer at the CG are described by the *"F=ma"* type of equation 2.1.2.

$$\begin{bmatrix} A_X \\ A_Y \\ A_Z \end{bmatrix}_{CG} = \begin{bmatrix} \left(F_{Xeng} + F_{Xaero} + F_{Xslosh} + F_{Xgust}\right)/M_T \\ \left(F_{Yeng} + F_{Yaero} + F_{Yslosh} + F_{Ygust}\right)/M_V \\ \left(F_{Zeng} + F_{Zaero} + F_{Zslosh} + F_{Zgust}\right)/M_V \end{bmatrix} \qquad (2.1.2)$$

Note that, M_T represents the total vehicle mass including the slosh masses, gimbaling engines, and aero-surfaces. M_V represents the vehicle mass that excludes the moving masses (slosh, engines, and aero-surfaces), because in the y and z directions the moving masses are implemented as separate bodies interacting with the vehicle through forces. The difference between the inertial accelerations (A_{XI}, A_{YI}, A_{ZI}) and the accelerations measured by an accelerometer at the CG (A_X, A_Y, A_Z) is the gravity acceleration components:

$$A_{XI} = A_X - g\sin\Theta$$

$$A_{YI} = A_Y + g\cos\Theta\sin\Phi \qquad (2.1.3)$$

$$A_{ZI} = A_Z + g\cos\Theta\cos\Phi$$

When the TWD dynamics are included in the model, the masses of the engines and the control surfaces should not be included in the calculation of vehicle mass properties, CG, or moments of inertia calculations. The tail-wags-dog equations generate reaction forces and moments on the vehicle due to the rotational accelerations of the engines or the control surfaces about the hinge. The effects of the swiveling masses are included by the forces and torques in the equations of motion.

Otherwise, if the TWD dynamics is not used, the vehicle mass (M_T), the CG, and the moments of inertia should include the masses of the engines and the control surfaces. Also, if an engine is defined as "fixed", that is, "Throttling" and not "Gimbaling", such as, for a reaction control jet that is not gimbaling, but fixed and throttling, then the TWD option is not introduced in the dynamic model and the engine masses should be included in the vehicle mass properties calculation.

Accelerations due to External Forces

The acceleration of a rotating vehicle in the body frame that has a rotational rate ω_b is defined by equation 2.1.4a.

$$\dot{v} + \omega_b \times v = \frac{\sum F_i}{M_V}$$

(2.1.4a)

Where: M_V is the vehicle mass and F_i is the external forces. This equation is resolved along the 3 body axes to calculate accelerations along x, y, z, as shown in Equation 2.1.4b, where P, Q, and R are the body rates.

$$\dot{U} + QW - RV = \sum \frac{F_X}{M_V}$$

$$\dot{V} + RU - PW = \sum \frac{F_Y}{M_V}$$

$$\dot{W} + PV - QU = \sum \frac{F_Z}{M_V}$$

(2.1.4b)

The left side of the equations represents the rate of change of linear momentum. The right side shows the summations: $\sum F_x$ $\sum F_y$ $\sum F_z$ of all external forces including gravity. The vehicle velocities U, V, W, along the body axes are obtained by integrating Equations 2.1.4b. The velocity components U, V, and W, along the body x, y, and z axes are also related to the angles of attack and sideslip as shown in Equation 2.1.5, where V_0 is the total vehicle velocity along the flight path.

$$U = V_0 \cos\alpha \ \cos\beta \qquad\qquad \alpha = \sin^{-1}\left(\frac{W}{V_0 \cos\beta}\right)$$

$$V = V_0 \sin\beta$$

$$W = V_0 \sin\alpha \ \cos\beta \qquad\qquad \beta = \sin^{-1}\left(\frac{V}{V_0}\right)$$

$$V_0 = \sqrt{U^2 + V^2 + W^2}$$

(2.1.5)

Where: α and β are the aerodynamic angles of attack and sideslip. After substituting U, V, and W from equations 2.1.4b in 2.1.5, the acceleration equations become:

$$\dot{U} = \dot{V}_0 \cos\alpha \ \cos\beta \quad = V_0 \sin\alpha \cos\beta \left(\dot{\alpha} - Q\right) + V_0 \cos\alpha \ \sin\beta \ \dot{\beta}$$

$$+ V_0 R \sin\beta + \sum {F_X}\big/{M_V}$$

$$\dot{V} = \dot{V}_0 \sin\beta \quad = -V_0 \cos\beta \ \dot{\beta} + V_0 \cos\beta \left(P\sin\alpha - R\cos\alpha\right)$$

$$+ \sum {F_Y}\big/{M_V}$$

$$\dot{W} = V_0 \cos\alpha \ \cos\beta \ \dot{\alpha} = -\dot{V}_0 \sin\alpha \ \cos\beta + V_0 \sin\alpha \ \sin\beta \ \dot{\beta} - V_0 P \sin\beta$$

$$+ V_0 Q \cos\alpha \ \cos\beta + \sum {F_Z}\big/{M_V}$$

Equation (2.1.6) Nominal acceleration equations as a function of external forces and body rates

Variations in the external forces δF$_x$, δF$_y$, δF$_z$ along the vehicle x, y, and z axes respectively produce variations in vehicle acceleration ($\dot{u}, \dot{v}, \dot{w}$), as shown in equations 2.1.7. Equations 2.1.7 calculate also the changes in the angles of attack and sideslip and the change in vehicle velocity δV as a function of the external forces. Note that, δV represents the change in velocity along the velocity vector V$_0$. Equations 2.1.7 are obtained by linearizing the non-linear equations 2.1.6, and substituting (w and v) with (α and β) respectively from equations 2.1.8.

$$\dot{u} = \delta\dot{V}\cos\alpha_0 = V_0 \sin\alpha_0 \left(\dot{\alpha} - q\right) + V_0 \left(\frac{(\dot{\alpha}_0 - Q_0)}{\cos\alpha_0} + R_0\beta_0 \tan\alpha_0\right)\alpha + V_0 \ \beta_0 r$$

$$+ V_0 \left(R_0 + \dot{\beta}_0 \cos\alpha_0\right)\beta + V_0\beta_0 \cos\alpha_0 \ \dot{\beta} + \left[\beta_0 \dot{\beta}_0 \cos\alpha_0 + R_0\beta_0 + (\dot{\alpha}_0 - Q_0)\sin\alpha_0\right]\delta V + \frac{\delta F_X}{M_V}$$

$$\dot{v} = V_0 \dot{\beta} = V_0 \sin\alpha_0 \ p - V_0 \cos\alpha_0 \ r + V_0 \left(R_0 \sin\alpha_0 + P_0 \cos\alpha_0\right)\alpha - \beta_0 \ \delta\dot{V} - \dot{V}_0\beta$$

$$+ \left[\frac{V_0\beta_0}{V_0} - R_0 \cos\alpha_0\right]\delta V + \frac{\delta F_Y}{M_V}$$

$$\dot{w} = V_0 \cos\alpha_0 \ \dot{\alpha} = V_0 \cos\alpha_0 \ q + V_0 \left(\dot{\beta}_0 \sin\alpha_0 - P_0\right)\beta - \sin\alpha_0 \ \delta\dot{V} + V_0\beta_0 \left(\sin\alpha_0 \ \dot{\beta} - p\right)$$

$$+ \left[\frac{(V_0\beta_0\dot{\beta}_0 - \dot{V}_0)}{\cos\alpha_0} - P_0\beta_0 V_0 \tan\alpha_0\right]\alpha + \left[\frac{V_0 \sin\alpha_0}{V_0} + Q_0 \cos\alpha_0\right]\delta V + \frac{\delta F_Z}{M_V}$$

Equation (2.1.7) Changes in vehicle accelerations due to external force variations

Small changes in the velocities along z and y (w and v) create variations in the angles of attack and sideslip α and β relative to the trim angles α$_0$ and β$_0$ respectively, as shown in Equations 2.1.8.

$$\alpha = \frac{w}{V_0 \cos\alpha_0} \qquad \beta = \frac{v}{V_0} \qquad\qquad (2.1.8)$$

Linear Accelerations at the Engine Gimbals

The translational accelerations at the TVC engine gimbals are used in the load-torque calculations. They include the effects of the vehicle rotations plus bending. The accelerations at the kth gimbal consist of the following three terms:

(a) Linear acceleration at the CG
(b) Contributions due to the vehicle angular acceleration, and
(c) Translational acceleration components due to structural flexibility at the gimbals.

$$a_{xe}(k) = \ddot{x}_{CG} + l_{Zek}\dot{q} - l_{Yek}\dot{r} + \sum_{j=1}^{Nm} \phi_{xe}(k,j)\ddot{\eta}(j)$$

$$a_{ye}(k) = \ddot{y}_{CG} + l_{Xek}\dot{r} - l_{Zek}\dot{p} + \sum_{j=1}^{Nm} \phi_{ye}(k,j)\ddot{\eta}(j) \qquad (2.1.9)$$

$$a_{ze}(k) = \ddot{z}_{CG} + l_{Yek}\dot{p} - l_{Xek}\dot{q} + \sum_{j=1}^{Nm} \phi_{ze}(k,j)\ddot{\eta}(j)$$

Where:

$\phi_{xe}(k,j)$ is the modal shape along x of mode (j) at the engine (k) location
$\eta(j)$ is the modal displacement for mode (j)
$l_{Xek}, l_{Yek},$ are the moment arms between an engine (k) and the vehicle CG
l_{Zek} in the x, y, and z directions respectively, $l_{Zek} = Z_{e(k)} - Z_{CG}$

Linear Accelerations at the Control Surface Hinges

Similarly, the acceleration along x, y, and z, at the mid-point of the kth control surface hinge line is calculated from equation 2.1.10. The accelerations at the control surfaces are used in the hinge moment equations.

$$a_{xcs}(k) = \ddot{x}_{CG} + l_{Zsk}\dot{q} - l_{Ysk}\dot{r} + \sum_{j=1}^{Nm} \phi_{xcs}(k,j)\ddot{\eta}(j)$$

$$a_{ycs}(k) = \ddot{y}_{CG} + l_{Xsk}\dot{r} - l_{Zsk}\dot{p} + \sum_{j=1}^{Nm} \phi_{ycs}(k,j)\ddot{\eta}(j) \qquad (2.1.10)$$

$$a_{zcs}(k) = \ddot{z}_{CG} + l_{Ysk}\dot{p} - l_{Xsk}\dot{q} + \sum_{j=1}^{Nm} \phi_{zcs}(k,j)\ddot{\eta}(j)$$

The moment arm distances between the center of an aerosurface k^{th} hinge line and the vehicle CG are defined in the following equations:

$$l_{XSk} = X_{Sk} - X_{CG} \qquad l_{YSk} = Y_{Sk} - Y_{CG} \qquad l_{ZSk} = Z_{Sk} - Z_{CG} \qquad (2.1.11)$$

18

2.2 Moment and Angular Acceleration Equations

The vehicle roll, pitch, and yaw body rates (P, Q, R) about its center of mass are obtained by integrating the non-linear rate of change of angular momentum equations 2.2.1.

$$I_{xx}\dot{P} = I_{xy}\left(\dot{Q} - PR\right) + I_{xz}\left(\dot{R} + PQ\right) + I_{yz}\left(Q^2 - R^2\right) + \left(I_{yy} - I_{zz}\right)QR + \sum L_X$$

$$I_{yy}\dot{Q} = I_{xy}\left(\dot{P} + QR\right) + I_{yz}\left(\dot{R} - PQ\right) + I_{xz}\left(R^2 - P^2\right) + \left(I_{zz} - I_{xx}\right)PR + \sum M_Y \qquad (2.2.1)$$

$$I_{zz}\dot{R} = I_{xz}\left(\dot{P} - QR\right) + I_{yz}\left(\dot{Q} + PR\right) + I_{xy}\left(P^2 - Q^2\right) + \left(I_{xx} - I_{yy}\right)PQ + \sum N_Z$$

Where: $\sum L_X$, $\sum M_Y$, and $\sum N_Z$ are the total externally applied (roll, pitch, and yaw) torques. They are due to aerodynamics, TVC forces, propellant sloshing, and external disturbances. The moments and products of inertia and the vehicle CG are calculated without the slosh masses and the gimbaling engines in the mass properties, because their presence in the vehicle equations is taken care by the slosh and the tail-wag-dog forces which are treated as separate bodies.

Equations 2.2.2 are derived by linearizing equations 2.2.1 at trim flight condition. They calculate variations in body rates (p, q, r) about its center of mass relative to the vehicle nominal rates (P0, Q0, R0) as a function of variations in the externally applied (roll, pitch, and yaw) torques: $\sum L_x$, $\sum M_y$, and $\sum N_z$.

$$I_{xx}\dot{p} = I_{xy}\left(\dot{q} - P_0 r - R_0 p\right) + I_{xz}\left(\dot{r} + Q_0 p + P_0 q\right) + 2I_{yz}\left(Q_0 q - R_0 r\right)$$

$$+\left(I_{yy} - I_{zz}\right)\left(Q_0 r + R_0 q\right) + \sum L_x$$

$$I_{yy}\dot{q} = I_{xy}\left(\dot{p} + Q_0 r + R_0 q\right) + I_{yz}\left(\dot{r} - Q_0 p - P_0 q\right) + 2I_{xz}\left(R_0 r - P_0 p\right)$$

$$+\left(I_{zz} - I_{xx}\right)\left(P_0 r + R_0 p\right) + \sum M_y \qquad (2.2.2)$$

$$I_{zz}\dot{r} = +I_{yz}\left(\dot{q} + P_0 r + R_0 p\right) + I_{xz}\left(\dot{p} - Q_0 r - R_0 q\right) + 2I_{xy}\left(P_0 p - Q_0 q\right)$$

$$+\left(I_{xx} - I_{yy}\right)\left(Q_0 p + P_0 q\right) + \sum N_z$$

The combined external torques: $\sum L_x$, $\sum M_y$, and $\sum N_z$ in equations 2.2.2 are due to variations in engine TVC forces, jet firing, aerodynamic forces, wind gust disturbances, sloshing, etc. as shown in Equation 2.2.3.

$$\sum L_X = L_{Xaero} + L_{X_{eng}} + L_{Xslosh} + L_{Xdist}$$

$$\sum M_Y = M_{Yaero} + M_{Y_{eng}} + M_{Yslosh} + M_{Ydist} \qquad (2.2.3)$$

$$\sum N_Z = N_{Zaero} + N_{Z_{eng}} + N_{Zslosh} + N_{Zdist}$$

The moment equations may be dynamically coupled together. The pitch axis is usually decoupled from the lateral axes, and the coupling is almost negligible in cylindrical boosters. Aircraft and rocket-plane type of vehicles, such as the Space Shuttle and most atmospheric vehicles have a significant amount of coupling between the roll and yaw axes due to the I_{xz} product of inertia term and also due to the aerodynamic coefficients $C_{l\beta}$, $C_{n\beta}$, etc. Coupling between all three: roll, pitch, and yaw moment axes can occur, mainly due to the products of inertia, steady vehicle rates (P0, Q0, R0), CG offsets, lack of

symmetry in the aerodynamic coefficients, and asymmetric TVC forces. It can also happen when an aircraft is flying at constant bank angle Φ_0 and sideslip β_0, or when a rocket vehicle is experiencing a steady sideslip angle β_0 due to cross-wind or because of the loss of thrust in an off-centered engine. Therefore, in the equations of motion we are not ignoring the cross-coupling terms between axes.

2.3 Gravitational Forces

The earth gravity force acting on the vehicle CG can be resolved along the body x, y, and z axes as a function of the pitch and roll Euler angles relative to the local horizontal axes.

$$\begin{pmatrix} F_{Xgrav} \\ F_{Ygrav} \\ F_{Zgrav} \end{pmatrix} = M_V g \begin{pmatrix} -\sin\Theta \\ \cos\Theta\sin\Phi \\ \cos\Theta\cos\Phi \end{pmatrix}$$

$where\ the\ gravity\ const.\ (g)\ is:$ \hspace{2cm} (2.3.1)

$$g = g_0 \left(\frac{R_e}{R_e + h_0}\right)^2 - \left(\frac{V_0^2}{R_e + h_0}\right)$$

The gravity acceleration constant (g) varies with altitude. The (g) equation also takes into consideration the orbital effect due to the vehicle velocity V_0 which causes a centripetal force, where: (g_o) is the gravity constant at the earth's surface. By applying small variations in equation 2.3.1, we obtain the following equation 2.3.2 which calculates variations in gravity forces as a function of variations in (α, δh, θ, ϕ, δV).

$$\frac{F_{Xgrav}}{M_V} = -g\cos\Theta_0\,\theta - g\sin\Theta_0\tan\alpha_0\,\alpha$$
$$+ \frac{\sin\Theta_0}{(R_e + h_0)^2}\left[\frac{2gR_e^2}{R_e + h_0} - V_0^2\right]\delta h + \left[\frac{2V_0}{R_e + h_0}\right]\sin\Theta_0\,\delta V$$

$$\frac{F_{Ygrav}}{M_V} = g\left(\cos\Theta_0\cos\Phi_0\phi - \sin\Theta_0\sin\Phi_0\theta\right)$$
$$- \frac{\cos\Theta_0\sin\Phi_0}{(R_e + h_0)^2}\left[\frac{2gR_e^2}{R_e + h_0} - V_0^2\right]\delta h - \left[\frac{g}{V_0} + \frac{2V_0}{R_e + h_0}\right]\cos\Theta_0\sin\Phi_0\,\delta V$$

$$\frac{F_{Zgrav}}{M_V} = -g\left(\sin\Theta_0\cos\Phi_0\theta + \cos\Theta_0\sin\Phi_0\phi\right) + g\left(\cos\Theta_0\cos\Phi_0\tan\alpha_0\right)\alpha$$
$$- \frac{\cos\Theta_0\cos\Phi_0}{(R_e + h_0)^2}\left[\frac{2gR_e^2}{R_e + h_0} - V_0^2\right]\delta h - \left[\frac{g}{V_0} + \frac{2V_0}{R_e + h_0}\right]\cos\Theta_0\cos\Phi_0\,\delta V$$

Equation (2.3.2) Variations in Gravity Forces

Where:

R_e is the radius of the earth
h_0 is the vehicle altitude from sea level
V_0 is the vehicle horizontal velocity
α_0, α are the nominal angle of attack and its variation from nominal
Φ_0, Θ_0 are the nominal vehicle roll and pitch Euler angles
ϕ, θ are the attitude variation angles in roll and pitch
g, g_0 is the nominal gravity acceleration, and at zero altitude

2.4 Engine Forces and Moments due to Gimbaling and Throttling
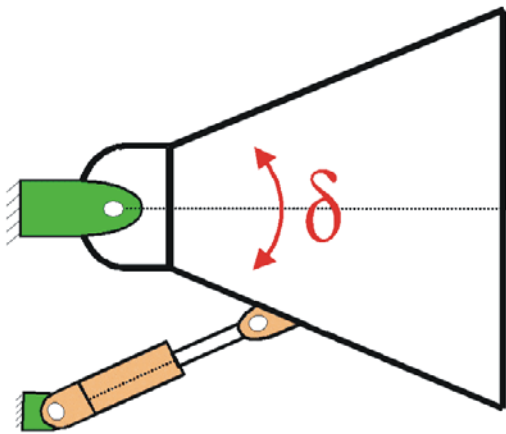
The attitude and direction of a rocket vehicle is controlled either by gimbaling the thrust vector control (TVC) engines, or by varying the thrust of the engines (throttling), or both. In our models the TVC nozzles are attached to the vehicle by means of spherical pivots that allow them to pivot in two directions. By deflecting the engine nozzles the TVC generates force variations at the gimbals perpendicular to the vehicle direction that are used to guide and stabilize the vehicle. Typically, two orthogonal actuators per engine are used to provide the forces needed to rotate the nozzle in pitch δ_y and in yaw δ_z directions. The max gimbal angles in typical launch vehicles may vary between $\pm 5°$ and $\pm 10°$. The vehicle velocity can be controlled by varying the engine thrust.

Engine Forces at the Gimbals

A typical engine nozzle (k) with a nominal thrust (T_{ek}) is not necessarily aligned with the vehicle x axis, but it is tilted in pitch and yaw at angles Δ_E and Δ_Z respectively, see Figure 2.4.4. This non-zero position is either due to intentional mounting of the nozzle, scheduling, or trimming, as the engines rotate in order to balance the aerodynamic moments. Δ_E is the elevation angle which is between the nozzle thrust direction and the vehicle x-y plane, and it is positive down. Δ_Z is the yaw rotation angle of the nozzle and the thrust vector at the gimbal. It is the rotation angle of the thrust vector projection in the x-y plane about the z-axis, measured from to the -x direction.

Total Deflection at an Engine Gimbal

The engine nozzles deflect further from their trim positions (Δ_E and Δ_Z) by some smaller angles (δ_{ye} and δ_{ze}) in pitch and yaw, in order to guide the vehicle and to stabilize it against aero disturbances. They may also vary their thrust from nominal. The additional deflections and thrust variations generate force variations at the engine gimbals. The forces which are perpendicular to the flight direction control attitude and flight path, and the thrust variations control the vehicle speed.

The actuators provide the forces required to rotate the nozzles in pitch and in yaw (δ_{ya} and δ_{za}) from trim (Δ_E and Δ_Z). The intended deflections, however, are corrupted by flexibility of the structure at the engine gimbal, and the total deflections of the nozzle in pitch and yaw consist of two components: the rotation of the nozzle about its gimbal as a result of the actuator displacement, and an additional

deflection resulting from the elastic deformation of the vehicle structure at the gimbal, equation (2.4.2), where: $(\sigma_{yek}\ \sigma_{zek})$ are the pitch and yaw modal slopes at the engine (k) gimbal. The pitch engine deflection δ_{yek} is measured with respect to the trim position Δ_{Ek} and along the same direction. When Δ_{Zk} is zero, the pitch deflection δ_{yek} is exactly in the pitch direction. Figure 2.4.6 illustrates the total nozzle deflection at the pivot, consisting of two rotational components: a component due to the nozzle rotation relative to the gimbal, plus a component due to structural deformation at the gimbal as described in equation (2.4.2).

$$\delta_{ye}(k) = \delta_{ya}(k) + \sum_{j=1}^{N\,\mathrm{mod}} \sigma_{ye}(k, j)\eta(j)$$

$$\delta_{ze}(k) = \delta_{za}(k) + \sum_{j=1}^{N\,\mathrm{mod}} \sigma_{ze}(k, j)\eta(j)$$

Equation 2.4.2 Total Nozzle deflection is due to rotation at the gimbal plus structure deformation

The relative rotation, rate, and acceleration at the gimbals are calculated from separate actuator models for each TVC rotation. The total deflection and acceleration at the gimbal term must include the structural deformation component calculated from the modes as in equation (2.4.2). The gimbal forces, therefore, contain undesirable low-damped oscillatory components due to structural flexibility at the gimbals.

Forces at the Engine Gimbals

Each engine at its trimmed position generates a force vector on the vehicle that can be resolved in three components $F_{XE}(k)$, $F_{YE}(k)$, and $F_{ZE}(k)$ along the vehicle body axes. Equations 2.4.1 calculate the trim forces along x, y, and z, at an engine (k) gimbal as a function of thrust and the trim angles (Δ_{Ek} and Δ_{Zk}). These are the steady-state forces that accelerate the vehicle and balance the steady aerodynamic moments.

$$
\begin{aligned}
F_{XE}(k) &= T_{ek}\cos\Delta_E(k)\cos\Delta_Z(k) \\
F_{YE}(k) &= T_{ek}\cos\Delta_E(k)\sin\Delta_Z(k) \\
F_{ZE}(k) &= -T_{ek}\sin\Delta_E(k)
\end{aligned}
\tag{2.4.1}
$$

Equation (2.4.3) calculates the force variations: δF_{xek}, δF_{yek}, and δF_{zek} at the engine gimbal due to pivoting relative to the trim angles (Δ_{Ek} and Δ_{Zk}) and throttling about nominal thrust T_{ek}. It is derived from equation (2.4.1) by replacing the nozzle trim angles (Δ_E and Δ_Z) by ($\Delta_E+\delta_y$) and ($\Delta_Z+\delta_z$), and the thrust T_{ek} with ($T_{ek}+\delta T_{ek}$) and solving for variations. They consist of four parts:

- Forces due to small pitch engine deflections (δ_{yek}) from trim
- Forces due to small yaw engine deflections (δ_{zek}) from trim about the local z-axis
- Force variation due to engine thrust variations ($\pm\delta T_{ek}$) relative to nominal thrust (T_{ek}), and
- Tail-wag-dog forces caused by angular accelerations of the engine nozzles.

$$F_{xe}(k) = T_{ek}\left(-\cos\Delta_{Z_k}\sin\Delta_{E_k}\delta_{yek} - \cos\Delta_{E_k}\sin\Delta_{Z_k}\delta_{zek} + \cos\Delta_{Z_k}\cos\Delta_{E_k}\,\delta T_{Thr_k}\right)$$
$$-m_{ek}l_{ek}\left(\cos\Delta_{Z_k}\sin\Delta_{E_k}\ddot{\delta}_{yek} + \cos\Delta_{E_k}\sin\Delta_{Z_k}\ddot{\delta}_{zek}\right)$$
$$F_{ye}(k) = T_{ek}\left(-\sin\Delta_{Z_k}\sin\Delta_{E_k}\delta_{yek} + \cos\Delta_{E_k}\cos\Delta_{Z_k}\delta_{zek} + \sin\Delta_{Z_k}\cos\Delta_{E_k}\,\delta T_{Thr_k}\right)$$
$$+m_{ek}l_{ek}\cos\Delta_{Z_k}\ddot{\delta}_{zek}$$
$$F_{ze}(k) = -T_{ek}\left(\cos\Delta_{E_k}\delta_{yek} + \sin\Delta_{E_k}\delta T_{Thr_k}\right) - m_{ek}l_{ek}\cos\Delta_{E_k}\ddot{\delta}_{yek}$$

$$\text{where the Throttle Control} \quad \delta T_{Thr_k} = \left(\frac{\delta T_{ek}}{T_{ek}}\right)$$

(2.4.3)

For a thrust varying engine, the ratio of thrust variation divided by the nominal engine thrust ($\delta T_{ek}/T_{ek}$) is defined to be the throttle control input $\delta_{Thr}(k)$. The maximum throttle control indicates the maximum amount of thrust variation that the engine is capable of providing, above and below nominal thrust. A positive value for δ_{Thr} indicates a thrust increase from the nominal thrust. A negative value indicates a thrust reduction from nominal. For example, if the thrust of an engine can be made to vary from 80 pounds to 120 pounds by means of a throttle control valve, the thrust variation in the equations should be represented by a nominal thrust $T_{ek}=100$ pounds and a throttle control input $\delta_{Thr}(k)=(\pm 0.2)$. In order to avoid confusion in Flixan, the maximum throttling capability of each engine is taken into consideration and the program automatically scales the model so that each input is expected to assume values between +1 and -1. In this example, an input of +1 corresponds to the max thrust of 120 (lb), zero corresponds to the nominal thrust of 100 (lb), and -1 corresponds to the minimum thrust of 80 (lb). Inputs of magnitude greater than one would violate the engine throttling specs.

On-off RCS jets can be modeled similar to the thrust varying engines using Equations (2.4.3). In the case of an "on/off" RCS jet capable of producing either zero or 100 lb of thrust, we can model this thruster as having a nominal thrust equal to zero and a max thrust equal to 100 pounds, in which case, the normalized throttle control input $\delta_{Thr}(k)$ in the vehicle model must be either: 0 or +1. This model can also be used to represent a pair of reaction control jets (ex. 100 pounds each) mounted back-to-back in the same location with their nozzles in the opposite directions producing a thrust between zero and ±100 pounds. In this case the throttle control input $\delta_{Thr}(k)$ in the normalized system can assume three distinct values {-1, 0, and +1} to represent the three extreme thrust values. Differential throttling of propulsion engines for attitude control can be used in vehicles that have the engines located with big enough moment arms from the vehicle CG. In simulations, the throttle control inputs $\delta_{Thr}(k)$ in the vehicle model are received from a jet selection logic that generates throttle control signals. They must be normalized and limited to values which are less than one in magnitude, otherwise, they would be off-limits.

The last term in equations 2.4.3 represent the reaction forces at the gimbal due to the angular acceleration of the engine nozzle about the pivot. This term creates the *"tail-wags-dog"* dynamics. We assume that the engine nozzles are rigid and when they rotate, they generate reaction forces against the vehicle at the gimbals. The TWD terms consist of two components: the angular acceleration of the nozzle relative to the gimbal and the acceleration of the structure around the gimbal. The TWD terms create a pair of zeros in the transfer function. The location of the zeros in the complex s-plane depends on the sign of the nozzle moment arm (l_{ek}), which is the distance of the nozzle's center of mass from its pivot. A typical engine nozzle has its center of mass further back from the pivot point ($l_{ek} > 0$), and the

TWD zeros create a complex pair along the (jω) axis. If the moment arm is negative (nozzle mass center is above gimbal) the zeros are along the real axis.

Total Engine Forces

The total TVC forces which are applied on the vehicle along x, y, and z, are the forces which maneuver the vehicle around, and they are obtained by combining the individual engines. The engine forces are combined to calculate the total vehicle force and moment variations due to the combined TVC. Note, that when the inertial coupling coefficients (h_e) are not included in the flex equations, the gimbal accelerations (pitch and yaw) should include the flexibility components as shown in equations (2.4.2). Otherwise, when they are included, the gimbal accelerations in equations (2.4.3) should not include the flex acceleration terms because the coupling of the vehicle structure with the gimbal accelerations is captured by the inertial coupling coefficients which are provided by the FEM. The combined TVC forces from all engines along the x, y, and z axes consist of the summation of the components from each individual engine as shown in equation (2.4.5). Figure (2.4.6) illustrates the total deflection of an engine at the gimbal as described in equation (2.4.2).

$$F_{X_{Eng}} = \sum_{k=1}^{Neng} F_{xe}(k) \qquad F_{Y_{Eng}} = \sum_{k=1}^{Neng} F_{ye}(k) \qquad F_{Z_{Eng}} = \sum_{k=1}^{Neng} F_{ze}(k) \qquad (2.4.5)$$
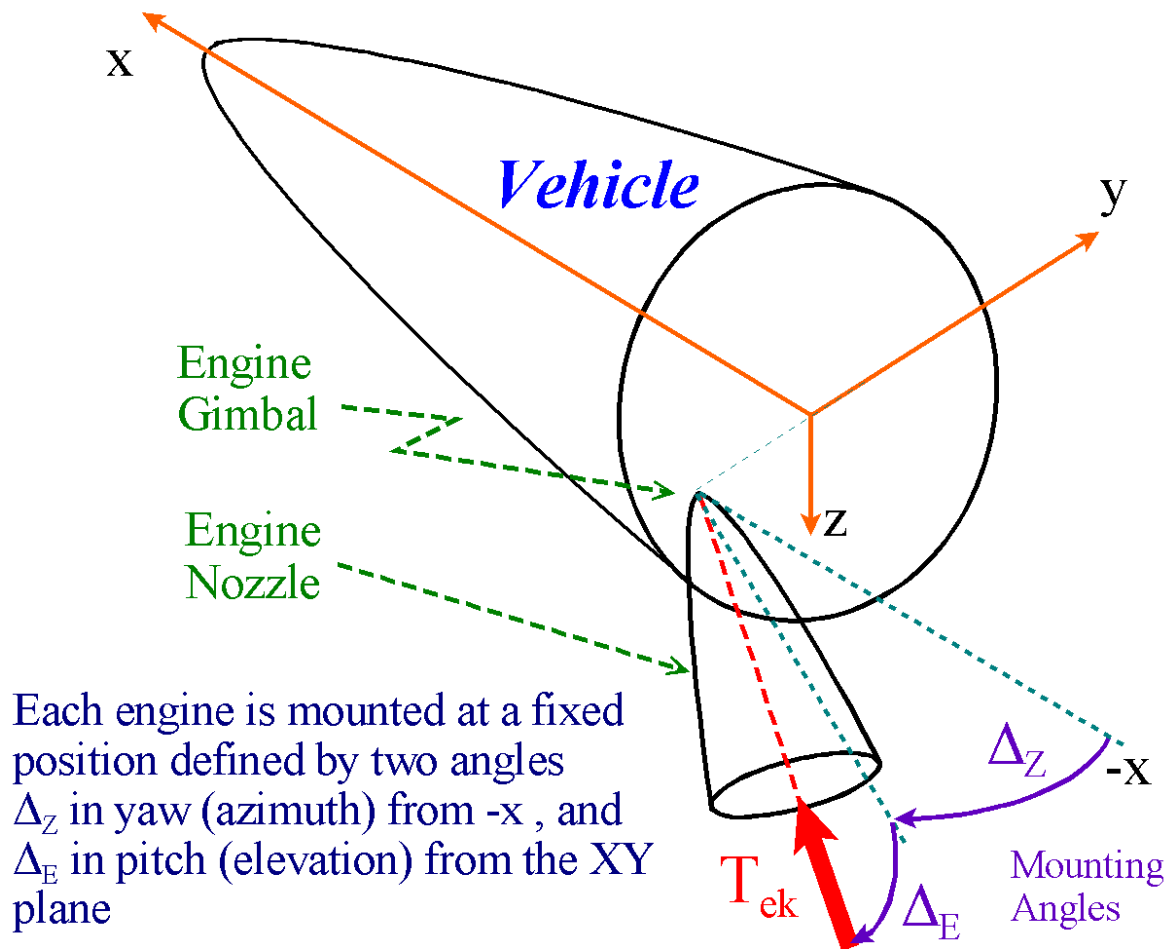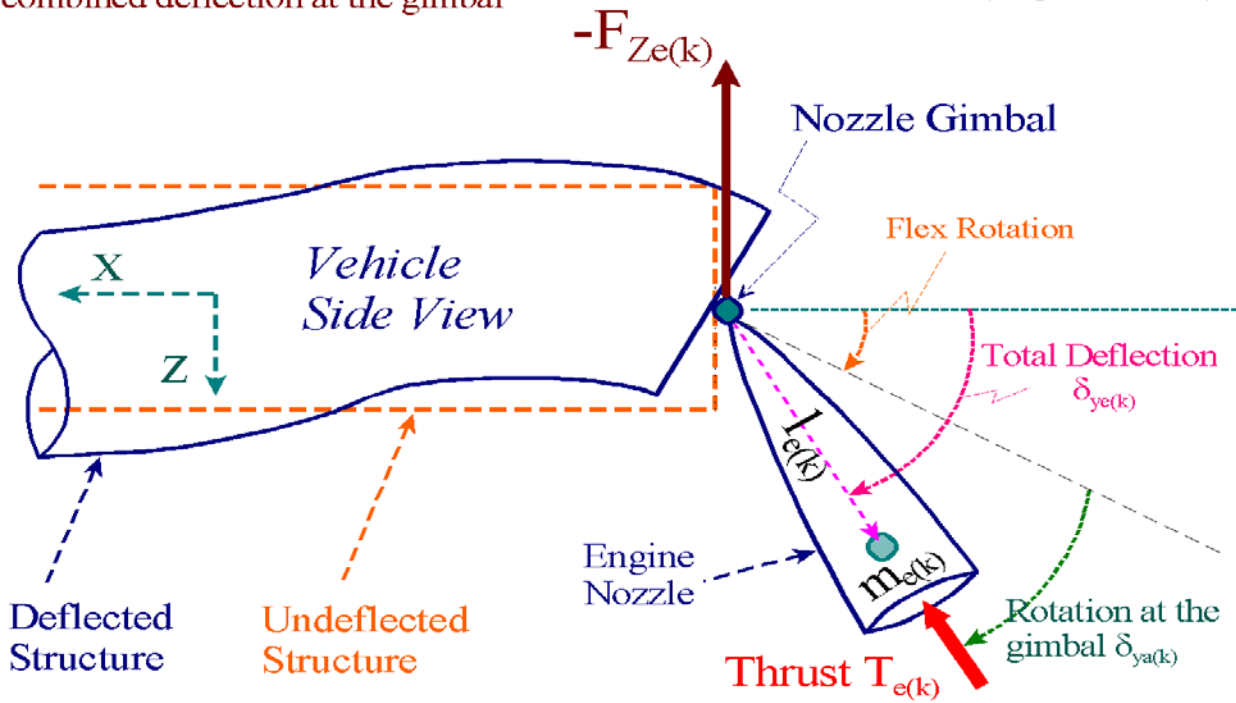

Figure (2.4.4) Engine Nozzle Orientation Angles with respect to the Vehicle

24

Normal Force perpendicular to the vehicle X axis resulting from the combined deflection at the gimbal

Total Pitch Deflection at the Gimbal (Rigid + Flex)

$-F_{Ze(k)}$

Nozzle Gimbal

Flex Rotation

X

Vehicle Side View

Z

Total Deflection $\delta_{ye(k)}$

$L_{e(k)}$

Engine Nozzle

$m_{e(k)}$

Rotation at the gimbal $\delta_{ya(k)}$

Thrust $T_{e(k)}$

Deflected Structure

Undeflected Structure

Lateral Force perpendicular to the vehicle X axis resulting from the combined deflection at the gimbal
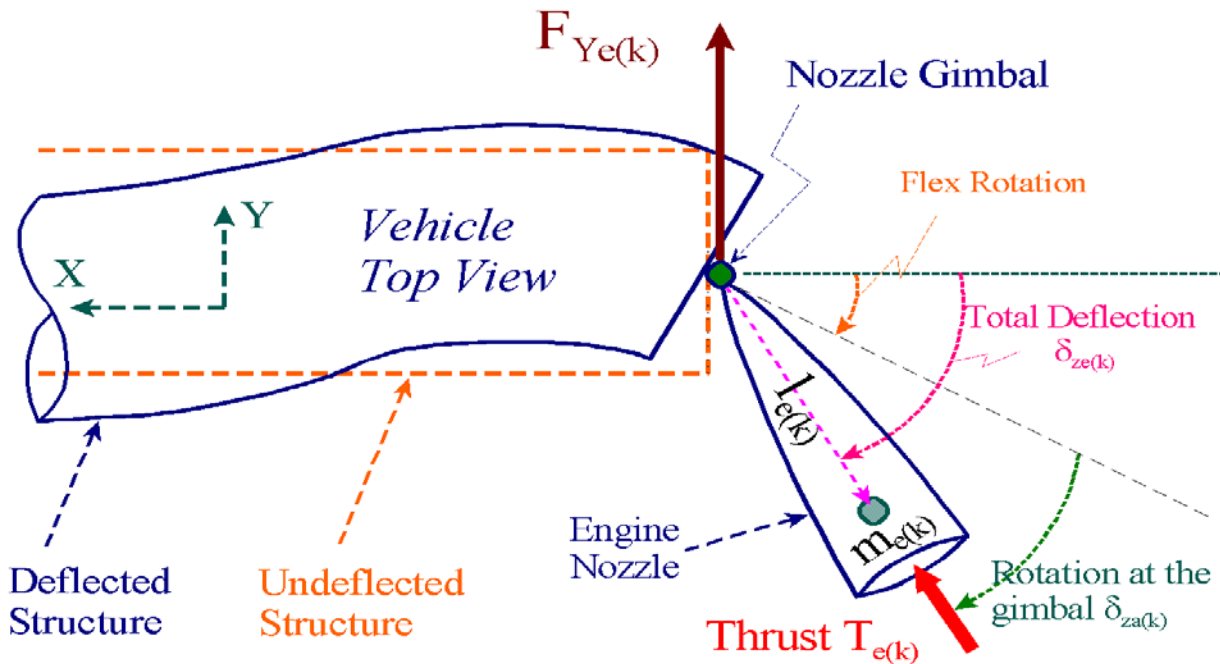
Total Engine Deflection in Yaw (Rigid + Flex)

$F_{Ye(k)}$

Nozzle Gimbal

Flex Rotation

Y

X

Vehicle Top View

Total Deflection $\delta_{ze(k)}$

$L_{e(k)}$

Engine Nozzle

$m_{e(k)}$

Rotation at the gimbal $\delta_{za(k)}$

Thrust $T_{e(k)}$

Deflected Structure

Undeflected Structure

Figure (2.4.6) Total Engine Deflections Consists of Rigid plus Flex Components

25

Moments due to Engine TVC Forces

Equations (2.4.7) calculate the roll, pitch, and yaw TVC moments on the vehicle generated by the force variations at the gimbals Equations (2.4.3), from all engines combined. The equations also include the reaction forces and moments created by the nozzle accelerations.

$$L_{X_{Eng}} = \sum_{k=1}^{Neng} \left(F_{ze(k)} l_{yek} - F_{ye(k)} l_{zek} \right)$$

$$M_{Y_{Eng}} = \sum_{k=1}^{Neng} \left\{ \begin{array}{l} F_{xe(k)} l_{zek} - F_{ze(k)} l_{xek} - I_{ek} \ddot{\delta}_{ye(k)} - m_{ek} l_{ek} A_X \cos\Delta_{E(k)} \delta_{ye(k)} \\ + \left(T_{ek} \cos\Delta_{E(k)} \cos\Delta_{Z(k)} - m_{ek} A_X \right) \sum_{j=1}^{N\,\mathrm{mod}} \phi_{ze}(k,j) \eta(j) \end{array} \right\}$$

$$N_{Z_{Eng}} = \sum_{k=1}^{Neng} \left\{ \begin{array}{l} F_{ye(k)} l_{xek} - F_{xe(k)} l_{yek} - I_{ek} \ddot{\delta}_{ze(k)} - m_{ek} l_{ek} A_X \cos\Delta_{E(k)} \cos\Delta_{Z(k)} \delta_{ze(k)} \\ - \left(T_{ek} \cos\Delta_{E(k)} \cos\Delta_{Z(k)} - m_{ek} A_X \right) \sum_{j=1}^{N\,\mathrm{mod}} \phi_{ye}(k,j) \eta(j) \end{array} \right\}$$

Equation (2.4.7) Vehicle Moments due to Combined TVC Forces

The first two terms in equations (2.4.7) consist of the cross-products between x, y, z engine forces times the moment arms from the vehicle CG to the engine gimbals. The third terms in the pitch and yaw equations are TWD torques due to engine rotational accelerations. The fourth term represents the moment caused by an engine that has its center of mass displaced due to gimbal rotation (δ_{ye}, δ_{ze}) and coupling with the vehicle acceleration (A_x). The fifth term in the pitch and yaw equations represents the moment variation caused by an engine thrust that has its application point displaced from its nominal position due to normal or lateral flex displacement at the gimbal. The sixth term is the additional moment due to the flex displacement at the gimbal coupling with the vehicle acceleration (A_x). The relationship between the inertial and the sensed accelerations is shown in equation (2.1.3).

The engine forces {$F_{xe(k)}$, $F_{ye(k)}$, $F_{ze(k)}$} are calculated in equation (2.4.3) and, as it was previously discussed, the implementation of the force equation depends on whether or not the inertial coupling coefficients (h_e) are included in the bending equations. When they are not available, the pitch and yaw gimbal accelerations are calculated with flexibility included as shown in equations (2.4.2). Otherwise, only the rigid component of the gimbal acceleration is used because the flex coupling effect is introduced by the inertial coupling coefficients (h_e) in the bending equation. The moment arms between the engine (k) gimbal and the vehicle CG are defined by the following equations:

$$l_{xek} = X_{ek} - X_{CG} \qquad l_{yek} = Y_{ek} - Y_{CG} \qquad l_{zek} = Z_{ek} - Z_{CG}$$

2.5 Aerodynamic Forces and Moments

The aerodynamic forces and moments which are applied on the flight vehicle as it flies through the atmosphere are based on an aerodynamic model that calculates the forces along the x, y, and z body axes, and also the moments, as a function of the Mach number, the angles of attack and sideslip, the body rates, and surface deflections. The aerodynamic model consists of a set of coefficients for the base vehicle, plus increment coefficients for each aerosurface. The aerodynamic forces along the x, y, and z axes are defined in equations 2.5.1, and the aerodynamic moments in equations 2.5.2. They are used in 6-dof simulations and not for linear analysis. They calculate the base forces and moments which are functions of Mach number and the angles of attack and sideslip relative to the airflow. They also include forces and moments generated by the control surfaces combined. The basic aerodynamic coefficients are (C_A, C_Y, C_Z, C_l, C_m, and C_n). They are non-dimensional and vary as a function of Mach number and the angles of attack and sideslip. The equations include damping terms which are functions of body rates and damping derivative coefficients. The coefficients are obtained from wind-tunnel tests, or analytically from CFD models. The vehicle "feels" the presence of a wind-shear or a gust in the equations by the changes that it produces in the angles of attack and sideslip (α_w, β_w) and also in the velocity V_w relative to the airflow, because those variables are affected by variations in the wind velocity, see figures (2.9.1- 2.9.3). The equations also include damping terms which are functions of body rates and damping derivative coefficients. The damping coefficients vary with Mach and alpha. In 6-DOF simulations the coefficients are stored in multi-dimensional look-up matrix tables and are interpolated.

$$F_{Xaero} = -\overline{Q}S_{ref} C_A(M, \alpha_w, \beta_w) + \sum_{k=1}^{Ncs} F_{Xcs}(k)$$

$$F_{Yaero} = \overline{Q}S_{ref}\left(C_Y(M, \alpha_w, \beta_w) + \left(\frac{l_{sp}}{2V_0}\right)\left(C_{Yp}\ p + C_{Yr}\ r + C_{Y\dot\beta}\ \dot\beta_w\right)\right) + \sum_{k=1}^{Ncs} F_{Ycs}(k)$$

$$F_{Zaero} = \overline{Q}S_{ref}\left(C_Z(M, \alpha_w, \beta_w) + \left(\frac{l_{ch}}{2V_0}\right)\left(C_{Zq}\ q + C_{Y\dot\alpha}\ \dot\alpha_w\right)\right) + \sum_{k=1}^{Ncs} F_{Zcs}(k)$$

$$where: \alpha_w = \alpha + \frac{w_{gust}}{V_0 \cos\alpha_0}\ ;\ \beta_w = \beta + \frac{v_{gust}}{V_0}$$

Equation (2.5.1) Aerodynamic Forces on the Vehicle

$$L_{Xaero} = \overline{Q}S_{ref}l_{sp}\left(C_l(M, \alpha_w, \beta_w) + \frac{l_{sp}}{2V_0}\left(C_{lp}\ p + C_{lr}\ r + C_{l\dot\beta}\ \dot\beta_w\right)\right) + \sum_{k=1}^{Nsurf} L_{Xs}(k)$$

$$M_{Yaero} = \overline{Q}S_{ref}l_{ch}\left(C_m(M, \alpha_w, \beta_w) + \frac{l_{ch}}{2V_0}\left(C_{mq}\ q + C_{m\dot\alpha}\ \dot\alpha_w\right)\right) + \sum_{k=1}^{Nsurf} M_{Ys}(k)$$

$$N_{Zaero} = \overline{Q}S_{ref}l_{sp}\left(C_n(M, \alpha_w, \beta_w) + \frac{l_{sp}}{2V_0}\left(C_{np}\ p + C_{nr}\ r + C_{n\dot\beta}\ \dot\beta_w\right)\right) + \sum_{k=1}^{Nsurf} N_{Zs}(k)$$

Figure (2.5.2) Aerodynamic Moments on the Vehicle

Equations 2.5.3 calculate the additional forces on the vehicle $F_{Xcs}(k)$, $F_{Ycs}(k)$, $F_{Zcs}(k)$, and the moments $L_{Xcs}(k)$, $M_{Ycs}(k)$, $N_{Zcs}(k)$ generated by the deflection and acceleration of an aerosurface (k). The aerosurface aerodynamic coefficients are functions of four variables: Mach number, angles of attack and sideslip relative to the airflow, and control surface increment from zero position δ_s. There are also damping terms due to the aerosurface rate $\dot{\delta}_s$. The equations also include "tail-wag-dog" forces generated at the hinges due to the aerosurface accelerations. In 6-dof simulations the coefficients are stored in four-dimensional look-up matrices and interpolated.

$$F_{Xcs}(k) = -\overline{Q}S_{ref}\left[C_{A\delta(k)}\left(M,\alpha_w,\beta_w,\delta_{s(k)}\right)+\left(\frac{\overline{c}_{sk}}{2V_0}\right)C_{A\dot{\delta}(k)}\dot{\delta}_{s(k)}\right] + F_{XS_{TWD}}(k)$$

$$F_{Ycs}(k) = \overline{Q}S_{ref}\left[C_{Y\delta(k)}\left(M,\alpha_w,\beta_w,\delta_{s(k)}\right)+\left(\frac{\overline{c}_{sk}}{2V_0}\right)C_{Y\dot{\delta}(k)}\dot{\delta}_{s(k)}\right] + F_{YS_{TWD}}(k)$$

$$F_{Zcs}(k) = \overline{Q}S_{ref}\left[C_{Z\delta(k)}\left(M,\alpha_w,\beta_w,\delta_{s(k)}\right)+\left(\frac{\overline{c}_{sk}}{2V_0}\right)C_{Z\dot{\delta}(k)}\dot{\delta}_{s(k)}\right] + F_{ZS_{TWD}}(k)$$

$$L_{Xs}(k) = \overline{Q}S_{ref}\,l_{sp}\left[C_{l\delta(k)}\left(M,\alpha_w,\beta_w,\delta_{s(k)}\right)+\left(\frac{\overline{c}_{sk}}{2V_0}\right)C_{l\dot{\delta}(k)}\dot{\delta}_{s(k)}\right] + F_{ZS_{TWD}(k)}l_{Ysk} - F_{YS_{TWD}(k)}l_{Zsk}$$

$$M_{Ys}(k) = \overline{Q}S_{ref}\,l_{ch}\left[C_{m\delta(k)}\left(M,\alpha_w,\beta_w,\delta_{s(k)}\right)+\left(\frac{\overline{c}_{sk}}{2V_0}\right)C_{m\dot{\delta}(k)}\dot{\delta}_{s(k)}\right]$$
$$+ F_{XS_{TWD}(k)}l_{Zsk} - F_{ZS_{TWD}(k)}l_{Xsk} - I_{hs(k)}\cos\phi_{h(k)}\ddot{\delta}_{s(k)}$$

$$N_{Zs}(k) = \overline{Q}S_{ref}\,l_{sp}\left[C_{n\delta(k)}\left(M,\alpha_w,\beta_w,\delta_{s(k)}\right)+\left(\frac{\overline{c}_{sk}}{2V_0}\right)C_{n\dot{\delta}(k)}\dot{\delta}_{s(k)}\right]$$
$$+ F_{YS_{TWD}(k)}l_{Xsk} - F_{XS_{TWD}(k)}l_{Ysk} - I_{hs(k)}\sin\phi_{h(k)}\ddot{\delta}_{s(k)}$$

$$where: F_{XS_{TWD}}(k), etc.\ are\ the\ TWD\ forces$$
$$F_{XS_{TWD}}(k) = -m_{sk}\,L_{hs(k)}\cos\lambda_{hs(k)}\sin\Delta_{s(k)}\ddot{\delta}_{s(k)}$$
$$F_{YS_{TWD}}(k) = +m_{sk}\,L_{hs(k)}\sin\phi_{hs(k)}\ddot{\delta}_{s(k)}$$
$$F_{ZS_{TWD}}(k) = -m_{sk}\,L_{hs(k)}\cos\phi_{hs(k)}\cos\Delta_{s(k)}\ddot{\delta}_{s(k)}$$
$$l_{Xsk} = X_{sk} - X_{CG} \qquad l_{Ysk} = Y_{sk} - Y_{CG} \qquad l_{Zsk} = Z_{sk} - Z_{CG}$$

Figure (2.5.3) Forces and Moments on the Vehicle Created by the Deflection and Acceleration of a Surface (k)

Linearized Equations

Equations 2.5.4 are used in linear control analysis, and they calculate the variations in the aerodynamic trim forces from steady-state, as a function of variations in vehicle variables, structural elasticity, and aero-surface forces. They are derived by linearizing equations 2.5.1. The angles of attack and sideslip (α_w, β_w) describe variations from trim (α_0, β_0) and they include the effects due to wind velocity disturbance, as shown in Section 2.9. The change in vehicle velocity (δV_w) includes also the effect due to the wind velocity. The variables w_{gust} and v_{gust} are the wind gust velocity components relative to the vehicle in the z and y directions respectively. The forces $F_{Xs}(k)$, $F_{Ys}(k)$, and $F_{Zs}(k)$ in this case represent additional forces due to an aerosurface (k) deflection and they are defined in equation 2.5.5. The coefficients $C_{Z\eta_j}$, $C_{Y\eta_j}$ etc. are aero-elastic coefficients that define variations in the aerodynamic forces along the y and z axes due to the generalized modal displacements (η_j) and their derivatives. They define, for example, the normal force variations on a flexible wing as a result of structural wing oscillations.

$$
F_{Xaero} = -\overline{Q}S_{ref}\left[
\begin{aligned}
&C_{A0}\tan\alpha_0\,\alpha + C_{A\alpha}\alpha_w + C_{A\beta}\beta_w + \left(\frac{l_{ch}}{2V_0}C_{Aq}\right)q \\
&+\left(\frac{2C_{A0}}{V_0} + \frac{\partial C_A}{\partial V}\right)\delta V_w + \left(\frac{\partial C_A}{\partial h} + \frac{\partial \rho}{\partial h}\left(\frac{V_0^2}{2\overline{Q}}\right)C_{A0}\right)\delta h
\end{aligned}
\right] + \sum_{k=1}^{Ncs}F_{Xs}(k)
$$

$$
F_{Yaero} = \overline{Q}S_{ref}\left[
\begin{aligned}
&C_{Y\alpha}\alpha_w + C_{Y\beta}\beta_w + \left(\frac{l_{sp}}{2V_0}\right)\left(C_{Yp}\,p + C_{Yr}\,r + C_{Y\dot{\beta}}\,\dot{\beta}_w\right) + \left(\frac{2C_{Y0}}{V_0}\right)\delta V_w \\
&+\frac{\partial\rho}{\partial h}\left(\frac{V_0^2}{2\overline{Q}}\right)C_{Y0}\delta h + \sum_{j=1}^{N\,mod}\left(C_{Y\eta_j}\eta_j + \frac{C_{Y\dot{\eta}_j}}{V_0}\dot{\eta}_j\right)
\end{aligned}
\right] + \sum_{k=1}^{Ncs}F_{Ys}(k)
$$

$$
F_{Zaero} = \overline{Q}S_{ref}\left[
\begin{aligned}
&C_{Z0}\tan\alpha_0\,\alpha + C_{Z\alpha}\alpha_w + C_{Z\beta}\beta_w + \left(\frac{l_{ch}}{2V_0}\right)\left(C_{Zq}\,q + C_{Z\dot{\alpha}}\,\dot{\alpha}_w\right) \\
&+\left(\frac{2C_{Z0}}{V_0} + \frac{\partial C_Z}{\partial V}\right)\delta V_w + \left(\frac{\partial C_Z}{\partial h} + \frac{\partial\rho}{\partial h}\left(\frac{V_0^2}{2\overline{Q}}\right)C_{Z0}\right)\delta h \\
&+\sum_{j=1}^{N\,mod}\left(C_{Z\eta_j}\eta_j + \frac{C_{Z\dot{\eta}_j}}{V_0}\dot{\eta}_j\right)
\end{aligned}
\right] + \sum_{k=1}^{Ncs}F_{Zs}(k)
$$

$$
where: \alpha_w = \alpha + \frac{w_{gust}}{V_0\cos\alpha_0}\;;\;\beta_w = \beta + \frac{v_{gust}}{V_0}
$$

Equation (2.5.4) Variations in Aerodynamic Forces along X, Y, and Z

Forces Generated by a Control Surface

In the equations that follow each aerosurface is considered to be a separate control input. Each rotating panel must be defined as a separate panel and not a combination of aerosurfaces, such as an aileron which is the differential deflection of two flaps, or an elevon that is the average deflection of two flaps. The transformation from roll, pitch, and yaw flight control demands to the individual panel deflections

is defined by the mixing-logic matrix and therefore it is not necessary to combine aerosurfaces together in the dynamic model. The reason is because it makes it easier to include flexibility and TWD forces at the hinges of each aerosurface because each aerosurface generates a separate force and torque on the vehicle at a specific location and direction. It is difficult to model the tail-wag-dog forces when the aerosurfaces are combined together as a single control input. Because, the forcing functions on the vehicle are not only from aerodynamic forces, which are defined by the aero coefficients, but they are also affected by tail-wags-dog forces and structural deformations which are specific to each aerosurface. This information may become corrupted when you combine aero-surfaces together. Figure 2.5.3 shows a typical aerosurface (k) rotating about a hinge vector. A positive deflection $(+\delta_s)$ is defined to be a clockwise rotation of the panel about its hinge vector. The orientation of the hinge vector with respect to the vehicle axes is defined in terms of two angles:

1. The back-sweep angle $\lambda_{hs}(k)$ which is the angle between the hinge vector and the y-z plane that slices the vehicle perpendicular to the x axis. In most airplanes the hinge line is perpendicular to the vehicle x axis and $\lambda_{hs}=0°$, or it may be slightly positive. It would be negative on a forward-sweep aircraft.
2. The aerosurface bank angle $\phi_{hs}(k)$ is defined between the projection line OP of the hinge line on the y-z plane and the vehicle x-y plane. For example, a left elevator or flap has $\phi_{hs}=0°$, a right elevator has $\phi_{hs}=180°$, and a rudder has $\phi_{hs}=90°$.
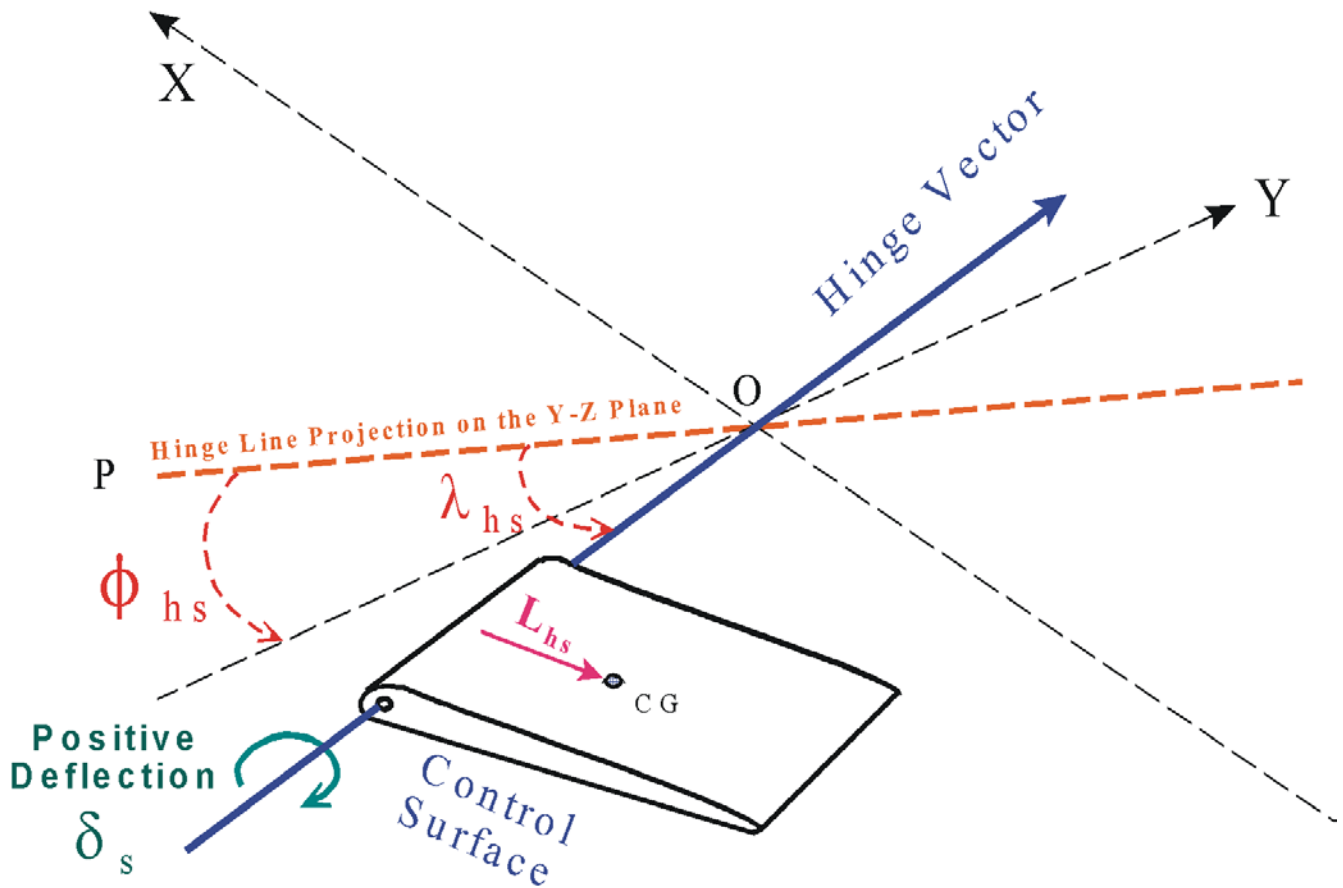

Figure (2.5.3) Definition of the Hinge Vector Orientation Angles

30

Other aerosurface parameters that may be necessary to define in addition to the hinge vector orientation angles are: the mid-point location of the hinge in vehicle coordinates, and the mass properties of each aerosurface such as: mass, moment of inertia about the hinge, and the distance (L_{hs}) between the hinge and surface CG. They are needed for the calculation of the TWD forces. Each individual rotating panel must be defined as a separate aerosurface and not as a combination of aerosurfaces, unless the TWD, load-torque feedback, and flexibility are not included, in which case it does not matter if surfaces are combined. The inputs to the flight vehicle dynamic model are control surface deflections in (radians), rates and accelerations for each individual rotating panel as already mentioned. They come from the corresponding actuator model. The transformation from roll, pitch, and yaw flight control demands to the individual aerosurface deflections is defined by the mixing-logic matrix that connects between the flight control system output and the actuator inputs. The derivation of the mixing logic matrix is discussed in Section 5.

Figure 2.5.4 is an example of a vehicle that has five control surfaces: a body-flap, two flaps, and two rudders that form a V-tail. The hinge vectors of the body-flap and the two flaps are pointing in the y direction. The hinge lines of the two flaps are slightly tilted from the y axis because the wing has a small dihedral. The aerosurface bank angle (φ_{hs}) is measured between the hinge vector and the vehicle x-y plane. The left flap has a small bank angle ($\varphi_{hs}=+2°$) and the right flap has an angle ($\varphi_{hs}=-2°$). The flaps have a small back-sweep angle ($\lambda_{hs}=5°$). The two rudders are tilted more, forming a 45º V-tail. The hinge vector of the left rudder is pointing towards the vehicle and has a bank angle ($\varphi_{hs}=+45°$) relative to the (x-y) plane. The hinge vector of the right rudder is pointing away from the vehicle and has a ($\varphi_{hs}=135°$ or $-45°$). Both rudders have a positive back-sweep angle ($\lambda_{hs}=10°$).

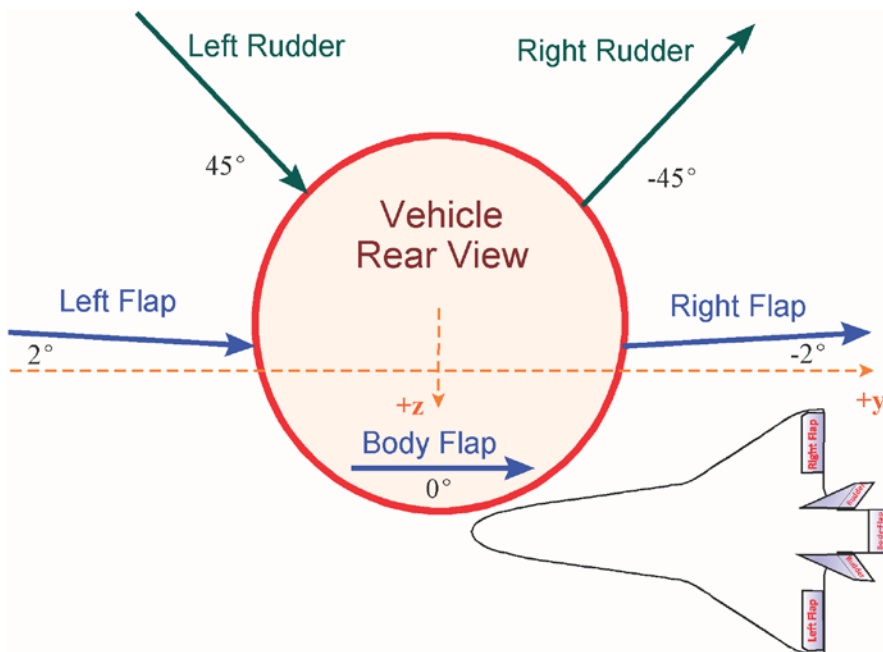

Figure (2.5.4) Directions of hinge lines on a Lifting-Body aircraft showing the angles (ϕ_{hs}) in the vehicle y-z plane

Equation 2.5.5 calculates force variations at the hinge of the kth aero-surface, along the vehicle x, y, and z axes, as a function of aerosurface deflection, deflection rate, and angular acceleration. It consists of three terms:

1. An aerodynamics force term that calculates the aero force increments along x, y, and z, as a function of aerosurface deflection (δ_s) and the aerosurface coefficients which are functions of: Mach, alpha, and beta.
2. An aerodynamic damping term that calculates the damping force as a function of the damping coefficients and the aerosurface rate ($\dot{\delta}_s$). The damping coefficients are usually functions of: Mach and alpha.
3. A reaction "tail-wags-dog" force term that is generated by the angular acceleration of the control surface and the structural deformation at the hinge.

$$F_{Xcs}(k) = -\overline{Q}S_{ref}\left[C_{A\delta(k)}\,\delta_{s(k)} + \left(\frac{\overline{c}_{sk}}{2V_0}\right)C_{A\dot{\delta}(k)}\,\dot{\delta}_{s(k)} \right] + F_{XS_{TWD}}(k)$$

$$F_{Ycs}(k) = \overline{Q}S_{ref}\left[C_{Y\delta(k)}\,\delta_{s(k)} + \left(\frac{\overline{c}_{sk}}{2V_0}\right)C_{Y\dot{\delta}(k)}\,\dot{\delta}_{s(k)} \right] + F_{YS_{TWD}}(k)$$

$$F_{Zcs}(k) = \overline{Q}S_{ref}\left[C_{Z\delta(k)}\,\delta_{s(k)} + \left(\frac{\overline{c}_{sk}}{2V_0}\right)C_{Z\dot{\delta}(k)}\,\dot{\delta}_{s(k)} \right] + F_{ZS_{TWD}}(k)$$

$$where: F_{XS_{TWD}}(k), etc.\ are\ the\ TWD\ forces$$

$$F_{XS_{TWD}}(k) = -m_{sk}\,L_{hs(k)}\cos\lambda_{hs(k)}\sin\Delta_{s(k)}\,\ddot{\delta}_{s(k)}$$

$$F_{YS_{TWD}}(k) = +m_{sk}\,L_{hs(k)}\sin\phi_{hs(k)}\,\ddot{\delta}_{s(k)}$$

$$F_{ZS_{TWD}}(k) = -m_{sk}\,L_{hs(k)}\cos\phi_{hs(k)}\cos\Delta_{s(k)}\,\ddot{\delta}_{s(k)}$$

Equation 2.5.5 Forces on the Vehicle due to a Control Surface (k)

L_{hs} is the moment arm distance between the hinge line and the control surface CG $\{L_{hs} = X_{hinge} - X_{cscg}\}$. It is positive when the surface cg is behind the hinge.

$\delta_s(k)$ is a small deflection angle in (radians) of the control surface (k) about its hinge vector, measured from its nominal trim angle.

$\Delta_s(k)$ is the nominal trim position angle of the control surface (k) about its hinge line. It is defined in the input data in (deg).

C_{Ydk}, C_{Zdk} are the aero force increments due to surface deflection, defined in (1/deg)

c_{sk} is the aero chord of surface (k), (part of the aero data)

m_{sk} is the mass of surface (k) in (slugs)

In Equation 2.5.5 the surface acceleration inputs $\ddot{\delta}_{s\,(k)}$ excite the TWD forces at the surface hinges. The surface acceleration, however, should also include the rotational acceleration at the hinge caused by the deformation of the structure at the hinge, as shown for the deflection in Equation 2.5.6. However, when the inertial coupling coefficients are included in the model the cross-coupling between surface flexing and structure excitation is captured by the h-parameters in the finite-elements-model and the surface acceleration inputs $\ddot{\delta}_{s\,(k)}$ in this case should only include hinge acceleration due to the actuator alone without the structural deformation term.

In the absence of the inertial coupling coefficients, on the other hand, the flexibility at the surfaces is approximated by assuming that the surfaces themselves are rigid, but the hinges where they are attached to have rotational stiffness. In this case, the total surface rotation consists of the rigid deflection due to the relative motion at the hinge plus the deformation of the supporting structure at the hinge. In this case, the surface acceleration about the hinge vector input $\ddot{\delta}_{s\,(k)}$ in equation 2.5.5 must be $\ddot{\delta}_{fs\,(k)}$ which includes the structural deformation term as shown in equation 2.5.6. Similarly, the deflection rates and accelerations at the control surfaces are calculated as a function of modal rates and accelerations, as in equation 2.5.6. The slope σ_{hs} at the hinge is determined by the orientation of the control surface hinge vector with respect to the vehicle axes, which is defined by the angles (ϕ_h and λ_h).

$$\delta_{fs}(k) = \delta_s(k) + \sum_{j=1}^{N\,\mathrm{mod}} \sigma_{hs}(k,j)\eta(j) \qquad where:$$

$$\sigma_{hs}(k) = \left(\sigma_{Ys}(k)\cos\phi_{h(k)} + \sigma_{Zs}(k)\sin\phi_{h(k)}\right)\cos\lambda_{h(k)} + \sigma_{Xs}(k)\sin\lambda_{h(k)}$$

Equation 2.5.6 Total Aero-Surface Deflection at a Hinge (k)

$\sigma_{hs}(k,j)$ is the modal slope for mode (j) at the kth hinge line, resolved about the hinge vector as shown in Figure 2.5.3.

Aerodynamic Moments

Equations 2.5.7 calculate the variations in the base vehicle aerodynamic moments about roll, pitch, and yaw, as a result of variations in the angles of attack and sideslip (α_w, β_w), variations in velocity (δV_w), altitude (δh), vehicle rates (p, q, r), and aerosurface deflections (δ_{si}). Notice that the changes in the angles of attack and sideslip and also in velocity include the effects due to the wind-gust as it is described in section 2.9.

The terms ($\Sigma L_{xs(k)}$, $\Sigma M_{ys(k)}$, and $\Sigma N_{zs(k)}$) are the combined moments on the vehicle generated by the deflections of N_{surf} control surfaces, (k=1,N_{surf}). The moments due to a single control surface are shown in equation 2.5.8. The aerodynamic coupling coefficients $C_{l\alpha}$, $C_{m\beta}$, and $C_{n\alpha}$ are zero when the vehicle is aerodynamically symmetric. They become significant when the vehicle loses symmetry, which increases the dynamic coupling between pitch and lateral. The coefficients $C_{l\eta j}$, $C_{m\eta j}$, $C_{n\eta j}$ are aero-elastic moment derivatives. They define variations in vehicle moments due to the excitation of a structural mode (η_j). For example, the flexing of a wing mode causes oscillatory moments on the vehicle. The aero-elastic coefficients are obtained by combining fluid aerodynamic models with finite element models, and it will be discussed in section 2.7.

$$L_{Xaero} = \overline{Q} S_{ref} l_{sp} \left(\begin{array}{l} C_{l\alpha}\alpha_w + C_{l\beta}\beta_w + \dfrac{l_{sp}}{2V_0}\left(C_{lp}\,p + C_{lr}\,r + C_{l\dot{\beta}}\,\dot{\beta}_w\right) + \left(\dfrac{2C_{l0}}{V_0}\right)\delta V_w \\[2ex] + \sum\limits_{j=1}^{N\,\mathrm{mod}}\left(C_{l\eta_j}\eta_j + \dfrac{C_{l\dot{\eta}_j}}{V_0}\dot{\eta}_j\right) + C_{l0}\left(\dfrac{V_0^2}{2\overline{Q}}\right)\dfrac{\partial\rho}{\partial h}\delta h \end{array} \right) + \sum\limits_{k=1}^{Nsurf} L_{Xs}(k)$$

$$M_{Yaero} = \overline{Q} S_{ref} l_{ch} \left(\begin{array}{l} C_{m\alpha}\alpha_w + C_{m\beta}\beta_w + \dfrac{l_{ch}}{2V_0}\left(C_{mq}\,q + C_{m\dot{\alpha}}\,\dot{\alpha}_w\right) + \left(\dfrac{2C_{m0}}{V_0} + \dfrac{\partial C_m}{\partial V}\right)\delta V_w \\[2ex] + \sum\limits_{j=1}^{N\,\mathrm{mod}}\left(C_{m\eta_j}\eta_j + \dfrac{C_{m\dot{\eta}_j}}{V_0}\dot{\eta}_j\right) + \left(\dfrac{\partial C_m}{\partial h} + C_{m0}\left(\dfrac{V_0^2}{2\overline{Q}}\right)\dfrac{\partial\rho}{\partial h}\right)\delta h \end{array} \right) + \sum\limits_{k=1}^{Nsurf} M_{Ys}(k)$$

$$N_{Zaero} = \overline{Q} S_{ref} l_{sp} \left(\begin{array}{l} C_{n\alpha}\alpha_w + C_{n\beta}\beta_w + \dfrac{l_{sp}}{2V_0}\left(C_{np}\,p + C_{nr}\,r + C_{n\dot{\beta}}\,\dot{\beta}_w\right) + \left(\dfrac{2C_{n0}}{V_0}\right)\delta V_w \\[2ex] + \sum\limits_{j=1}^{N\,\mathrm{mod}}\left(C_{n\eta_j}\eta_j + \dfrac{C_{n\dot{\eta}_j}}{V_0}\dot{\eta}_j\right) + C_{n0}\left(\dfrac{V_0^2}{2\overline{Q}}\right)\dfrac{\partial\rho}{\partial h}\delta h \end{array} \right) + \sum\limits_{k=1}^{Nsurf} N_{Zs}(k)$$

Equation 2.5.7 Aerodynamic Moment Variations in Roll, Pitch, and Yaw

$\overline{Q}$ S_{ref}	is the dynamic pressure in (lb/ft^2), and reference area in (ft^2).
$C_{l\beta}$, $C_{m\alpha}$, $C_{n\beta}$	are the aerodynamic moment derivatives due to the angles of attack and sideslip, in (1/deg).
$C_{l\delta i}$, $C_{m\delta i}$, $C_{n\delta i}$	are the aerodynamic derivatives for the control aero-surfaces (δ_{si} where i=1,.. N_{surf}) in (1/deg).
l_{sp} and l_{ch}	are the wing span and mean aerodynamic chord respectively in (feet).
L_{xs} M_{ys} $N_{zs}(k)$	are the moments about x, y, and z axes generated by the control surface (k) deflections (δ_{sk}).

Vehicle Moments due to Control Surface Deflections

Equations 2.5.8 calculate the roll, pitch, and yaw variations in vehicle moments generated by the deflection $\delta_{s(k)}$ of a control surface (k) from trim position $\Delta_{s(k)}$. The orientation of the control surface hinge line is with respect to the vehicle axes is defined by the angles $\varphi_{hs(k)}$ and $\lambda_{hs(k)}$, as shown in Figure 2.5.3. The aerosurface coefficients $C_{l\delta(k)}$, $C_{m\delta(k)}$, etc. are the aerodynamic moment increments that generate the aero moment variations due to surface deflection δ_{sk} from trim. They are functions of Mach, α, and β, for each panel, and are generated from wind tunnel or CFD models. They are originally calculated relative to a fixed moment reference center (MRC) point, and they must be transformed from the MRC to the vehicle CG using equation 2.5.10. The equations also include aerodynamic damping terms that calculate the damping moment as a function of damping coefficients and the aerosurface rate $\dot{\delta}_s$. The damping coefficients are usually functions of: Mach and alpha. The equations also include tail-wag-dog terms due to the TWD forces from equation 2.5.5 and due to aerosurface angular accelerations. There are also terms due to coupling of the vehicle acceleration with the normal and lateral displacements of the aerosurface center of mass.

$$L_{Xs}(k) = \overline{Q}\, S_{ref}\, l_{sp} \left[C_{l\delta(k)}\, \delta_{s(k)} + \left(\frac{\overline{c}_{sk}}{2V_0} \right) C_{l\dot{\delta}(k)}\, \dot{\delta}_{s(k)} \right] + F_{ZS_{TWD}(k)} l_{Ysk} - F_{YS_{TWD}(k)} l_{Zsk}$$

$$M_{Ys}(k) = \overline{Q}\, S_{ref}\, l_{ch} \left[C_{m\delta(k)}\, \delta_{s(k)} + \left(\frac{\overline{c}_{sk}}{2V_0} \right) C_{m\dot{\delta}(k)}\, \dot{\delta}_{s(k)} \right] + F_{XS_{TWD}(k)} l_{Zsk} - F_{ZS_{TWD}(k)} l_{Xsk}$$

$$\qquad - I_{hs(k)} \cos\phi_{h(k)}\, \ddot{\delta}_{s(k)} + m_{sk}\left(A_Z d_{Xsk} - A_X d_{Zsk} \right)$$

$$N_{Zs}(k) = \overline{Q}\, S_{ref}\, l_{sp} \left[C_{n\delta(k)}\, \delta_{s(k)} + \left(\frac{\overline{c}_{sk}}{2V_0} \right) C_{n\dot{\delta}(k)}\, \dot{\delta}_{s(k)} \right] + F_{YS_{TWD}(k)} l_{Xsk} - F_{XS_{TWD}(k)} l_{Ysk}$$

$$\qquad - I_{hs(k)} \sin\phi_{h(k)}\, \ddot{\delta}_{s(k)} + m_{sk} A_X d_{Ysk}$$

$$where: l_{Xsk} = X_{sk} - X_{CG} \qquad l_{Ysk} = Y_{sk} - Y_{CG} \qquad l_{Zsk} = Z_{sk} - Z_{CG}$$

Equation 2.5.8 Vehicle Moments (roll, pitch, yaw due to Control Surface (k) deflections

Equations 2.5.9 calculate the displacements d_{Xsk}, d_{Ysk}, d_{Zsk} along x, y, and z of the aero surface center of mass and they have two components: a component due to surface rotation δ_s, and a component due to structural deformation at the hinge (η). When the displacements couple with the vehicle A_X and A_Z accelerations they create additional moments on the vehicle. The moment arm l_{Xsk} of a control surface (k) is the distances between the middle point of its hinge line and the vehicle CG.

$$d_{Zsk} = L_{hs(k)} \cos\Delta_s \cos\phi_{h(k)}\, \delta_{s(k)} + \sum_{j=1}^{N\,\mathrm{mod}} \phi_{Zs}(k,j)\eta(j)$$

$$d_{Ysk} = -L_{hs(k)} \cos\Delta_s \sin\phi_{h(k)}\, \delta_{s(k)} + \sum_{j=1}^{N\,\mathrm{mod}} \phi_{Ys}(k,j)\eta(j)$$

$$d_{Xsk} = L_{hs(k)} \sin\Delta_s \cos\lambda_{h(k)}\, \delta_{s(k)} + \sum_{j=1}^{N\,\mathrm{mod}} \phi_{Xs}(k,j)\eta(j)$$

(2.5.9)

$C_{mh\delta(k)}$, $C_{nh\delta(k)}$ are the aerodynamic moment derivatives for the control aero-surfaces (δ_{sk} where k=1,.. N_{surf}) in (1/deg). They are obtained with respect to the MRC and transformed by the program from the MRC to the vehicle CG.

F_{YStwd}, F_{ZStwd} are the tail-wag-dog forces at the hinges of the control surfaces as shown in equation (2.5.5)

$m_{s(k)}$ & $I_{hs(k)}$ are the mass and the Moment of Inertia of Surface (k) about its hinge

Δ_s is the surface trim position with respect to the vehicle x-axis

In equation 2.5.8, the total moment variations generated by a control surface, in addition to the aero moments, it includes also moments created by the TWD forces from Equation (2.5.5) due to the surface accelerations. Notice, that when the inertial coupling coefficients (h_s) of the control surfaces are not available, we assume that surface panels are rigid and they are attached on a flexible hinge, and the structure is excited by the TWD forces generated by the surface inertial accelerations, which

include rotation at the hinge plus deformation of the hinge structure, defined as $\ddot{\delta}_{fs(k)}$ in Equation 2.5.6. However, when the inertial coupling coefficients are included in the flex modes and in the hinge moment equations, only the surface acceleration $\ddot{\delta}_{s(k)}$ relative to the hinge should be used from Equation 2.5.6 and not the flex component, because the flex coupling effect is introduced via the h-parameters.

Transforming the Aerodynamic Moment Coefficients

The aerodynamic moment coefficients C_L, C_M, and C_N, and their derivatives with respect to (α, β, p, q, r, η, etc) in Equations (2.5.7) and (2.5.8) are assumed to be defined about the vehicle center of mass. However, they are originally calculated relative to a fixed location on the vehicle, called the Moments Reference Center (MRC). This is because the CG usually varies during flight and the aero moment coefficients, therefore, must be transformed from the MRC to the vehicle CG before they can be used in the equations of motion. Flixan automatically performs this transformation using the input data. The location of the MRC (X_{MRC}, Y_{MRC}, Z_{MRC}) with respect to the vehicle coordinates is defined in the aerodynamic data. The following equations are used to transform the aero moment coefficients and the derivatives from the MRC to the vehicle center of mass, where (X_{CG}, Y_{CG}, Z_{CG}) are the CG coordinates.

$$C_{L_{CG}} = C_{L_{MRC}} + C_Y \frac{Z_{CG} - Z_{MRC}}{l_{sp}} - C_Z \frac{Y_{CG} - Y_{MRC}}{l_{sp}}$$

$$C_{M_{CG}} = C_{M_{MRC}} + C_Z \frac{X_{CG} - X_{MRC}}{l_{ch}} + C_A \frac{Z_{CG} - Z_{MRC}}{l_{ch}}$$

$$C_{N_{CG}} = C_{N_{MRC}} - C_Y \frac{X_{CG} - X_{MRC}}{l_{sp}} - C_A \frac{Y_{CG} - Y_{MRC}}{l_{sp}}$$

Equation 2.5.10 Aero Moment Transformation Equations from MRC to CG
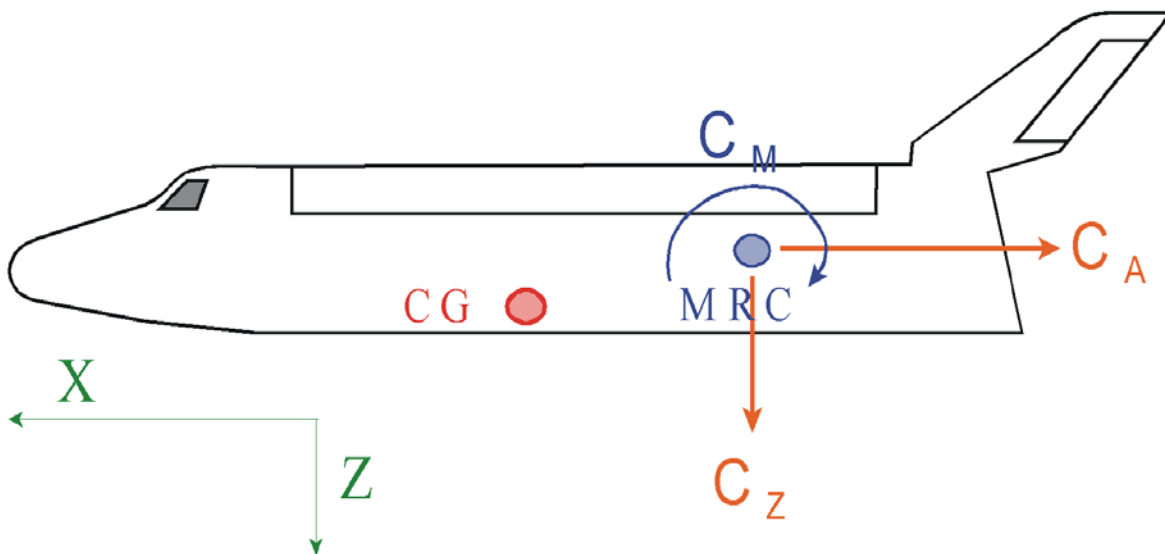

Figure 1.5.11 Pitch Moment Transformation from MRC to CG

The following flight vehicle (mainly aircraft) performance parameters are included for reference.

- The aerodynamic center (AC) is the point on the vehicle about which the pitching moment coefficient remains unchanged, that is, the partial of C_M with respect to (á) becomes zero.

$$X_{AC} = X_{MRC} - \frac{C_{m\alpha}(MRC)}{C_{Z\alpha}} l_{ch}$$

- The Center of Pressure (CP) is the point where the total aerodynamic force acts on the vehicle, that is, the point where the moments balance.

$$X_{CP} = X_{MRC} - \frac{C_M(MRC)}{C_Z} l_{ch}$$

- The Static Margin (SM) in terms of percentage body length is defined as:

$$SM = \frac{X_{CG} - X_{AC}}{Body\_Length} 100$$

Definition of the Aero Coefficients

The coefficients $C_{z\alpha}$ and $C_{y\beta}$ are the aerodynamic force derivatives in units of (1/deg). They are used to calculate changes in aerodynamic forces due to small variations in the angles of attack and sideslip. The coefficients $C_{z\delta si}$ and $C_{y\delta si}$ are aerodynamic force increments in units of (1/deg) and they calculate changes in aerodynamic forces due to small deflections of the control surfaces. The aero derivative coefficients are defined in units (1/deg) but they are converted internally by the program into units (1/rad) because alpha, beta and the surface deflections are calculated in radians. The axial force coefficients C_{Au} and $C_{A\alpha}$ calculate the force variation along the x axis due to changes in the velocity along the x axis and the angle of attack respectively. They are defined as positive along the negative vehicle x axis because they generate drag forces on the vehicle. The cross coupling coefficients $C_{Z\beta}$, $C_{Y\alpha}$ and $C_{A\beta}$ are usually very small and in most cases they can be set to zero.

Force Derivatives: The force derivatives $C_{A\alpha}$, $C_{Z\alpha}$, and $C_{Y\beta}$ define variations in vehicle forces along the -x, z and y axes respectively due to small changes of angle of attack and sideslip in (radians). They are defined as follows

$$\frac{\partial F_Z}{\partial \alpha} = \overline{Q} S_r C_{Z\alpha} \qquad\qquad \frac{\partial F_Y}{\partial \beta} = \overline{Q} S_r C_{Y\beta} \qquad\qquad etc.$$

Moment Derivatives: The moment derivatives $C_{m\alpha}$, $C_{n\beta}$, $C_{l\beta}$, etc. define variations in roll, pitch, and yaw vehicle moments due to small changes of angle of attack or sideslip in. They are defined by the following equations

$$\frac{\partial M_Y}{\partial \alpha} = \overline{Q} S_r l_{ch} C_{m\alpha} \qquad\qquad \frac{\partial L_X}{\partial \beta} = \overline{Q} S_r l_{sp} C_{l\beta} \qquad\qquad etc.$$

Force Rate Derivatives: The force rate derivatives C_{Zq}, C_{Yr}, C_{Yp}, etc, define force variations along the z and y axes due to variations in the vehicle body rates p, q, r in (radians/sec). They are defined as follows

$$\frac{\partial F_Z}{\partial q} = \left(\frac{\overline{Q} S_r l_{ch}}{2V_0} \right) C_{Zq} \qquad\qquad \frac{\partial F_Y}{\partial p} = \left(\frac{\overline{Q} S_r l_{sp}}{2V_0} \right) C_{Yp}$$

Moment Rate Derivatives: The moment rate derivatives C_{mq}, C_{nr}, C_{lp}, etc, define variations in roll, pitch, and yaw vehicle moments due to variations in vehicle body rates p, q, r in (radians/sec). They are defined as follows

$$\frac{\partial M_Y}{\partial q} = \left(\frac{\overline{Q} S_r l_{ch}^2}{2V_0} \right) C_{mq} \qquad\qquad \frac{\partial N_Z}{\partial r} = \left(\frac{\overline{Q} S_r l_{sp}^2}{2V_0} \right) C_{nr}$$

Velocity Derivatives: The velocity derivatives C_{Av}, and C_{Zv}, etc, define the change in vehicle force along the negative x axis, and along the z axis respectively due to changes in vehicle velocity in (feet/sec). They are defined as follows

$$\frac{\partial F_X}{\partial V} = -\left(\frac{\overline{Q} S_r}{V_0} \right) C_{AV} \qquad\qquad \frac{\partial F_Z}{\partial V} = \left(\frac{\overline{Q} S_r}{V_0} \right) C_{ZV}$$

Steady state Force and Moment Coefficients: The coefficients C_{mo}, C_{Ao}, and C_{Zo}, etc, are not derivatives. They are aerodynamic force and moment coefficients at the trim condition. They are dimension-less, functions of (a, b, and Mach) and they define the nominal forces (F_{X0}, F_{Z0}) and moments (M_{y0}, N_{z0}) on the vehicle (not variations), at the trim condition. They are defined by the following equations

$$M_{Yo} = \overline{Q} S_r l_{ch} C_{mo} \qquad L_{Xo} = \overline{Q} S_r l_{sp} C_{lo} \qquad F_{Xo} = -\overline{Q} S_r C_{Ao} \qquad F_{Zo} = \overline{Q} S_r C_{Zo}$$

Variations in Dynamic Pressure due to δV and δh: The change in dynamic pressure due to changes in vehicle velocity (δV), and the change in dynamic pressure due to changes in altitude (δh) can be obtained from the following equations, where h_0 is the vehicle altitude and b_0 is constant.

$$\frac{\partial \overline{Q}}{\partial V} = \rho_o V_0 e^{-b_o h_o} \qquad\qquad \frac{\partial \overline{Q}}{\partial h} = \rho_o \left(\frac{b_o V_0^2}{2} \right) e^{-b_o h_o}$$

Velocity Derivatives: The velocity derivatives define the effect of velocity variations (δV) on the vehicle forces and moments. They are used in equations (**x**) and are defined as follows:

$$\frac{\partial F_X}{\partial V} = -\overline{Q} S_r \left(\frac{2}{V_0} \right) (C_{AV} + C_{Ao}) \qquad where \qquad C_{AV} = \frac{V_0}{2} \left(\frac{\partial C_A}{\partial V} \right)$$

$$\frac{\partial F_Z}{\partial V} = \overline{Q} S_r \left(\frac{2}{V_0} \right) (C_{ZV} + C_{Zo}) \qquad where \qquad C_{ZV} = \frac{V_0}{2} \left(\frac{\partial C_Z}{\partial V} \right)$$

$$\frac{\partial F_Y}{\partial V} = \overline{Q} S_r \left(\frac{2}{V_0} \right) C_{Yo}$$

$$\frac{\partial M_y}{\partial V} = \overline{Q} S_r l_{ch} \left(\frac{2}{V_0} \right) (C_{mV} + C_{mo}) \qquad where \qquad C_{mV} = \frac{V_0}{2} \left(\frac{\partial C_m}{\partial V} \right)$$

Altitude Derivatives: They define the effects of altitude variations from nominal on the vehicle forces and moments.

$$\frac{\partial F_X}{\partial h} = -\overline{Q}S_r\left(\frac{\partial C_A}{\partial h} + \frac{\partial \rho}{\partial h}\left(\frac{V_0^2}{2\overline{Q}}\right)C_{A0}\right) \qquad \frac{\partial F_Z}{\partial h} = \overline{Q}S_r\left(\frac{\partial C_Z}{\partial h} + \frac{\partial \rho}{\partial h}\left(\frac{V_0^2}{2\overline{Q}}\right)C_{Z0}\right) \qquad \frac{\partial F_Y}{\partial h} = \overline{Q}S_r\frac{\partial \rho}{\partial h}\left(\frac{V_0^2}{2\overline{Q}}\right)C_{Y0}$$

$$\frac{\partial M_y}{\partial h} = \overline{Q}S_r l_{ch}\left(\frac{\partial C_m}{\partial h} + \frac{\partial \rho}{\partial h}\left(\frac{V_0^2}{2\overline{Q}}\right)C_{m0}\right) \qquad \frac{\partial N_z}{\partial h} = \overline{Q}S_r l_{sp}\left(\frac{\partial \rho}{\partial h}\left(\frac{V_0^2}{2\overline{Q}}\right)C_{n0}\right)$$

Angle of Attack Rate Derivatives: The derivatives $C_{Z\alpha\_dot}$, $C_{Y\beta\_dot}$, $C_{m\alpha\_dot}$ define the changes in vehicle forces and moments due to variations in the rates of the angles of attack and sideslip. They are used in the force and moment equations (2.5.4 and 2.5.7), and are defined as follows:

$$\frac{\partial F_Z}{\partial \dot{\alpha}} = \overline{Q}\,S_r\left(\frac{l_{ch}}{2V_0}\right)C_{Z\dot{\alpha}} \qquad\qquad \frac{\partial M_y}{\partial \dot{\alpha}} = \overline{Q}\,S_r\,l_{ch}\left(\frac{l_{ch}}{2V_0}\right)C_{m\dot{\alpha}}$$

Generalized Aero Force and Moment Derivatives (GAFD): The aero-elastic coefficients are not always available. They are included only when the aero/ flex coupling is significant. They are defined by the following equations. The generalized aero moment derivatives ($C_{l\eta j}$ $C_{m\eta j}$ $C_{n\eta j}$) define the change in vehicle roll, pitch and yaw moments due to variations in the generalized modal displacement $\eta(j)$ of mode (j). Similarly, the generalized aero moment derivatives ($C_{l\eta j\_dot}$ $C_{m\eta j\_dot}$ $C_{n\eta j\_dot}$) define the change in vehicle roll, pitch and yaw moments due to variations of the generalized modal rates of a mode (j). Where l_{ch} and l_{sp} are the vehicle mean aero chord and span reference lengths, and S_{ref} is the vehicle reference area.

$$\frac{\partial M_y}{\partial \eta_{(j)}} = \overline{Q}\,S_r\,l_{ch}\,C_{m\eta(j)} \qquad\qquad \frac{\partial M_y}{\partial \dot{\eta}_{(j)}} = \overline{Q}\,S_r\,l_{ch}\left(\frac{C_{m\dot{\eta}(j)}}{V_0}\right)$$

$$\frac{\partial N_z}{\partial \eta_{(j)}} = \overline{Q}\,S_r\,l_{sp}\,C_{n\eta(j)} \qquad\qquad \frac{\partial N_z}{\partial \dot{\eta}_{(j)}} = \overline{Q}\,S_r\,l_{sp}\left(\frac{C_{n\dot{\eta}(j)}}{V_0}\right)$$

The generalized aero force derivatives define also the variations in vehicle forces along the y and z axes due to variations in the modal displacement $\eta(j)$ and also the displacement rate $\eta(j)_{dot}$ of mode (j).

$$\frac{\partial F_Y}{\partial \eta_{(j)}} = \overline{Q}\,S_r\,C_{Y\eta(j)} \qquad\qquad \frac{\partial F_Y}{\partial \dot{\eta}_{(j)}} = \overline{Q}\,S_r\left(\frac{C_{Y\dot{\eta}(j)}}{V_0}\right)$$

$$\frac{\partial F_Z}{\partial \eta_{(j)}} = \overline{Q}\,S_r\,C_{Z\eta(j)} \qquad\qquad \frac{\partial F_Z}{\partial \dot{\eta}_{(j)}} = \overline{Q}\,S_r\left(\frac{C_{Z\dot{\eta}(j)}}{V_0}\right)$$

The GAFD derivatives ($C_{\eta j \alpha}$ $C_{\eta j \beta}$ $C_{\eta j p}$ $C_{\eta j q}$ $C_{\eta j \delta s}$ etc.) define the amount of modal excitation $\eta(j)$ of a mode (j) caused by the variations in (α, β, p, q, r, δ_s) etc, and also their rates. The reference length (l_{chg}) is used to normalize the data, and it may not be the same as the vehicle reference length (l_{ch}).

$$\frac{\partial \eta_j}{\partial \alpha} = \overline{Q} S_{ref} C_{\eta j \alpha} \qquad \frac{\partial \eta_j}{\partial \delta_{sk}} = \overline{Q} S_{ref} C_{\eta_j \delta_{sk}}$$

$$\frac{\partial \eta_j}{\partial \dot{\alpha}} = \overline{Q} S_{ref} \left(\frac{l_{chg}}{2V_0}\right) C_{\eta j \dot{\alpha}} \qquad \frac{\partial \eta_j}{\partial \dot{\delta}_{sk}} = \overline{Q} S_{ref} \left(\frac{\overline{c}_k}{2V_0}\right) C_{\eta_j \dot{\delta}_{sk}}$$

$$\frac{\partial \eta_j}{\partial p} = \overline{Q} S_{ref} \left(\frac{l_{chg}}{2V_0}\right) C_{\eta j p} \qquad \frac{\partial \eta_j}{\partial q} = \overline{Q} S_{ref} \left(\frac{l_{chg}}{2V_0}\right) C_{\eta j q}$$

$$\frac{\partial \eta_j}{\partial \dot{p}} = \overline{Q} S_{ref} \left(\frac{l_{chg}}{2V_0}\right)^2 C_{\eta j \dot{p}} \qquad \frac{\partial \eta_j}{\partial \dot{q}} = \overline{Q} S_{ref} \left(\frac{l_{chg}}{2V_0}\right)^2 C_{\eta j \dot{q}}$$

$$\frac{\partial \eta_j}{\partial \eta_i} = \overline{Q} S_{ref} C_{\eta_j \eta_i} \qquad \frac{\partial \eta_j}{\partial \dot{\eta}_i} = \overline{Q} S_{ref} \left(\frac{1}{V_0}\right) C_{\eta_j \dot{\eta}_i}$$

The hinge moment derivatives { $C_{h\alpha(k)}$ $C_{h\beta(k)}$ $C_{hq(k)}$ $C_{hp(k)}$ $C_{hr(k)}$ } define how the moments (HM_k) at the hinge of a control surface (k) vary as a result of variations in vehicle states: (α, β, q, p, r) and the derivatives of these states. The hinge moment derivatives $C_{h\delta(k,i)}$ define how the moments at the hinge of a control surface (k) vary as a result of surface (i) deflections (δ_{si}), and the hinge moment derivatives $C_{h\eta(k,j)}$ define how the moments at the hinge vary as a result of mode (j) generalized displacement (η_j). Similarly for the rates of surface deflections and modal displacements. The parameters (c_k) and (s_k) are the chord reference length and the surface area respectively for each control surface (k). The hinge moments are defined as follows:

$$\frac{\partial HM_k}{\partial \alpha} = \overline{Q} s_k \overline{c}_k C_{h\alpha (k)} \qquad \frac{\partial HM_k}{\partial \dot{\alpha}} = \overline{Q} s_k \overline{c}_k \left(\frac{l_{ch}}{2V_0}\right) C_{h\dot{\alpha} (k)}$$

$$\frac{\partial HM_k}{\partial q} = \overline{Q} s_k \overline{c}_k \left(\frac{l_{ch}}{2V_0}\right) C_{hq (k)} \qquad \frac{\partial HM_k}{\partial \dot{q}} = \overline{Q} s_k \overline{c}_k \left(\frac{l_{ch}}{2V_0}\right)^2 C_{h\dot{q} (k)}$$

$$\frac{\partial HM_k}{\partial \delta_{si}} = \overline{Q} s_k \overline{c}_k C_{h\delta (k,i)} \qquad \frac{\partial HM_k}{\partial \dot{\delta}_{si}} = \overline{Q} s_k \overline{c}_k \left(\frac{\overline{c}_i}{2V_0}\right) C_{h\dot{\delta} (k,i)}$$

$$\frac{\partial HM_k}{\partial \eta_j} = \overline{Q} s_k \overline{c}_k C_{h\eta (k, j)} \qquad \frac{\partial HM_k}{\partial \dot{\eta}_j} = \overline{Q} s_k \overline{c}_k \left(\frac{1}{V_0}\right) C_{h\dot{\eta} (k, j)}$$

2.6 Propellant Sloshing

Propellant tanks in flight vehicles experience disturbance forces due to sloshing. Sloshing is defined to be the periodic motion of the free surface of a liquid in a partially filled container. In launch vehicles or spacecraft, sloshing can be excited by vehicle motion as a result of control system commands or from fluctuations in vehicle acceleration produced by thrust variations, jet firings, or gust disturbances. If the liquid is allowed to slosh freely, the uncontrolled oscillations can produce disturbance forces that cause additional accelerations on the vehicle. These accelerations are then sensed and responded to by the flight control system, forming a closed-loop that can lead to an oscillatory instability. A slosh-induced instability may lead to a structural failure, premature engine shutdown, or inability of the spacecraft to achieve upper-stage engine start through loss of propellant head at the drain port, loss of propellant through the vent system, and even loss of the vehicle itself. Even in a low or near zero-gravity environment, where the slosh frequencies and the torques exerted are low, instability can occur, due to coupling with the RCS or TVC, and the liquid motion can build up to amplitudes that may damage the vehicle. In general, the slosh frequencies should be greater than the control system bandwidth and below the fundamental bending mode frequency.

When a vehicle is accelerating the motion of the liquid fuel inside the tank can be approximated with a spring mass analogy model. We may assume that the propellant can be separated in two parts: (a) a solid mass that does not move relative to the tank and it is located near the bottom of the tank, and (b) a sloshing mass portion that oscillates slightly below the surface and its motion is perpendicular to the acceleration A_T, and the oscillations are excited by the vehicle lateral motion. The solid propellant weight is rigidly attached to the vehicle mass properties at a fixed point in the tank centerline located at the center of the non-sloshing propellant mass. This point mass is included in the calculations of the vehicle CG and moments of inertia, because, the moment of inertia of the non-sloshing propellant mass about its center of mass is zero, since it does not rotate with the vehicle.

The sloshing part of the liquid near the surface is approximated with a low damped, oscillating spring mass system whose weight and location depend on the properties of the liquid, the shape and size of the tank, and the liquid fill level. The mass is free to oscillate in two directions perpendicular to the steady-state acceleration vector A_T, which is mostly in the x direction, but there may also be a small acceleration component in the z direction (we ignore the y component). One side of the spring is attached at a fixed point in the tank centerline a little below the surface, and the other end of the spring is attached to a mass that represents the sloshing portion of the propellant. The frequency of the slosh oscillation is proportional to the square root of the acceleration A_T.

The slosh model can also be coupled with structural flexibility. The attachment point of the spring at the tank centerline is not necessarily rigid but it may oscillate due to structural bending. A structural node is required at that location in order to introduce flexibility by the mode shapes at the slosh mass attachment. The excitation is in both directions: that is, slosh is exciting flexibility and flexibility is exciting slosh. The non-sloshing portion of the propellant is attached at a fixed point below the slosh mass, near the bottom of the tank.
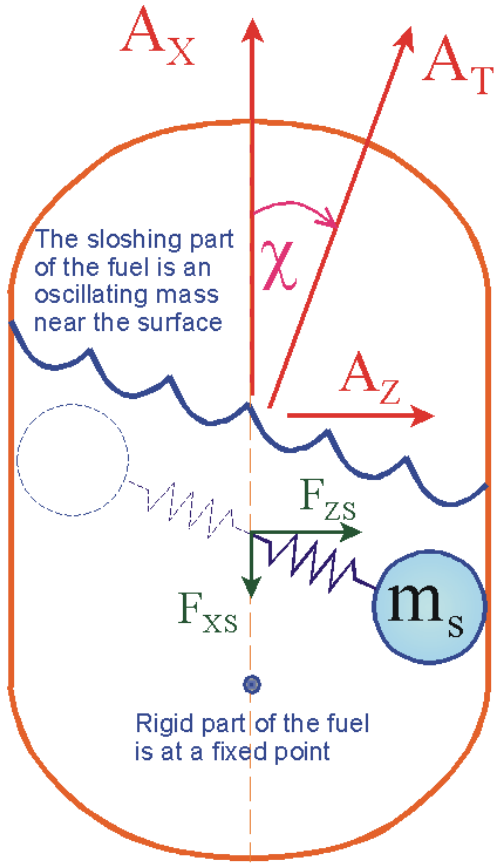
A_X and A_Z are the sensed vehicle accelerations along the body x and z directions. A_Y is assumed zero

$Total\ Acceleration:\ A_T = \sqrt{A_X^2 + A_Z^2}$

$\sin \chi = \dfrac{A_Z}{A_T}$

$The\ Slosh\ Frequency:$

$\omega_s = \omega_{s0} \sqrt{\dfrac{A_T}{g}}\ (rad\ /\ sec)$

$Forces\ due\ to\ slosh\ mass:$

$F_{ZS} = m_s \left(\omega_s^2 z_s + 2\zeta_s \omega_s \dot{z}_s \right) \cos \chi$

$F_{XS} = -m_s \left(\omega_s^2 z_s + 2\zeta_s \omega_s \dot{z}_s \right) \sin \chi$

$F_{YS} = m_s \left(\omega_s^2 y_s + 2\zeta_s \omega_s \dot{y}_s \right)$

Figure (2.6.1) The slosh mass oscillates in a plane that is perpendicular to the average total acceleration and it creates oscillatory forces on the vehicle

The slosh motion is excited by variations in vehicle normal and lateral accelerations at the point where the spring is attached to the tank centerline. The slosh mass cannot move along the acceleration vector A_T, which is the sensed acceleration: $(F_{thrust}-F_{aero})/M_T$, but the displacements are perpendicular to A_T. The displacements of the ith slosh mass, z_{si} and y_{si}, are measured relative to the spring attachment point at the tank centerline. If we assume that the steady-state A_Y acceleration is zero, the y_{si} slosh mass displacement is along the vehicle y axis. The z_{si} slosh displacement, however, is not necessarily along the vehicle z axis but it is slightly tilted by an angle χ in the x-z plane, perpendicular to A_T, see Figure 2.6.1.

The displacements of the slosh mass in two directions (z_s and y_s) relative to the tank and perpendicular to A_T are defined by two low damped 2nd order differential equations 2.6.2. The equations are excited by variations in the vehicle normal and lateral accelerations at the slosh mass attachment, perpendicular to the acceleration vector A_T.

$$z_{si}(s)\left(s^2 + 2\varsigma_i\omega_{si}\,s + \omega_{si}^2\right) = a_{xsi}\sin\chi - a_{zsi}\cos\chi - A_T\sum_{j=1}^{N\,\text{mod}}\sigma_{ysi}(j)\eta(j)$$

$$y_{si}(s)\left(s^2 + 2\varsigma_i\omega_{si}\,s + \omega_{si}^2\right) = -a_{ysi} + A_T\sum_{j=1}^{N\,\text{mod}}\sigma_{zsi}(j)\eta(j)$$

(2.6.2)

Where:

ω_{si}, ζ_{si} are the frequency of the ith slosh mass in (rad/sec) and the damping coefficient.

a_{xsi}, a_{zsi}, a_{ysi} are the translational accelerations of the vehicle at the ith slosh mass location along the x, z and y directions respectively, as defined in equations 2.6.3.

z_{si} and y_{si} are the displacements of the slosh mass relative to the tank centerline attachment point perpendicular to the acceleration A_T

χ is the angle between the acceleration vector A_T and the vehicle x axis

The slosh mass is excited to oscillations by variations in vehicle acceleration at the spring attachment point in the tank centerline. The vehicle accelerations along x, y, and z at that point consist of three components: (a) the linear accelerations at the vehicle CG, (b) the rotational acceleration components due to the vehicle angular accelerations, and (c) flex acceleration components because the tank structure is also flexing at the slosh mass attachment, see equation 2.6.3.

$$a_{xsi} = \ddot{x}_{CG} + l_{Zsi}\dot{q} - l_{Ysi}\dot{r} + \sum_{j=1}^{N\,\text{mod}}\phi_{xs}(i,j)\ddot{\eta}(j)$$

$$a_{ysi} = \ddot{y}_{CG} + l_{Xsi}\dot{r} - l_{Zsi}\dot{p} + \sum_{j=1}^{N\,\text{mod}}\phi_{ys}(i,j)\ddot{\eta}(j)$$

(2.6.3)

$$a_{zsi} = \ddot{z}_{CG} + l_{Ysi}\dot{p} - l_{Xsi}\dot{q} + \sum_{j=1}^{N\,\text{mod}}\phi_{zs}(i,j)\ddot{\eta}(j)$$

Where:

$\phi_{ys}(i,j)$, $\phi_{zs}(i,j)$ are the modal shapes along y and z of the jth mode at the ith slosh mass location

$\eta(j)$ is the generalized modal displacement for the jth mode

l_{Xsi}, l_{Ysi}, l_{Zsi} are the moment arms of slosh mass (i) from the vehicle CG in the x, y, and z directions respectively.

$$l_{Xsi} = x_{si} - x_{CG} \qquad l_{Ysi} = y_{si} - y_{CG} \qquad l_{Zsi} = z_{si} - z_{CG}$$

The parameters required to define propellant sloshing in a tank are: the slosh mass m_{si}, slosh frequency ω_{si} in (rad/sec), damping coefficient ζ_{si}, and the steady-state location of the slosh mass relative to the vehicle. They can be obtained from the tank geometry, propellant density, surface level, the vehicle acceleration, etc. The slosh frequency is typically defined at 1g acceleration, ω_{s0} in (rad/sec), and it is proportionally scaled with the square root of the steady-state acceleration in (g's), $\omega_s = \omega_{s0}\sqrt{A_T}$.

The derivation of slosh parameters as a function of tank geometry, propellant level and density, have been obtained experimentally and they are documented in NASA reports. Slosh stability is typically analyzed in the frequency domain by calculating the phase and gain margins using Nichols or Nyquist diagrams. The slosh modes are low damped and they are mostly phase-stable with the bubble resonances opening away from the -1 critical point. Sometimes, however, depending on vehicle CG and the slosh mass location relative to the vehicle's center of rotation (CR), the direction of the resonance is pointing towards or it is encircling the critical -1 point. This would indicate a reduced slosh margin and the possibility of closed-loop slosh instability (divergent oscillations at the slosh frequency). In general the slosh modes are phase-stable unless the location of slosh mass happens to be between the vehicle CG and the center of rotation (CR). This statement is valid if we ignore the TWD, otherwise, it is more complicated to predict the conditions of slosh stability.

The disturbance force on the vehicle generated at the spring attachment point by the oscillating motion relative to the tank of a single slosh mass $m_s(i)$, can be resolved in three components along the vehicle x, y, and z axes, as shown in equation 2.6.4.

$$
\begin{aligned}
F_{Zs}(i) &= m_s(i)\left(\omega_{si}^2 z_{si} + 2\varsigma_i \omega_{si} \dot{z}_{si}\right)\cos\chi \\
F_{Xs}(i) &= -m_s(i)\left(\omega_{si}^2 z_{si} + 2\varsigma_i \omega_{si} \dot{z}_{si}\right)\sin\chi \\
F_{Ys}(i) &= m_s(i)\left(\omega_{si}^2 y_{si} + 2\varsigma_i \omega_{si} \dot{y}_{si}\right)
\end{aligned}
$$

(2.6.4)

The combined slosh forces on the vehicle F_{Xsl}, F_{Zsl}, and F_{Ysl} along the x, z and y axes from all tanks are:

$$
F_{Xsl} = \sum_{i=1}^{Nsl} F_{Xs}(i) \qquad F_{Ysl} = \sum_{i=1}^{Nsl} F_{Ys}(i) \qquad F_{Zsl} = \sum_{i=1}^{Nsl} F_{Zs}(i)
$$

(2.6.5)

Equation 2.6.6 calculates the moments on the vehicle in roll, pitch, and yaw due to multiple propellants sloshing by combining the forces from all tanks. It also includes the moments generated by the displacements of the slosh mass coupling with the vehicle acceleration.
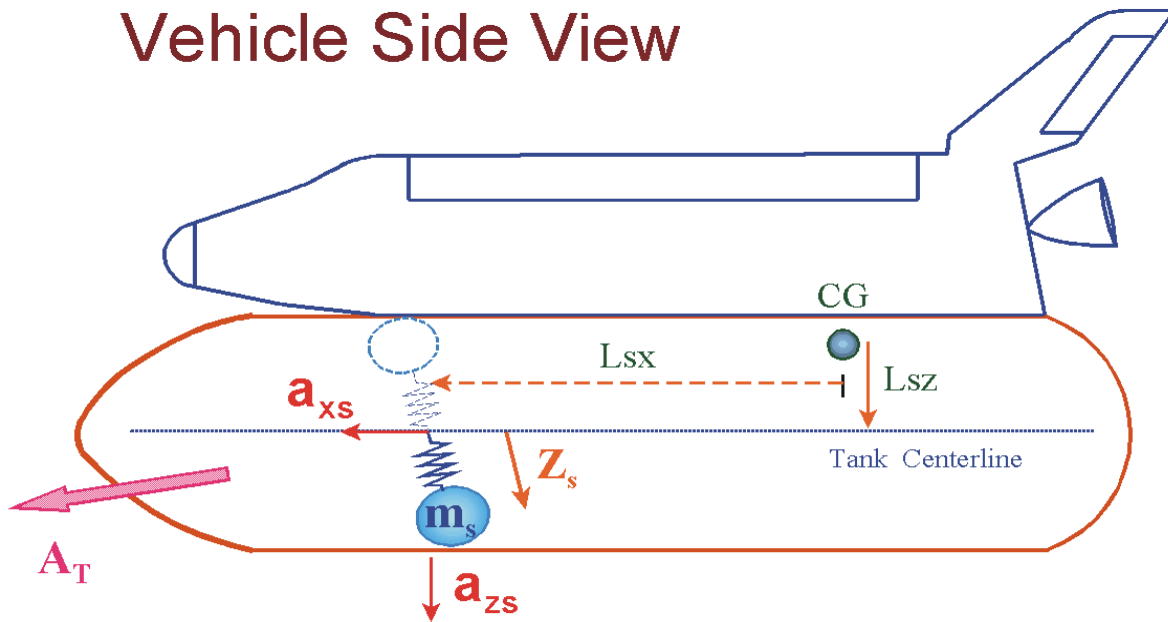
$$
\begin{aligned}
L_{XSL} &= \sum_{i=1}^{Nsl} \left\{ F_{Zsi} l_{syi} - F_{Ysi} l_{szi} - m_s(i) A_Z y_{si} \right\} \\
M_{YSL} &= \sum_{i=1}^{Nsl} \left\{ F_{Xsi} l_{szi} - F_{Zsi} l_{sxi} - m_s(i)\left[d_{si}^2 \dot{q} + A_T z_{si}\right] \right\} \\
N_{ZSL} &= \sum_{i=1}^{Nsl} \left\{ F_{Ysi} l_{sxi} - F_{Xsi} l_{syi} - m_s(i)\left[l_{syi}^2 \dot{r} - A_X y_{si}\right] \right\} \\
where&:\ A_T = \sqrt{A_X^2 + A_Z^2}
\end{aligned}
$$

(2.6.6)

d_{si} is the distance between the vehicle CG and the acceleration vector through the slosh mass, and it is calculated in Figure 2.6.8

A_T is the vehicle total sensed acceleration in the x-z plane

Vehicle Side View

CG

Lsx

Lsz

a_{xs}

Z_s

Tank Centerline

m_s

A_T

a_{zs}

Vehicle Acceleration at the
Slosh Mass (a_{xs} , a_{zs})

Reference Axes

Y

Z

Rear View

TVC
Engines

CG

L_{sz}

m_s

y_s

Tank Centerline

a_{ys}

Vehicle Side Acceleration
at the Slosh Mass

Figure (2.6.7) Spring-mass slosh model

45

$$A_T = -g$$

$$A_Z = -g\cos\theta \qquad A_X = g\sin\theta$$

$$\chi = \sin^{-1}\left[\frac{A_Z}{\sqrt{A_X^2 + A_Z^2}}\right] = -90 + \theta$$

$$l = \sqrt{(x_s - x_{CG})^2 + (z_s - z_{CG})^2}$$

$$\bar{u}_1 = \frac{(A_X, A_Z)}{\sqrt{A_X + A_Z}}; \qquad \bar{u}_2 = \frac{(x_s - x_{CG}, z_s - z_{CG})}{l}$$

$$\cos\gamma = \bar{u}_1^T * \bar{u}_2 \qquad d_s = l\sin\gamma$$

Calculating the distance (d_s) from the vehicle CG to the acceleration vector (A_T) through the slosh mass
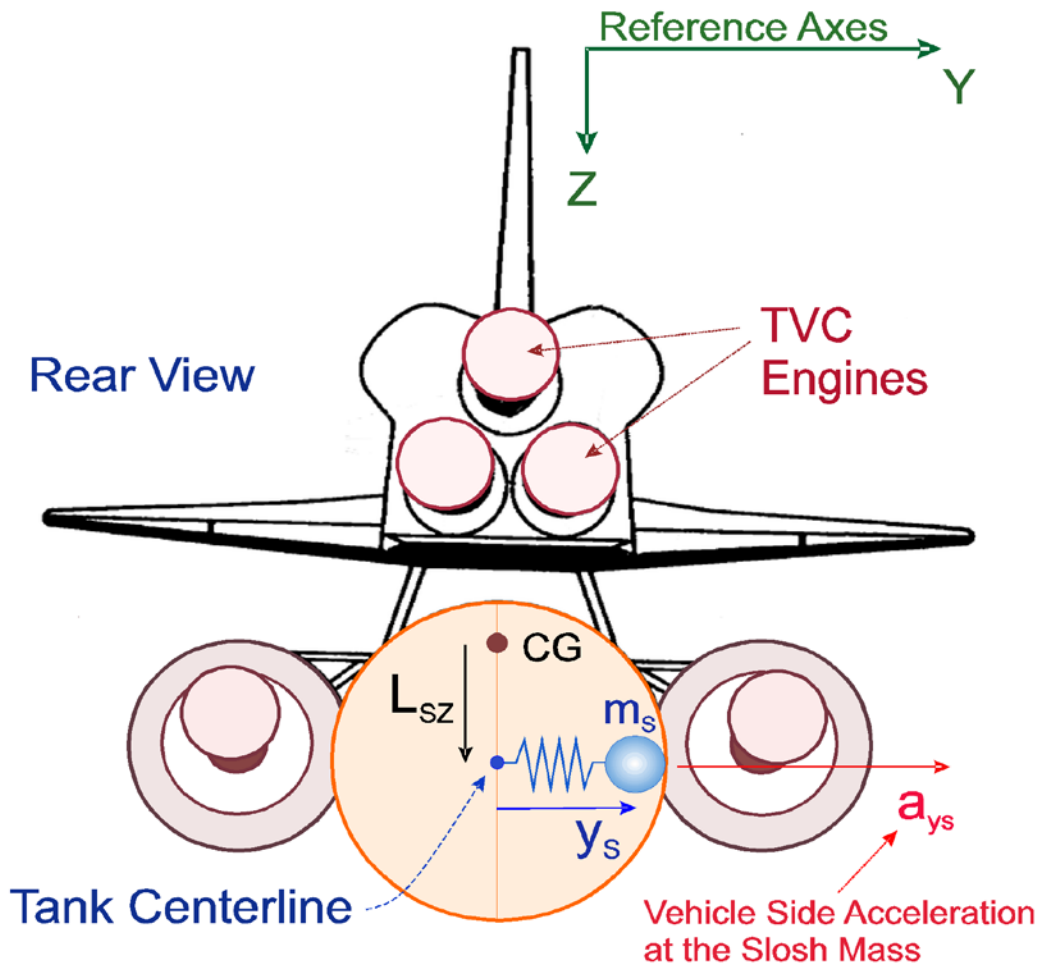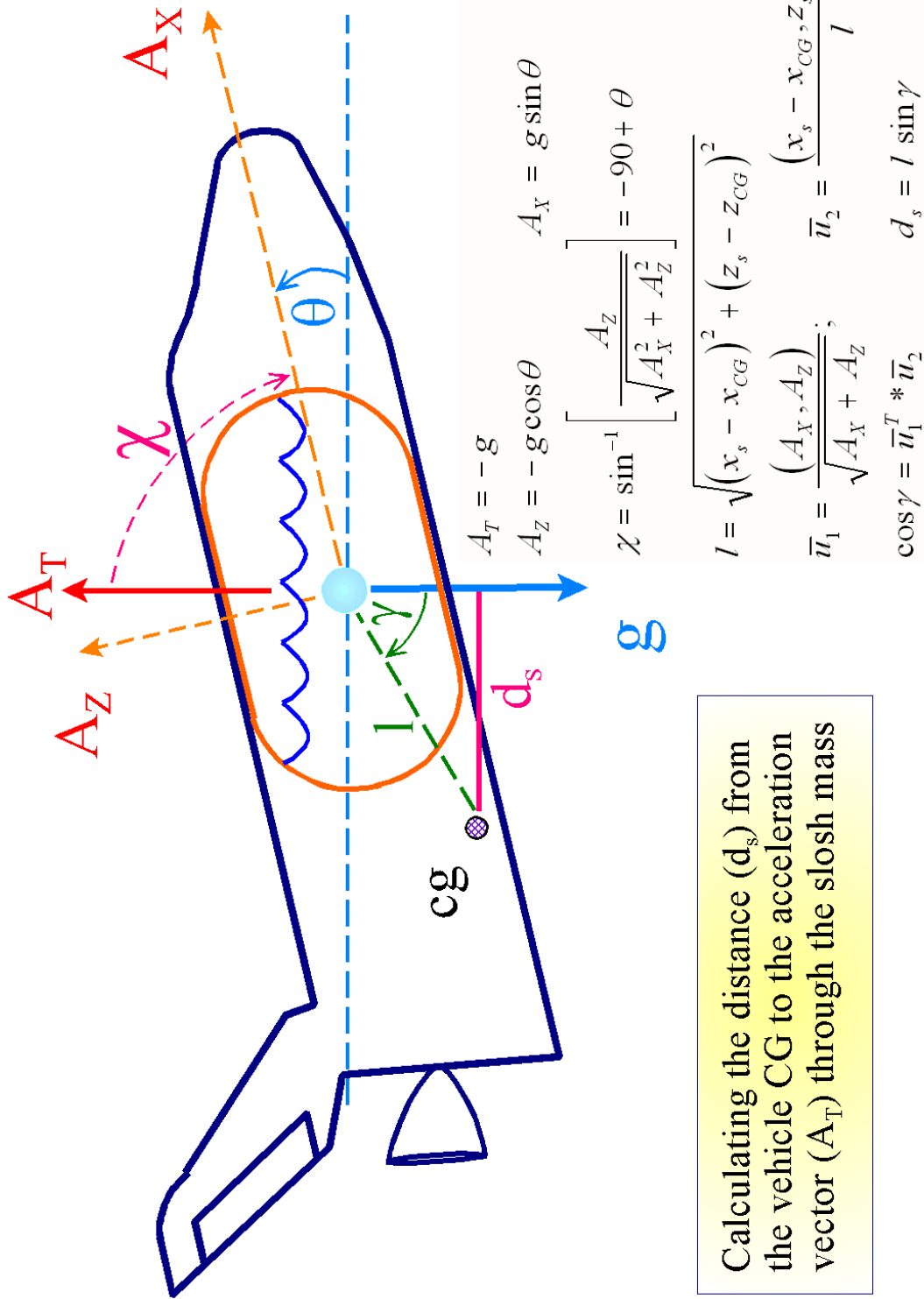
Figure (2.6.8) Equations for calculating the distance (d_s) between the acceleration vector at the slosh mass and the vehicle CG. In the above example the acceleration is upward in the vertical direction due to the lifting aerodynamic forces counteracting the gravity and the fuel level is horizontal.

Non-Linear Pendulum Slosh Model

The spring mass model used for linear analysis is not sufficient to analyze cases of slosh instability. In reality the slosh mass will not diverge to infinity because its deflection cannot exceed the tank radius even when it is unstable and, therefore, the force on the vehicle will be bounded. In fact, it won't even reach near the tank walls but if we assume a pendulum model, the pendulum angle will only swing up to 45° before the wave breaks and the oscillations will begin growing again from a lower amplitude. We therefore need to include a more efficient conical pendulum model in the simulation to analyze the vehicle response to slosh instabilities. The conical pendulum model captures not only the forces at the pendulum pivot point due to vehicle acceleration but it includes also the centripetal forces against the tank walls produced by the velocity of the slosh mass as it spins around the tank. We can therefore analyze vortex type of slosh instabilities as the mass motion couples with the TVC, by giving it an initial lateral spin velocity around the tank centerline and watch if it damps out or diverges. Figure 2.6.9 shows the pendulum model relative to tank for an arbitrary 60% fill level. We assume that only 20% of the total propellant is sloshing near the top and 40% is rigidly attached towards the bottom at its center of mass point on the tank centerline. The pendulum string is a little shorter than the local tank radius and it is attached at a point on the centerline a little below the sloshing surface.
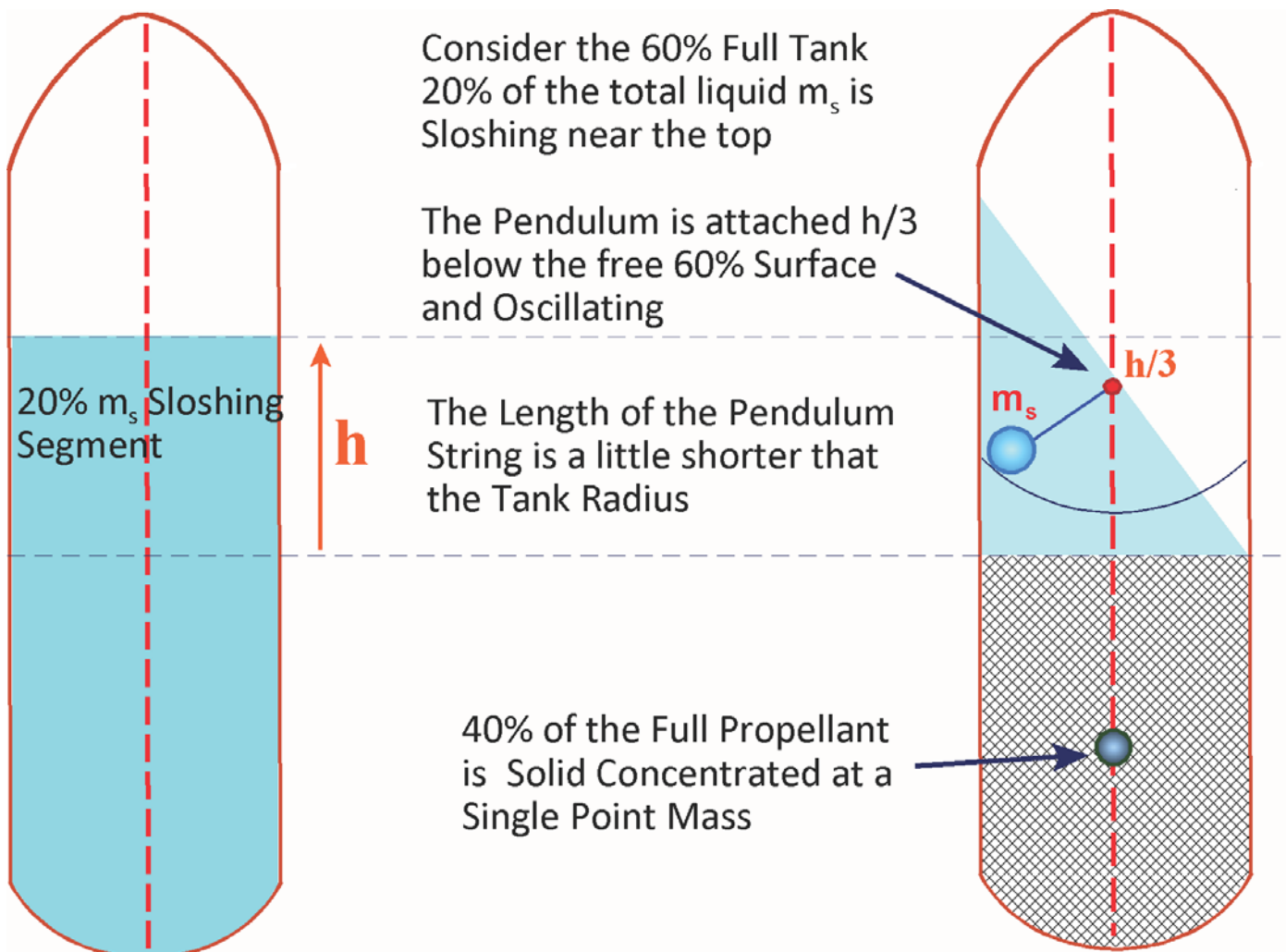

Figure 2.6.9 Pendulum Slosh Model

The model is more realistic if we assume a spherical tank and that the string is elastic and the slosh mass m_s is attached from the center of the tank as shown in Figure 2.6.10. This is also equivalent to a soft ball rolling inside the lower part of a spherical tank under the influence of the tank acceleration forces. This semi-sphere is not necessarily the tank itself but it approximates the region of slosh activity near the surface. It is the boundary of the slosh mass position. The mass can float inside the sphere and it doesn't apply a force on the vehicle until it reaches near the surface of the sphere and the string stretches r_s beyond its nominal length r_p which is a little shorter than the tank radius. The tank acceleration in the x-direction $\ddot{x}$ is equal to the vehicle g acceleration which keeps the mass oscillating near the bottom of the sphere. There are also lateral accelerations $\ddot{y}$ and $\ddot{z}$ produced by lateral disturbance forces that excite the pendulum motion.
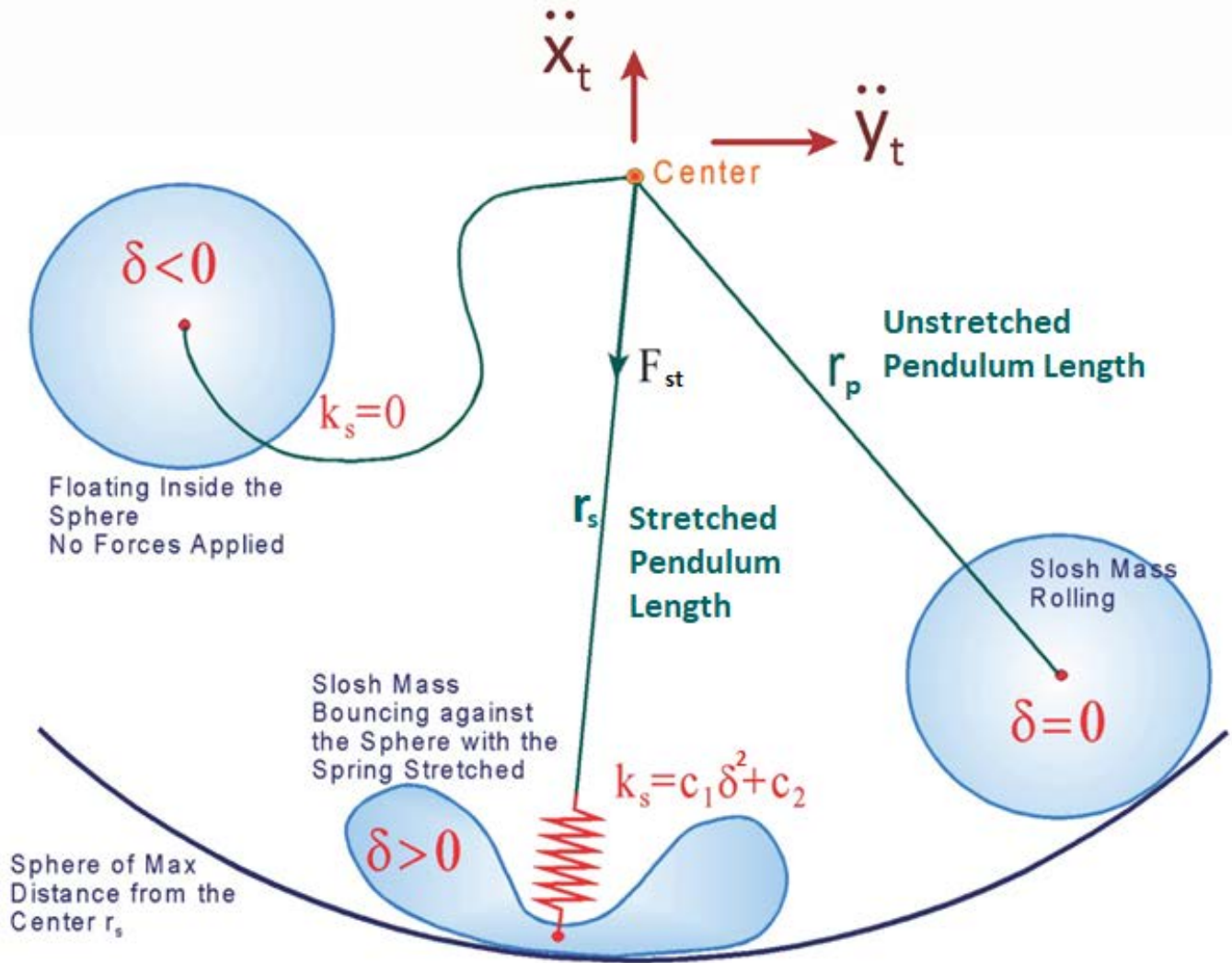

Figure 2.6.10 Non-Linear Slosh Model

The extension of the pendulum string δ is equal to the stretched length r_s minus the original unstretched length r_p. The spring constant of the string k_s is a non-linear function of the extension δ. It is adjusted to prevent the mass from extending too far beyond the tank wall.

$$\delta = r_s - r_p$$

The acceleration $\underline{a}_t$ of the vehicle at the location of the slosh mass is:

$$\underline{a}_t = -\underline{d}_s \times \underline{\dot{\omega}}_b + \underline{a}_{cg} \quad where: \ \underline{d}_s = \underline{l}_{piv} + \underline{x}_s - \underline{l}_{CG}$$

Where:
$\underline{d}_s$ is the distance between the slosh mass and the vehicle CG
$\underline{\dot{\omega}}_b$ is the vehicle angular acceleration
x_s is the slosh mass position relative to the tank center
l_{piv} is the location of the string pivot point
l_{cg} is the location of the vehicle CG
$\underline{a}_{cg}$ is the vehicle translational acceleration at the CG.

The pendulum string is elastic and it can be stretched by the vehicle acceleration at the pivot point. Its tension F_{st} in the following equation is produced by forces, consisting of 3 elements:

1. a centripetal force due to angular rate $\dot{\theta}$ of the mass as it rotates inside the sphere,
2. a non-linear spring force due to the extension of the string δ as it stretches beyond its length r, and
3. a viscous friction of the string proportional to its extension rate which is along the vector $\underline{u}_1$

$$F_{st} = m_s \left(r_p + \delta \right) \dot{\theta}^2 + k_s \left(\delta \right) \delta + k_{d1} \left(\underline{\dot{x}}_s \bullet \underline{u}_1 \right)$$

Where:
$\dot{\theta}$ is the angular rate of the pendulum as it rotates along the tank wall
$k_s(\delta)$ is the spring constant of the pendulum string which is a non-linear function of spring displacement δ;
        $k_s = c_1 \delta^2 + c_2$. It prevents it from stretching too much beyond the tank wall
k_{d1} is the axial damping coefficient of the string along $\underline{u}_1$
r_p is the unstretched length of the string, a little shorter than tank radius
$\underline{\dot{x}}_s$ is the slosh mass velocity relative to the tank, resolved along $\underline{u}_1$
$\underline{u}_1$ is the unit vector along the line from the tank center to the slosh mass

$$\underline{u}_1 = \frac{\underline{x}_s}{\left| \underline{x}_s \right|}$$

The inertial acceleration of the slosh mass consists of two acceleration components: the acceleration relative to the tank $\ddot{\underline{x}}_s$ plus the inertial acceleration $\underline{a}_t$ of the tank at the slosh mass which is close to the pivot point. This acceleration is produced by two forces: the axial tension of the string along the $\underline{u}_1$ vector, plus viscous friction force against the mass velocity as it rotates around the tank along $\underline{u}_2$ vector and is rubbing against the inside of the tank wall

$$m_s\left(\ddot{\underline{x}}_s + \underline{a}_t\right) = -F_{st}\underline{u}_1 - \left(k_{d2}\dot{\theta}\right)\underline{u}_2$$

Where:

k_{d2} is the tangential damping coefficient of the mass as it slides along the surface creating a force parallel to the surface resisting the mass velocity along $\underline{u}_2$

$\underline{u}_2$ is the unit vector parallel to the surface in the velocity direction

$$\underline{u}_v = \frac{\dot{\underline{x}}_s}{|\dot{\underline{x}}_s|} \qquad \underline{u}_2 = \left[\left(\underline{u}_1 \times \underline{u}_v\right) \times \underline{u}_1\right]$$

The force on the vehicle F_v generated by the slosh mass is equal and opposite to the force on the slosh mass and the torque on the vehicle is obtained by cross-multiplying F_v with the distance d_s of the slosh mass from the vehicle CG.

$$\underline{F}_v = F_{st}\underline{u}_1 + \left(k_{d2}\dot{\theta}\right)\underline{u}_2$$
$$\underline{T}_v = \left(\underline{d}_s \times \underline{F}_v\right) \ where: \underline{d}_s = \underline{l}_{tnk} + \underline{x}_s - \underline{l}_{CG}$$

The velocity and position of the slosh mass m_s with respect to the tank are obtained by integrating the slosh mass acceleration starting from known initial velocity and position conditions v_0 and p_0

$$\dot{\underline{x}}_s = \underline{v}_0 + \int_0^t \ddot{\underline{x}}_s(t)\,dt \qquad \underline{x}_s = \underline{p}_0 + \int_0^t \dot{\underline{x}}_s(t)\,dt$$

The slosh mass angular rate $\dot{\theta}$ is obtained by resolving the slosh mass velocity $\dot{\underline{x}}_s$ along the $\underline{u}_2$ direction. The pendulum angle θ relative to the tank centerline is obtained from the x-direction component of vector $\underline{u}_1$.

$$\dot{\theta} = \left(\frac{\dot{\underline{x}}_s}{r+\delta}\right)\bullet\underline{u}_2 \qquad \theta = \cos^{-1}\left[u_1(1)\right]$$
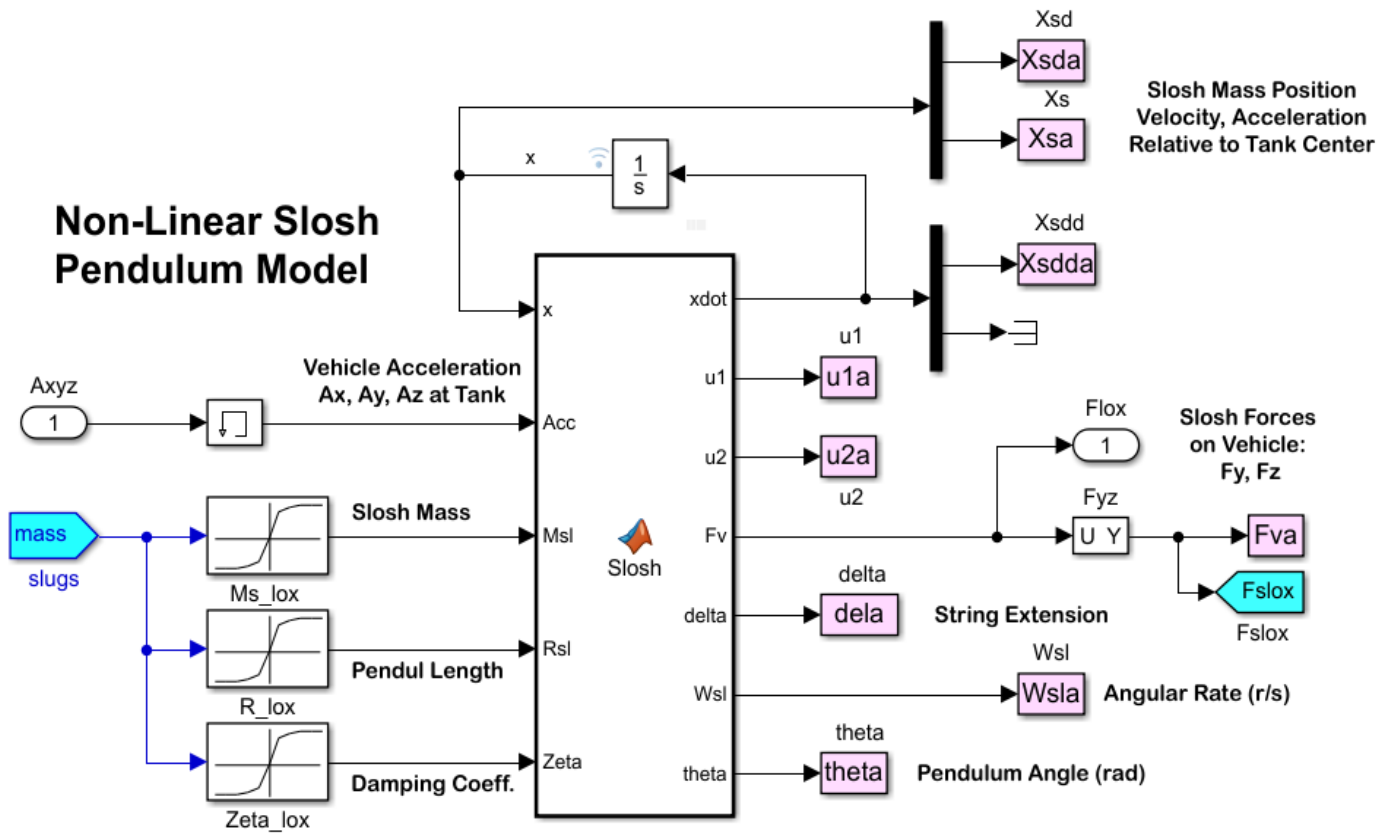
Figure 2.6.11 Pendulum Slosh Model Implementation Using Simulink

```matlab
function [xdot,u1,u2,Fv,delta,Wsl,theta]= Slosh(x,Acc,Msl,Rsl,Zeta)
% Slosh Model
% out= Slosh(x,Acc)
% Calculates the Slosh Forces on the Tank as a function of
% Vehicle acceleration at the Tank
%
% State Variables (x)
% x(1:3)  = Xsd Slosh Mass Velocity wrt Tank
% x(4:6)  = Xs Slosh Mass Position wrt Tank
% Acc(3}  = Vehicle Linear x,y,z Accelerat at Tank
% Msl     = Slosh Mass (slug)
% Rsl     = Pendulum length (ft)
% Ts      = Sampling Period (sec)

xdot=zeros(6,1);                             % Initialize
Xsd= x(1:3);                                 % Velocity of Msl (Tank Relative)
Xs = x(4:6);                                 % Position of Msl (Tank Relative)

% Find the Axial direction u1
rs= sqrt(Xs'*Xs);                            % Scalar Distance of Msl from center
if rs==0, rs=0.0001;                         % Avoid Xs in the center of sphere
    e=rand(3,1); Xs=e*rs/sqrt(e'*e);
end
u1= Xs/rs;                                   % Unit vector from center to mass
theta=acos(-u1(1));                          % Pendulum Angle wrt tank centerline

% Find the Tangential direction u2
vm= sqrt(Xsd'*Xsd);                          % Veloc magnit relative to tank
if vm==0, vm=0.0001;                         % Avoid Xsd being zero
    e=rand(3,1); Xsd=e*vm/sqrt(e'*e);
end
uv= Xsd/vm;                                  % Unit vector along veloc Xsd
u3= cross(u1,uv);                            % Unit Vect Perpendic to u1 & uv
u2= cross(u3,u1);                            % Unit Vect along vel, Tangent to surface

% Non-Linear Spring Deflection
delta= rs - Rsl;                             % Spring Extension
if delta>0                                   % Stretched Spring
    Kspr=(8000*delta^2 + 100)*Msl;           % Non-Linear Spring 2.e5*delta^2 + 5.0e3;
    Kdl=2+8*Msl;                             % Friction Coefficients 1000
    Wsl= dot((Xsd/rs),u2);                   % Slosh Mass angular rate tangent tank surf
    if Acc(1)>0
        Kfr=2*Msl*Zeta*sqrt(Acc(1)*Rsl);     % Friction Coefficient
    else, Kfr=0;
    end
else                                         % Free-Floating
    Kspr=0; Kfr=0; Kdl=0; Wsl=0; delta=0;    % Zero all External Forces
end

% Forces on Slosh Mass and Vehicle
Fd= Kfr*Wsl;                                 % Tangent Viscous Frict Force on Mass
Fst= Kspr*delta + Msl*(rs*Wsl^2) + dot(Kdl*Xsd,u1);  % Radial Centripet, Spring & Damping accel
Xsdd= - (Fst/Msl)*u1 - (Fd/Msl)*u2 - Acc;    % Slosh mass Acceler wrt tank center
Fv= Fst*u1 + Fd*u2; Fv(1)=0;                 % Y,Z Force on Vehicle, No X

% State Derivatives
xdot(1:3)= Xsdd;                             % Xs-dot-dot
xdot(4:6)= Xsd;                              % Xs-dot
end
```
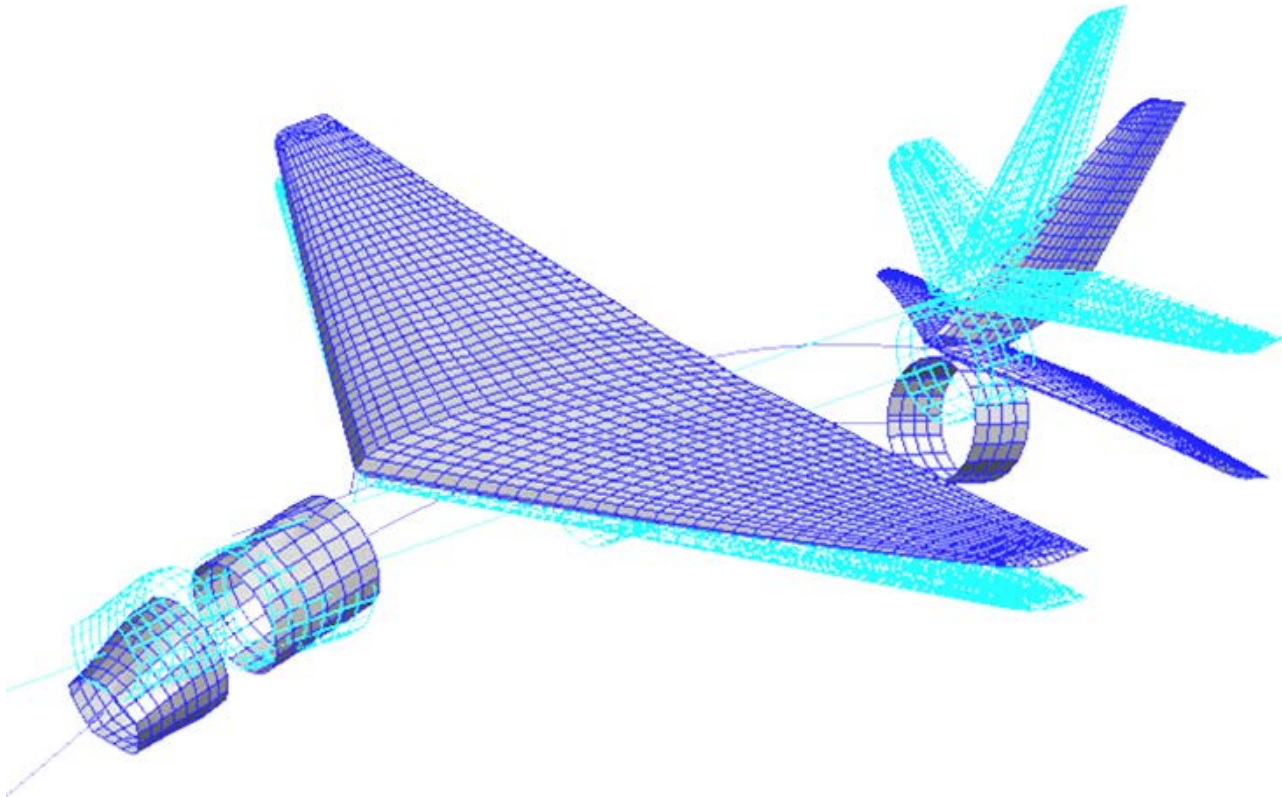
2.7 Structural Flexibility

Structural flexibility is a very important factor in flight control system stability and performance and it must properly be accounted for in the mathematical model and analysis. Flight vehicles are designed with minimum weight objectives, hence their structures exhibit some form of flexibility. Some parts of the vehicle can develop considerable amounts of displacement and acceleration as a result of structural flexibility in addition to the displacement and acceleration that arise owing to the rigid body motion. The primary function of the flight control system is to guide and stabilize the flexible vehicle without violating the operational requirements. It processes data from sensors to provide command signals to engines, control surfaces and RCS jets. The sensors measure angular or translational motion, which in additional to the rigid-body, it includes motion caused by structural deformation at the locations of the sensors.

These structural vibration signals affect the commands to the control effectors. Since the effectors apply forces to the structure, energy can be fed to the structure at various frequencies, including those where flex modes may be excited. Because structural damping is small, it is possible for the effectors to add energy faster than it is dissipated causing excessive structural deflections and possible structural failures. If the structural characteristics are ignored, the flight vehicle may not be properly controlled and in many instances it may exhibit self-excited divergent oscillations that can be destructive. The structural flexibility should, therefore, be considered in the control analysis, and the control system designer must be aware that divergent structural feedback can occur and must ensure that the flex phenomena are properly analyzed and compensated.

Problems arising from the dynamic interaction between the control system and the flexible structure are influenced by the sensor locations, the local structural flexibility, mode shapes, frequencies, and damping characteristics. The structure where the sensors are mounted may be excited by engine noise and local vibrations, and it may exhibit undesirable responses that can produce erroneous sensor signals or saturation which may seriously affect control system performance and operation. Local oscillations may also be reinforced by the control system. In adverse situations, an attempt is made to attenuate the interaction by modifying the control system, include filters, stiffening the sensor mounting structure, or relocating the sensors. If these modifications fail to resolve the interaction problem, structural redesign may be necessary. Improper determination and selection of dominant flexibility modes in the design has often led to catastrophic structural instability problems in flight vehicles. The design is therefore supplemented with frequency domain analysis, simulations, component tests, system vibration tests, and flight tests.

Flexibility in general limits the control system bandwidth. As a rule of thumb there should be a factor of 10 separation between the control system bandwidth and the first dominant flex resonance. It affects also the vehicle performance and usually requires filtering. The control system must be designed to process the sensor signals so that there is a net flow of energy out of the structure. First, the control system may filter sensor signals at resonant structural frequencies, thereby, preventing the effectors from supplying energy at those frequencies. This is called "gain stabilization" and it avoids excessive response in high frequency flex resonances. In general, however, one or more of the lower frequency modes are not sufficiently separated from the control system bandwidth to permit gain stabilization and the alternative is "phase-stabilization", where the controller is designed to adjust the phase of the control forces and remove energy from the modes, and hence actively attenuating rather than amplifying the mode. Most designs employ both methods, with phase stabilization of low frequency modes and gain stabilization of high frequency modes.

In launch vehicles the main source of flex mode excitation is the TVC. In aircraft, the acceleration of the vehicle in combination with the aerodynamic forces can excite the structure into bending motion especially in the wings and the tails. This causes significant aero-elastic phenomena to occur which may have a serious impact on vehicle stability and performance. The deflection of an elevator, for example, causes a torsional flexibility on the wing due to the aerodynamic loading in the opposite direction which reduces its effectiveness. Wing divergence is another aero-elastic phenomenon to be avoided. That is, when the aerodynamic center of the wing is in front of its centerline, the lift generated at high dynamic pressures has a tendency to rotate the wing (nose up), which increases the aero moment even further. This torsional moment is resisted by the wing stiffness. If the wing torsional stiffness is not enough, the wing will twist off. There are other factors to consider in the design of flex structures. Examine the external panels for the possibility of panel flutter. In digital control systems we must also consider the effect of high frequency aliasing where some vibration modes fold-back, excite and de-stabilize lower frequency modes. We may also have to include filters in the rate gyro and accelerometer signals before sampling to eliminate noise problems folding down and exciting structural modes. Furthermore, the frequency of programmed pitch and guidance commands should not coincide with either flexible or rigid-body mode frequencies. We should also consider filtering the input commands to remove signals that excite vibrations.

The oscillatory motion of a vehicle structure can be characterized with a combination of elastic modes which are excited by forcing functions generated from the TVC gimbaling, reaction jets, actuator forces, aerodynamic forces, propellant sloshing, aero-elastic coupling, reaction wheels, CMG, and other external disturbances. The term "elastic modes" or "structural modes", refers to the normalized mode shapes of the flight vehicle in *"free-free"* vibration. The mode shapes and frequencies (or modal data) of the vehicle are obtained from a finite element modeling program, such as Nastran. Each bending mode is represented by a second order differential equation, shown in equation 2.7.1, that has a low damping coefficient (ζ_j), a resonance frequency (ω_j) in (rad/sec), and a generalized mass $m_g(j)$ in units of (lb-sec^2/ft) that normalizes the equation. The equation is excited on the right hand side by external forces and torques acting on the vehicle structure in different locations. It calculates the modal excitation of each mode (j) responding at its natural frequency ω_j. The mode excitation is a time function called the generalized displacement $\eta_j(t)$ of mode (j) in units of (feet). The coefficients on the RHS of this equation include a set of translational mode shapes [$\varphi_{xn}(j)$, $\varphi_{yn}(j)$, $\varphi_{zn}(j)$] along the vehicle x, y, and z axes, and a set of rotational mode slopes [$\sigma_{xn}(j)$, $\sigma_{yn}(j)$, $\sigma_{zn}(j)$] about x, y, and z, at each excitation point, called "nodes", where a force or a torque is applied. They are obtained from the finite elements model.

The output from each flex mode function is the generalized displacement of a specific mode (j). These are not physical variables, but intermediate states that define the excitation of each natural frequency under the influence of the combined forces and torques. The amount and the direction of excitation, in terms of magnitude and phase of each modal displacement (η_j) depends, not only on the forcing function, but also on the mode shapes and slopes of the structure at the excitation point. When a sensor is mounted on the structure, in addition to the rigid body motion, it also measures a linear combination of displacements (η_j) from all the flex modes which are observable at that sensor. The elastic modes produce high frequency oscillations at the sensor, superimposed on the top of the rigid body measurements. Furthermore, the amount and the direction by which each mode is detected at a sensor depend on the mode shapes and slopes of the structure at the sensor location. Flexibility also affects the response of the vehicle at the engine gimbals or aerosurfaces to actuator forces. It produces additional loading torques on the actuator due to flexibility at the hinges, reaction torques against the actuator control torques, and sometimes tail-wag-dog type of oscillations at the hinges. See the load-torque-feedback effects in Section 2.10.

In some cases the structural modes are not only excited by the direct application of forces and torques at structural nodes, but the flexible structure can also be excited by aerodynamic forces generated due to the vehicle motion relative to the atmosphere, and specifically, the angles of attack and sideslip and the body rates. These are aero-elastic phenomena, where aerodynamic forces acting on a flexible structure couple rigid-body and flexible-body dynamics and they can affect the control system performance. The aero-elastic coupling may cause the vehicle resonant frequencies undergo substantial and irregular variations along its flight, tending sometimes for resonances to approach one another rather than to increase uniformly with time as it would result from the consumption of a propellant. Aero-elastic coupling can sometimes be destabilizing because it may lower the frequency of the first flex mode closer to the rigid-body bandwidth while reducing the vehicle static stability, and phase stabilization of the lowest frequency vibration modes may be required. To protect against adverse aero-elastic effects fins are sometimes installed to increase static stability and also stiffen the frequency of structural modes.

Aero-elastic excitation is characterized by a set of aero-elastic coefficients, the Generalized Aerodynamic Force Derivatives (GAFD), that couple the structural modes with aerodynamics, and specifically with variations in (α, β, body rates, and surface deflections). Aero-elasticity is more dominant in large and flexible aircraft because flexibility is affected not only by the TVC but also by the aerodynamic forces produced due to vehicle rigid-body motion in the atmosphere. In addition, the vehicle flexibility, such as a surfaces, wing or a tail, significantly affects the aerodynamic forces and moments and the overall vehicle performance, especially at high dynamic pressures. Complex CFD models are developed to study aero-elasticity and flutter effects and the aero-elastic coupling between structure and aerodynamics. Sometimes it becomes significant enough to include it in the control design and linear analysis. In some launch vehicle applications, such as the Space Shuttle during ascent, the flexure excitation due to the TVC is much more dominant and the aero-elastic effects were ignored. During descent, however, the aero-elastic effects were included.

Another factor that affects flexibility is the inertia forces produced by the pivoting of the massive engines or control surfaces. These forces can yield undesirable deformations of the supporting structure and they in turn produce control disturbances. This excitation is characterized by the "inertial coupling coefficients" which couple the structural modes with the rotational accelerations of the control surfaces or nozzles. The inertial coupling coefficients, otherwise known as *"h-parameters"*, are created from the finite-elements program, with the modal data. The modes are *"free-free"* and they are created with the control surfaces included in the Nastran model and the joints at the hinges are locked (infinitely stiff). The control surface hinges are released in the simulation model by the inclusion of the h-parameters in the equations of motion, see equations (2-3) and (2-4-2). In the early phases of a design the aero-elastic coefficients are not usually available for modeling flexibility because their creation involves extensive CFD modeling. In the flex equations that follow we present two approaches for modeling flexibility. One that does not include aero-elasticity and it does not require GAFD and h-parameters data and a second method that includes both. In the first method the surfaces are assumed to be rigid and they are attached at the hinge of a flexible structure. The structure does not include the surfaces. The structure is excited by aero and inertia forces produced at the hinges of the control surfaces, due to rigid surface deflections, rates and accelerations. This approximation model is shown in equations (2.7.1) and (2.7.2). The second method is obviously more efficient because it includes both: aero-elastic and inertial coupling coefficients, and it is shown in Equation (2.7.4). The FEM includes the aero-surfaces with the hinges locked.

The Structural Bending Equation:

External forces and torques are applied at different locations on the vehicle and excite the structural modes. Each mode is represented by a second order, low damped differential equation that calculates the mode excitation which is represented by the generalized displacement $\eta_{j(t)}$. Equation 2.7.1 calculates $\eta_{j(t)}$ as a function of the external forces and torques. The forcing functions are mainly due to forces and torques generated by the engines, RCS jets, aerosurface rotations, momentum exchange devices, and due to propellant sloshing. We are presenting two methods of modeling the flex mode excitation: a simple method that does not require GAFD, and a more efficient method that requires GAFD and inertial coupling coefficients.

Flex Mode Excitation without Aero-Elasticity and Inertial Coupling Coefficients

In this case the inertial coupling coefficients $h_{cs}(k,j)$ and the GAFD data are not included. Equation 2.7.1 calculates the generalized displacement of a flex mode (j) as a function of the external forces. The gimbaling engines, the slosh masses, and the aero-surfaces are attached as separate bodies that excite the flexible structure by generating reaction forces as a result of their motion.

$$
\begin{aligned}
m_g(j)\left(s^2 + 2\varsigma_j\omega_j s + \omega_j^2\right)\eta_j(s) = & \\
+ \sum_{i=1}^{Nslosh}\left[F_{Xsi}\,\phi_{xs}(i,j) + F_{Ysi}\,\phi_{ys}(i,j) + F_{Zsi}\,\phi_{zs}(i,j)\right] & \quad Slosh\ Forces \\
+ \sum_{k=1}^{Neng}\left[F_{Xek}\,\phi_{xe}(k,j) + F_{Yek}\,\phi_{ye}(k,j) + F_{Zek}\,\phi_{ze}(k,j)\right] & \quad Engine\ Forces \\
- \sum_{k=1}^{Neng}m_{ek}\left[\phi_{xe}(k,j)\,a_{xe(k)} + \phi_{ye}(k,j)\,a_{ye(k)} + \phi_{ze}(k,j)\,a_{ze(k)}\right] & \quad Eng\ Inertia\ Forces \\
- \sum_{k=1}^{Neng}I_{ek}\left[\sigma_{ye}(k,j)\,\ddot{\delta}_{ye(k)} + \sigma_{ze}(k,j)\,\ddot{\delta}_{ze(k)}\right] & \quad Engine\ Inertia\ Torques \\
+ \sum_{l=1}^{Nsurf}\left[F_{Xs(l)}\,\phi_{xcs}(l,j) + F_{Ys(l)}\,\phi_{ycs}(l,j) + F_{Zs(l)}\,\phi_{zcs}(l,j)\right] & \quad Surface\ Forces \\
- \sum_{l=1}^{Nsurf}m_{cs(l)}\left[\phi_{xcs}(l,j)\,a_{xcs(l)} + \phi_{ycs}(l,j)\,a_{ycs(l)} + \phi_{zcs}(l,j)\,a_{zcs(l)}\right] & \\
- \sum_{l=1}^{Nsurf}I_{hcs(l)}\,\sigma_{hcs}(l,j)\,\ddot{\delta}_{fcs(l)} & \quad Surface\ Inertia\ Torques
\end{aligned}
$$

Figure (2.7.1) Structural Mode excitation without GAFD and Inertial Coupling Coefficients

The total deflection at a control surface (k) including flexibility is obtained from equation (2.7.2), where: ϕ_{hsk} and λ_{hsk} are the orientation angles of the hinge vector.

$$
\begin{aligned}
\sigma_{hcs}(k) &= \left(\sigma_{ycs}(k)\cos\phi_{hsk} + \sigma_{zcs}(k)\sin\phi_{hsk}\right)\cos\lambda_{hsk} + \sigma_{xcsk}\sin\lambda_{hsk} \\
\delta_{fcs}(k) &= \delta_{cs}(k) + \sum_{j=1}^{N\,mod}\sigma_{hcs}(k,j)\,\eta(j)
\end{aligned}
\qquad (2.7.2)
$$

Where:

m_{ek}, I_{ek} are the mass and moment of inertia of engine (k) about its gimbal

a_{yek}, a_{zek} are the vehicle accelerations at engine (k) gimbal along the y and z axes.

F_{Yek}, F_{Zek} are the forces at engine (k) gimbal along the body y and z axes.

F_{Ysi}, F_{Zsi} are the slosh forces at tank (i) along the body y and z axes.

$\varphi_{zek}(j)$, $\varphi_{yek}(j)$ are the modal displacements for mode (j) at the engine (k) pivot, along the z and y axes respectively, in (ft/ft).

$\sigma_{zek}(j)$, $\sigma_{yek}(j)$ are the mode slopes of mode (j) at the engine (k) pivot, about z and y axes respectively, in units of (radians/ft).

$\varphi_{zsi}(j)$, $\varphi_{ysi}(j)$ are the modal displacements in (ft/ft) of mode (j) at the slosh mass (i) location.

$\varphi_{zcp}(j)$, $\varphi_{ycp}(j)$ are the mode displacements for mode (j) at the disturbance point in units of (ft/ft), (assuming that the disturbance is applied at a point).

$\varphi_{zasi}(j)$, $\varphi_{yasi}(j)$ are the mode displacements of mode (j) at the aero-surface (i) hinge, along the z and y axes respectively, in (ft/ft).

$\sigma_{zasi}(j)$, $\sigma_{yasi}(j)$ are the mode slopes of mode (j) at the aero-surface (i) pivot, about the z and y axes respectively, in (ft/ft).

η_j, ω_j are the generalized modal displacement, and mode frequency of mode (j)

$m_g(j)$ is the generalized mass for mode (j)

δ_{zek}, δ_{yek} are the deflections of engine (k) about z and y

$M_{hcs(k)}$ is the hinge moment due to aero forces at the surface (k) from equation (2.3-3)

$\delta_{fcs(k)}$ is the control surface deflection including flexibility from equation (2.3-3)

a_{zek} is the z-acceleration at the gimbal of engine (k) including flex

$a_{zs(l)}$ is the z-acceleration at the hinge of the control surface (l) including flex

$\sigma_{hcs(l)}$ is the modal slope at the center of the hinge line of surface (l) resolved about the hinge vector

ϕ_{hsk}, λ_{hsk} are the bank and sweep angles of the hinge vector

The bending modes are mainly excited by engine, aero-surface, and slosh forces. In the absence of aero-elastic data a bending mode is also excited by the aerodynamic forces created by surface deflections, equation (2.5.5), and they are applied at the center of the hinges. There are also forces generated at the gimbals and hinges due to variations in vehicle acceleration, from Equations (2.1.8 & 2.1.9). This model is obviously not as accurate as the aero-elastic model presented in Equation (2.7.4).

Modal Excitation Using GAFD and Inertial Flex Coupling Coefficients

Generalized Aerodynamic Force Derivatives and inertia coupling coefficients provide a more accurate modeling of the aero-elastic coupling between aerodynamics and structural flexibility and also the dynamic coupling between control surface accelerations and structural excitation. The GAFD data consists of three types of coefficients.

I.   A set of coefficients that define how the vehicle basic aerodynamic forces and moments, such as: C_Z, C_m, C_n, etc. are affected by flexibility, specifically, from the modal displacements (η_j), and the modal rates.

II.   Another set of coefficients define how the modal displacement variable (η_j) of a flex mode (j) from equation (2.3.1), is excited by the rigid vehicle motion, specifically by changes in the angles of attack and sideslip, body rates, control surface deflections, and by interactions with the other modes. Also by the rates of change of the above variables.

III.   The third set of coefficients are hinge moment coefficients. They define how the moment at the hinge of a control surface (i) is affected by changes in the vehicle angles of attack, sideslip, body rates, accelerations, modal displacements, modal rates, and also by the interactions with other control surface deflections (δ_{cs}) and rates. These coefficients are also be discussed in the Hinge Moment equations, Section (2.5.2).

The GAFD data are calculated using unsteady aerodynamic theory by post processing the generalized aerodynamic forces [Q_{ij}] which is an aerodynamic matrix obtained from the "Doublet Lattice" process. It requires a CFD model and a finite elements model. The [Q_{ij}] terms are also used for flutter and loads analysis. The generalized aerodynamic forces are complex matrices and they are functions of the vehicle Mach number, dynamic pressure, at reduced frequencies. The GAFD matrices are computed at specific frequencies that correspond to the modal frequencies plus one or two additional frequencies below the first flex mode. At each Mach number and reduced frequency a complex generalized force matrix is generated, a matrix for the real part and a matrix for the imaginary part. In flutter analysis, a Mach number and a reduced frequency is assumed and the flutter solution is calculated. For the development of a control analysis model, a single complex generalized aerodynamic force matrix, independent of frequency, is constructed by extracting the corresponding rows from the reduced frequency dependent matrices. The real part of this complex matrix consists of displacement coefficients and the imaginary part consists of the velocity coefficients. The inputs to the Doublet Lattice process are the modal data (mode shapes and mode frequencies) obtained from the finite elements model. The aerodynamic shape of the vehicle, including the fuselage, has been initially modeled by means of flat plates and the Doublet Lattice process calculates the generalized aerodynamic forces at different Mach numbers. When the fuselage is modeled as a slender body and an interference cylinder is included with the flat plates representing the lifting surfaces, adjustments can be made to the aero model to closely match measured data. For example, the rigid body aerodynamic derivatives, such as Cma, Cnb etc, derived from the Doublet Lattice output are compared with the aerodynamic derivatives obtained from wind tunnel data and appropriate model corrections are made. The program finally combines the FEM with the aerodynamic model and creates the Generalized Aerodynamic Forces, also known as the Q_{ij} matrix. The GAFD data used in the equations are extracted from the Q_{ij} matrix.

The aero-elastic model is more accurate because it is based on a detailed and more refined CFD aero-elastic model and it provides a more accurate formulation of flexibility and how it couples with aerodynamics. Equation (2.7.4), is similar to (2.7.1). It calculates the modal displacement (η_j) but the forcing functions from the control surfaces are calculated not by direct forces at the surface hinges, as in (2.7.1), but by using GAFD and h-parameters. The aero-elastic terms contribute to the modal excitation by the aerodynamic forces created as a result of the vehicle motion relative to wind (α_w, β_w, body rates), also the surface deflections $\delta_{s(k)}$), and also the rates of the above. The coefficients also include dynamic coupling with other modes (η_j).

$$m_g(j)\left(s^2 + 2\varsigma_j\omega_j s + \omega_j^2\right)\eta_j(s) =$$

$$+ \sum_{i=1}^{Nslosh}\left[F_{Xsi}\,\phi_{xs}(i,j) + F_{Ysi}\,\phi_{ys}(i,j) + F_{Zsi}\,\phi_{zs}(i,j)\right] \qquad Slosh\ Forces$$

$$+ \sum_{k=1}^{Neng}\left[F_{Xek}\,\phi_{xe}(k,j) + F_{Yek}\,\phi_{ye}(k,j) + F_{Zek}\,\phi_{ze}(k,j)\right] \qquad Engine\ Forces$$

$$- \sum_{k=1}^{Neng}\left[h_{ye}(k,j)\ddot{\delta}_{yek} + h_{ze}(k,j)\ddot{\delta}_{zek}\right] \qquad Engine\ Inert.Coupling$$

$$- \sum_{l=1}^{Nsurf} h_s(l,j)\ddot{\delta}_{cs(l)} \qquad Control\ Surf.Coupling$$

$$Aero - Elastic\ Terms$$

$$+ \overline{Q}\,S_{ref}^*\left[\begin{array}{l} + C_{\eta_j\alpha}\alpha_w + C_{\eta_j\beta}\beta_w + \left(\dfrac{l_{ch}^*}{2V_0}\right)\left(C_{\eta_j\dot\alpha}\dot\alpha_w + C_{\eta_j q}q\right) + \left(\dfrac{l_{ch}^*}{2V_0}\right)^2 C_{\eta_j\dot q}\dot q \\[2em] + \left(\dfrac{l_{sp}^*}{2V_0}\right)\left(C_{\eta_j\dot\beta}\dot\beta_w + C_{\eta_j p}p + C_{\eta_j r}r\right) + \left(\dfrac{l_{sp}^*}{2V_0}\right)^2\left(C_{\eta_j\dot p}\dot p + C_{\eta_j\dot r}\dot r\right) \\[2em] + \sum_{k=1}^{Nsurf}\left[C_{\eta(j)\delta(k)}\delta_{cs(k)} + \left(\dfrac{\overline{c}_{sk}}{2V_0}\right)C_{\eta(j)\dot\delta(k)}\dot\delta_{cs(k)}\right] + \sum_{i=1}^{N\mathrm{mode}}\left[C_{\eta(j)\eta(i)_i}\eta_i + \left(\dfrac{C_{\eta(j)\dot\eta(i)}}{V_0}\right)\dot\eta_i\right] \end{array}\right]$$

Equation (2.7.4) Bending Mode (j) Excitation Using GAFD and Inertial Coupling Coefficients

Where:

S^*_{ref}	is the surface reference area of the vehicle in (ft^2) used to scale the GAFD data.
l^*_{ch}, l^*_{sp}	are the chord and span reference lengths in (feet) used to normalize the GAFD data.
$\bar{c}_{sk}$	is the chord in (feet) of the control surface (k) used to normalize the GAFD data.
$\delta_{cs(k)}$	is the clockwise rotation in (radians) of a control surface (k) about its hinge vector. The rotation is only due to actuator displacement and it does not include structural flexibility.
$h_{s(k,j)}$	are the inertial coupling coefficients (h-parameters) in (lb-sec^2) which couple mode (j) excitation to surface (k) acceleration.
η_i	is the generalized modal displacement in (feet) of a flex mode (I).

The inertial coupling coefficients are the off-diagonal blocks in the mass matrix of the FEM that couple engine or surface accelerations with flexibility. They couple the angular acceleration of a control surface (k) to the excitation of a mode (j). This formulation is more accurate than equation (2.7.1), where the surfaces and nozzles are assumed to be rigid and the structure excitation is a result of inertial forces generated from rigid surface or nozzle accelerations. In Equation (2.7.4) the excitation of a mode (j) due to the control surface (k) accelerations is defined by the inertial coupling coefficients, or h-parameters $h_s(k,j)$. The mode is similarly excited by the pitch and yaw gimbal accelerations by the engine inertial coupling coefficients $h_{ye}(k,j)$ and $h_{ze}(k,j)$. This method is more accurate because it includes the flexibility of the effector itself and its interaction with the vehicle structure. Unlike equation (2.7.1) where the gimbaling engines and the control surfaces are separate bodies, in equation (2.7.4) the aero-elastic flex model includes the aero-surfaces with the hinges locked. The hinges in equation (2.7.4) are released by the h-parameters $h_s(l, j)$.

Note, in Equation (2.7.4) the aero-elastic coefficients were included only for the control surfaces. The inertia coupling, however, is implemented using h-parameters for both: surfaces and nozzles. Since the modal excitation due to engine and surface slewing is captured by the h-parameters, unlike equation (2.4.3), the engine forces in this case should include only the TVC and throttling terms, as shown in Equation (2.7.5), and they should exclude the inertial terms.

$$
\begin{array}{|l|}
\hline
F_{xe}(k) = T_{ek}\left(-\cos\Delta_{Z_k}\sin\Delta_{E_k}\delta_{yek} - \cos\Delta_{E_k}\sin\Delta_{Z_k}\delta_{zek} + \cos\Delta_{Z_k}\cos\Delta_{E_k}\,\delta T_{Thl_k}\right) \\
F_{ye}(k) = T_{ek}\left(-\sin\Delta_{Z_k}\sin\Delta_{E_k}\delta_{yek} + \cos\Delta_{E_k}\cos\Delta_{Z_k}\delta_{zek} + \sin\Delta_{Z_k}\cos\Delta_{E_k}\,\delta T_{Thl_k}\right) \\
F_{ze}(k) = -T_{ek}\left(\cos\Delta_{E_k}\delta_{yek} + \sin\Delta_{E_k}\delta T_{Thl_k}\right) \\
\\
\textit{where the Throttle Control}\quad \delta T_{Thl_k} = \left(\dfrac{\delta T_{ek}}{T_{ek}}\right) \\
\hline
\end{array}
$$

Equation (2.7.5) Engine Forces at the Gimbal due to Gimbaling and Throttling, Excluding the Inertial Terms

In the situation, however, where the gimbaling engines are assumed to be rigid enough to be modeled as separate bodies without h-parameters, then the engines should be implemented as in Equation (2.7.1), and the engine forces at the gimbals should be calculated from Equation (2.4.3) including the inertial forces.

2.8 Modeling Flexible Vehicle Interaction with Actuators

This section describes the interconnection and the dynamic coupling between the vehicle model and the actuators when the dynamic models include tail-wag-dog and load-torque feedback. Figure 2.8-1 shows the dynamic model of a flight vehicle that is controlled by three aerosurfaces (Elevon, Aileron, and Rudder), and each aerosurface is controlled by a separate actuator subsystem. A mixing-logic matrix receives the: roll, pitch and yaw acceleration demands from the flight control system and converts them to Elevon, Aileron and Rudder actuator commands. The actuator models used in our analysis are a little more complex than SISO transfer functions. In addition to the shaft control hydraulics they include the aerosurface inertia dynamics about the hinge. A shaft is driving the load dynamics through some stiffness and the aerosurface load is pivoting about a hinge. The actuator outputs in addition to deflection in (rad) they also include rate and rotational acceleration at the hinge. The gimbal acceleration inputs to the vehicle model produce the TWD dynamics. The actuator inputs, in addition to deflection command in (rad) they also include the external load torque at the hinges coming from the vehicle model. They feed-back to the actuator hinge moment inputs closing mechanical feedback loops, as shown in Figure 2.8-1. This load-torque is reacting against the actuator torque and the actuator control torque must be able to overcome it.
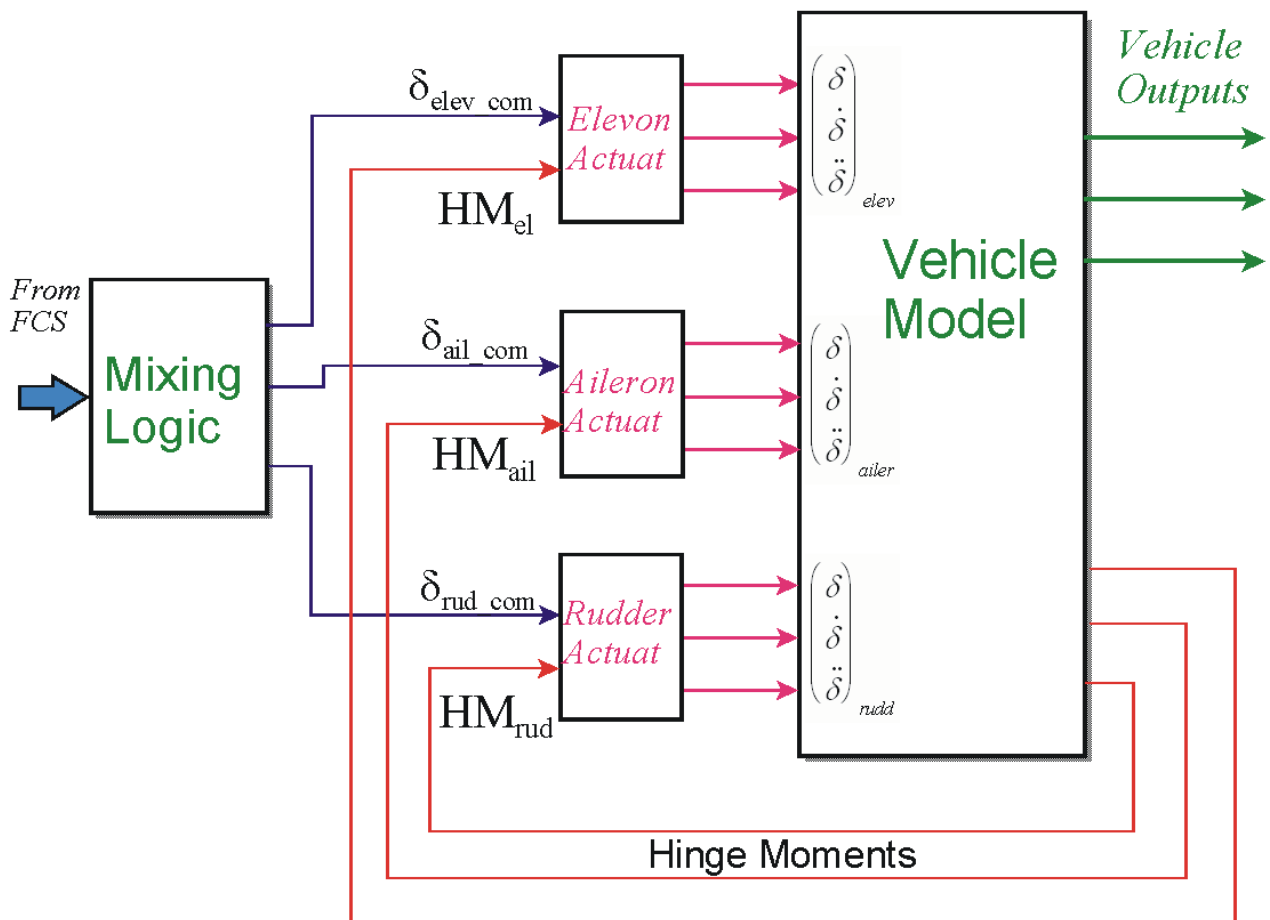

Figure (2.8.1) Block Diagram showing the interconnections between the Mixing Logic, the Vehicle and the Actuator dynamics

The dynamic interaction between actuator dynamics, the control system, non-linearities, and flexibility of the vehicle back-up structure and load, is very critical in the design because it affects performance and often causes "tail-wag-dog" type of oscillations if not properly implemented. Factors such as, hydraulic fluid compressibility, gimbal friction, nozzle or control surface flexibility, backup structure stiffness, load inertia, and other parameters should be included correctly in the actuator model and the analysis. It is a good practice, therefore, to keep the local resonant frequency at the hinge above the tail-wags-dog frequency. Figure (2.8.1) shows a typical vehicle and actuator interconnection consisting of three main elements: the vehicle model, the actuators (one actuator per control surface input), and the mixing logic that converts the FCS demands to deflection commands. The control surface deflection, rate, and acceleration outputs from the actuator model drive the vehicle dynamic model. The surface deflections generate the aero forces (or in the case of a gimbaling engine the TVC forces) that control the vehicle. The load accelerations create the tail-wag-dog forces. The rates create damping forces (not frequently used). The vehicle model creates hinge moment outputs at each hinge representing the external loading due to vehicle acceleration at the gimbals. They are undesirable because the actuator has to be powerful enough to "fight" against them. Each actuator model in addition to the deflection command it has a second HM input to receive the external load torques from the vehicle hinge moment outputs via a mechanical feedback loop. In the case of a TVC engine the vehicle model provides two load-torque outputs for pitch and yaw gimbaling.

The analyst must be very careful in selecting the stiffness coefficients in the actuator model in order to avoid double-booking them in both the actuator and the structural models. When modeling the servo system that controls the position of a surface or a nozzle relative to the vehicle it involves three types of stiffnesses, (a) the stiffness of the backup structure which is where the actuator is attached to the vehicle structure, (b) the actuator stiffness consisting of piston plus oil (or electrical) stiffness, and (c) the load stiffness due to flexing of the surface or nozzle. All three stiffnesses combine together to form a combined stiffness (K_T) that is associated with a resonance. When the analysis is based on rigid-body models the flexibility of the backup structure supporting the hinge can be included in the actuator model. In fact all three stiffnesses can be included and they will define the load resonance about the hinge as a function of the load moment of inertia and the combined stiffness coefficient (K_T). This implementation is useful in evaluating the actuator loop stability and performance because the flight control system interacts with the load dynamics, the actuator shaft, and the backup structure, and they often excite each other to instability, often due to stiction, backlash, and other non-linearities.

When structural flexibility is already included in the flexible vehicle model, including the actuator attachment, then it is no longer necessary to include the backup and load stiffnesses in the actuator because those resonances are already captured in the structural model by the modal data at the gimbal. The backup and load stiffnesses in the actuator model they should be set to infinity and only the actuator piston stiffness should be included in the actuator model. This applies in both cases: (a) when the flex model includes the control surfaces with the joints locked and released via the h-parameters, and (b) when the flex modes exclude the engine nozzles and the rigid engines are attached via the coupling equations. Actuator models which are intended to be used in rigid body vehicle models are referred to as "soft" because they include all three stiffnesses. A simplified soft actuator is shown in figure (2.8.2). The deflection (δ), rate, and acceleration outputs consist of: the rigid surface rotation, plus the additional deflection at the hinge caused by the combined structural compliance due to (K_T). The feedback loop in figure (2.8.2) represents the measurement of the actuator piston extension (x_{fb}) which is not exactly equal to the actual piston position (x_p) but it includes the backup structure and load deformation effects which corrupt the measurement. Under ideal conditions when those two stiffnesses are infinitely stiff, then the measurement ($x_{fb} = x_p$). In other words, the soft actuator captures the local resonance of an aero-surface about the hinge, or the so called "pendulum resonance" of a nozzle about its gimbal. The stiff actuator does not have it because the resonance is included in the Nastran model. In some cases it is okay to combine "soft" actuator models with flexible vehicle models when the backup and load stiffnesses in the finite elements model were taken out by setting them to very stiff values.

When the vehicle dynamic model includes inertial coupling coefficients (h-parameters), the actuator linkage dynamics are mechanized in the finite elements model. The backup stiffness and the load stiffness are also included in the flex model but the actuator piston is locked and the surfaces do not rotate at the hinges. The actuator is released in the simulation equations by the h-parameters $h_s(k,j)$. The h-parameters, also known as inertial coupling coefficients, are coupling the vehicle flexibility and surface accelerations. In this case the "stiff" actuators are used because the flexibility at the hinges is already captured in the flex model coefficients. Only the actuator piston stiffness in series with the oil stiffness (for hydraulic actuators), or in the case of an electro-mechanical actuator, the actuator shaft stiffness in series with the electrical stiffness, shown as K_{act} in figure (2.8.2), should be included in the "stiff" actuator model. In general, the actuator stiffness (K_{act}) is much larger than the total stiffness (K_T) used in the soft actuator model. Simple illustrations of "soft" and "stiff" types of actuator models are shown in figures (2.8.2 & 2.8.3).
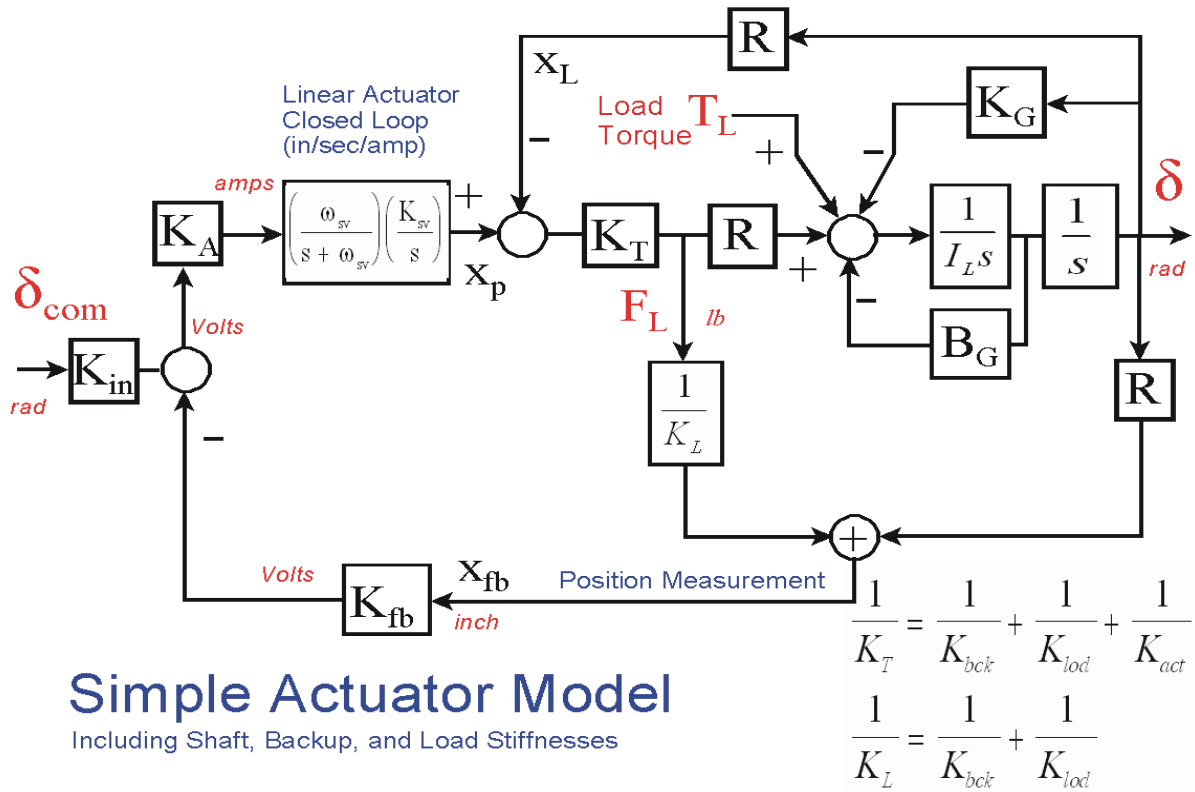
Simple Actuator Model
Including Shaft, Backup, and Load Stiffnesses

$$\frac{1}{K_T} = \frac{1}{K_{bck}} + \frac{1}{K_{lod}} + \frac{1}{K_{act}}$$

$$\frac{1}{K_L} = \frac{1}{K_{bck}} + \frac{1}{K_{lod}}$$

Figure (2.8.2) Soft Actuator Model that includes all three: Actuator, Backup, and Load Stiffnesses
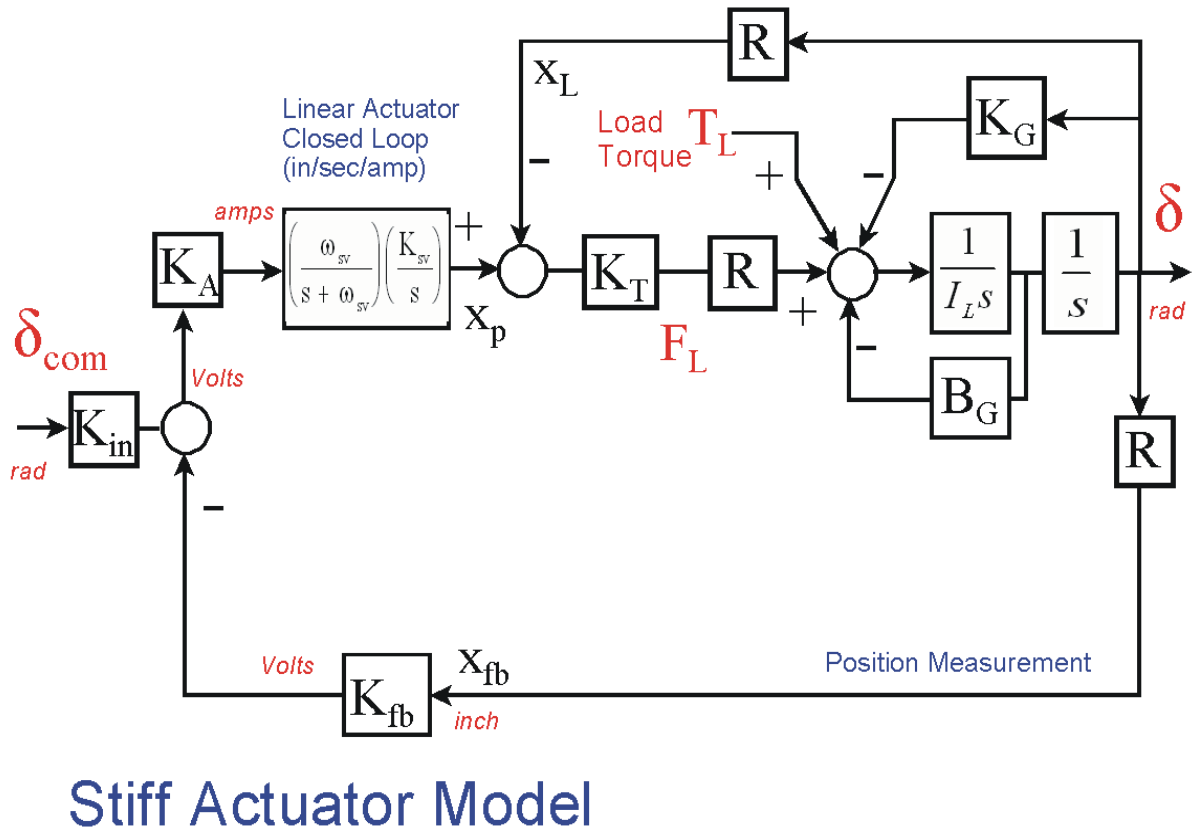

Stiff Actuator Model

Figure (2.8.3) Stiff Actuator Model that includes only the Shaft Stiffness in (K_T)

65

2.9 Modeling a Wind-Gust Disturbance

The air through which an aircraft flies is never still, and as a consequence, the wind causes disturbances on the flight vehicle, and its motion is always erratic. The total velocity of the vehicle relative to the air mass is obtained by the combination of two component vectors: a component due to the vehicle velocity relative to the earth, plus the velocity of the wind relative to the ground. The nature of those air disturbances is influenced by many factors, but it is usually turbulence which occurs in and around clouds, wind shears which are violent atmospheric phenomena caused due to severe downburst of air and sudden changes in the direction and velocity of the wind as the altitude changes, and gusts which are random, short duration sharp impulses of variations in wind velocity relative to the vehicle. In simulations, turbulence can be represented by a white noise generator passing through a low-pass second order filter. A wind-shear is a steady and persistent disturbance and it can be represented with a step in velocity filtered by a low-pass filter. A short wind gust W_{Gust} represents an unexpected change in the air-mass velocity in (feet/sec) with respect to the ground that must be added to the vehicle velocity relative to the ground. It can be defined by (1-cos) function.

$$w_G(t) = w_{Gust}\left(1 - \cos(\omega_G t)\right)$$

The wind disturbance causes variations in the angles of attack and sideslip (α_w and β_w) of the vehicle relative to the airflow, in comparison with the steady-state trim angles without the wind (α_0 and β_0). It also changes the magnitude and direction of the vehicle velocity relative to the air-mass (δV_w).
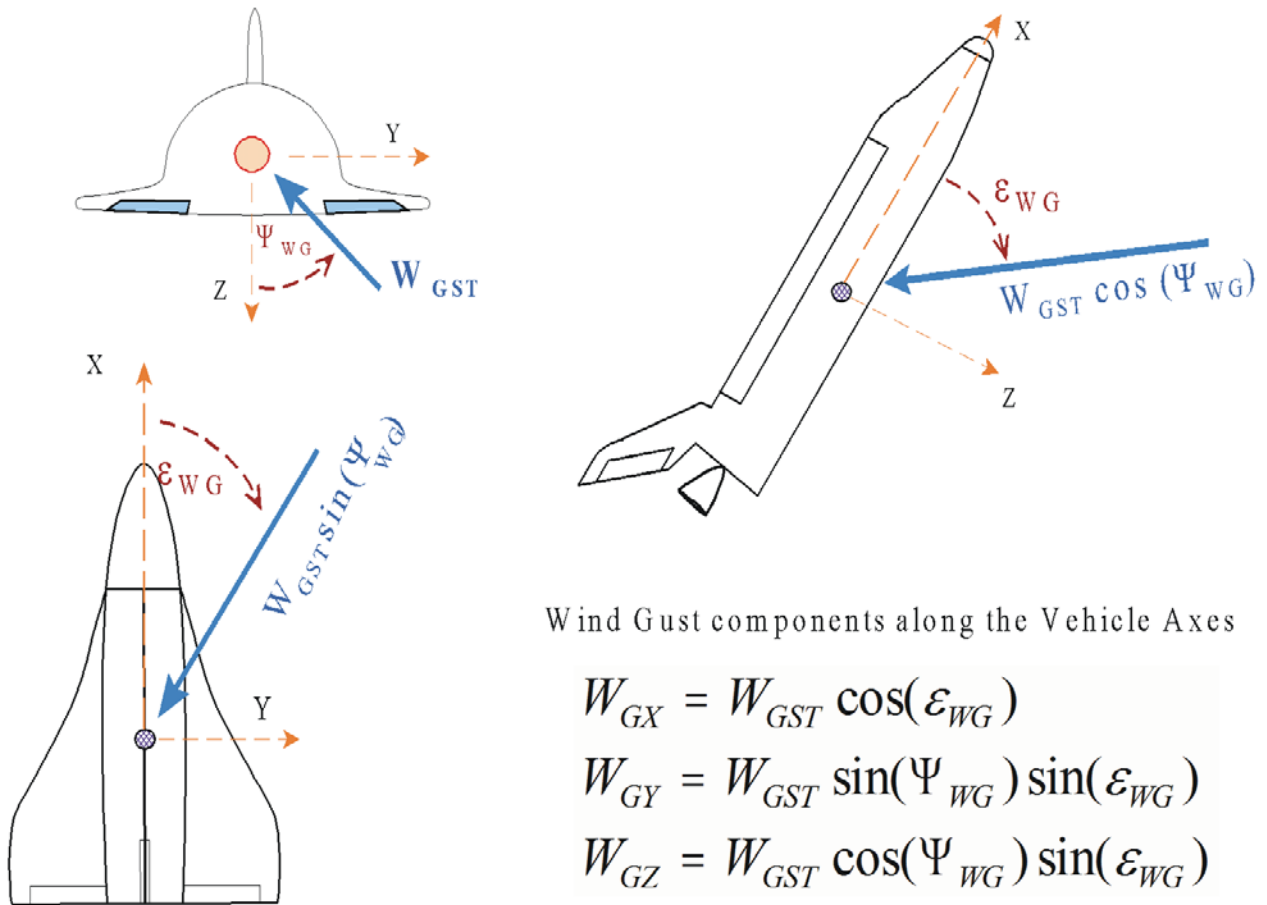

Wind Gust components along the Vehicle Axes

$$W_{GX} = W_{GST} \cos(\varepsilon_{WG})$$

$$W_{GY} = W_{GST} \sin(\Psi_{WG}) \sin(\varepsilon_{WG})$$

$$W_{GZ} = W_{GST} \cos(\Psi_{WG}) \sin(\varepsilon_{WG})$$

Figure 2.9.1 Wind-Gust velocity vector W$_{GST}$ is resolved along the vehicle body axes

66

The velocity and direction of the winds vary considerably with seasons and altitude. Prior to launching a vehicle the average wind velocity above and around the launch site is measured at different altitudes by releasing weather balloons, and the wind data received are used to adjust the vehicle trajectory in order to maximize performance.

In this model, the wind direction relative to the vehicle body axes is fixed and it is defined by two angles: an elevation angle (ε_{WG}) of the wind vector with respect to the vehicle x axis, and an azimuth angle (Ψ_{WG}) which is the angle between the vehicle z axis and the projection of W_{GST} in the y-z plane, see Figure 2.9.1. The gust vector W_{Gust} can then be resolved in three velocity components (W_{GX}, W_{GY}, and W_{GZ}) along the vehicle body axes, as shown in this Figure 2.9.1.

In a typical airplane, for example, when the elevation gust angle ($\varepsilon_{WG} = 0$) means that the wind gust direction is coming head-on towards the vehicle, along the -x axis. When the azimuth and elevation angles are both equal to 90 degrees, it means that the wind gust direction is coming toward the pilot from the right side along the -y axis. When $\Psi_{WG}=0$ and $\varepsilon_{WG}=90$ degrees, it means that the gust is coming from the bottom of the aircraft along the -z axis, towards the pilot's feet.

Change in Angle of Sideslip

$$\beta_w = \beta + \beta_g \quad where$$

$$\beta_g = \tan^{-1}\left\{ \frac{W_{GY} \cos\beta_0}{V_0 \cos\alpha_0 + W_{GY} \sin\beta_0} \right\}$$

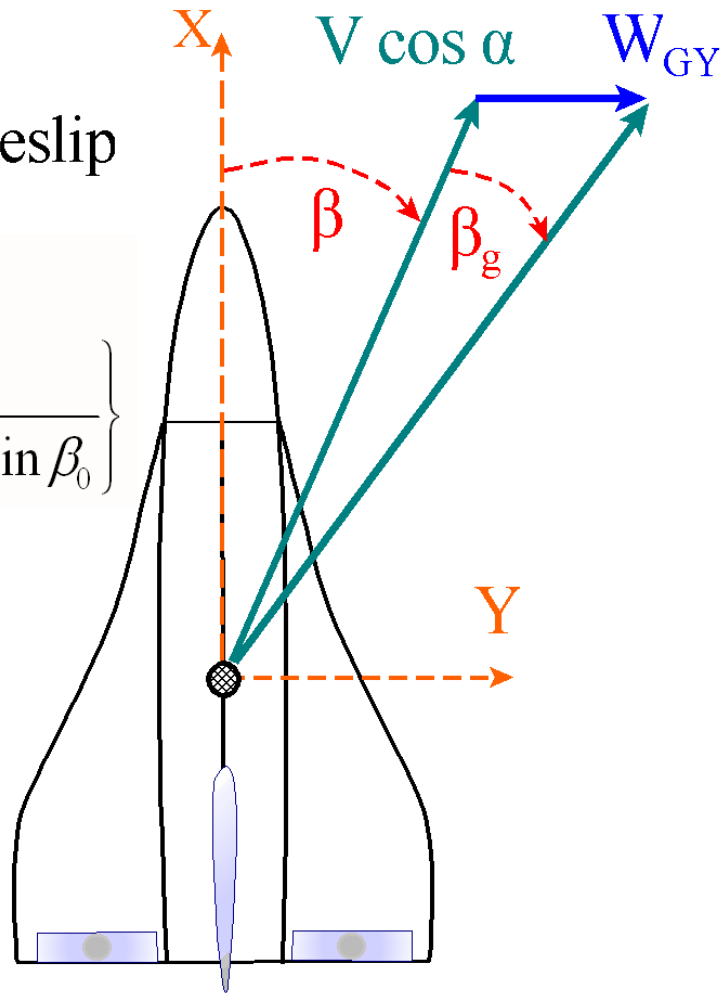**Figure 2.9.2 Change in the Angle of Sideslip due to the Wind-Gust**

The angles of attack and sideslip (α, β) are calculated in equations 2.1.5 from the normal and lateral velocity relative to earth alone, assuming that the air mass is not moving. In the presence of wind, however, the angles of attack and sideslip and also the vehicle velocity are modified to: (α$_w$, β$_w$ and δV$_w$) relative to the airflow. The equations in Figures (2.9.2 and 2.9.3) calculate the total angles of attack and sideslip relative to the air mass which includes the effects of the gust velocity. Instead of (α, β, and δV), the variables (α$_w$, β$_w$, and δV$_w$) which include the wind effect are used in equations (2.5.4 and 2.5.7) to calculate the total aerodynamic forces and moments acting on the vehicle.

Change in Veleocity

$$\delta V_W = \delta V + W_{GX} \cos\alpha + W_{GZ} \sin\alpha$$

Total Angle of Attack

$$\alpha_w = \alpha + \alpha_g$$
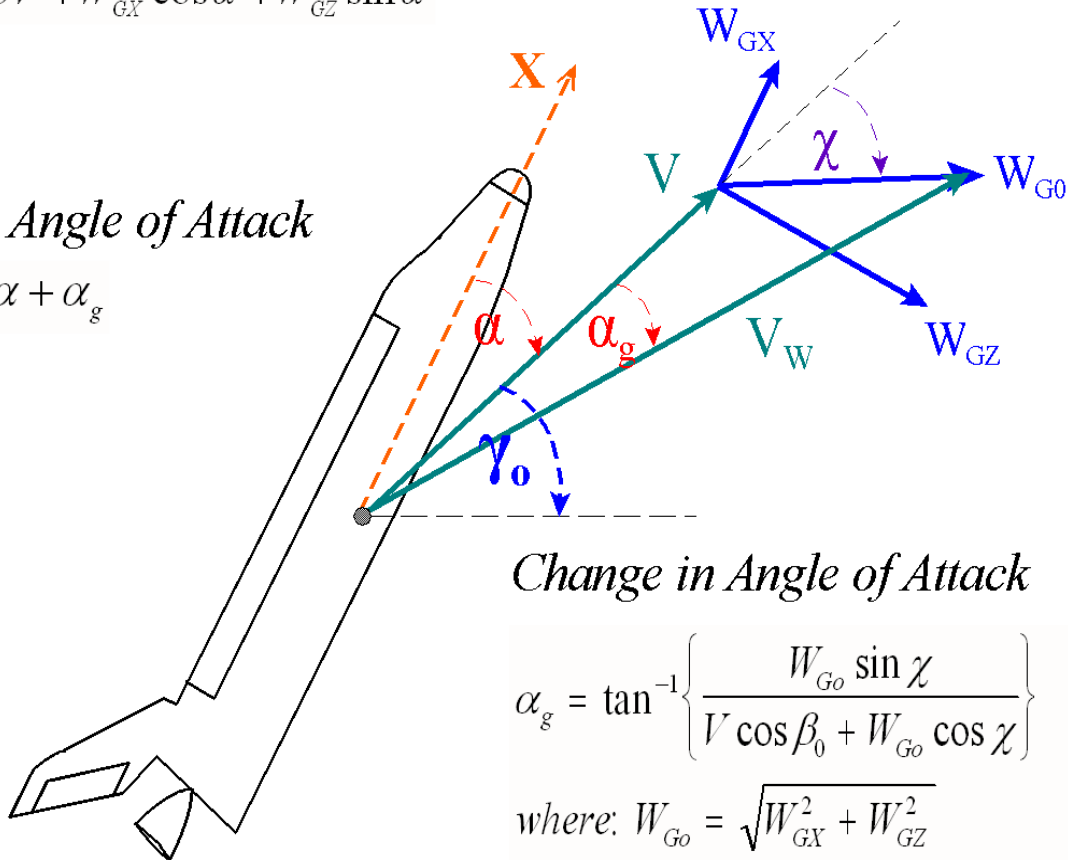
Change in Angle of Attack

$$\alpha_g = \tan^{-1}\left\{\frac{W_{Go} \sin\chi}{V \cos\beta_0 + W_{Go} \cos\chi}\right\}$$

$$\text{where: } W_{Go} = \sqrt{W_{GX}^2 + W_{GZ}^2}$$

$$\chi = \tan2^{-1}\left(W_{GZ}, W_{GX}\right) - \alpha_0$$

Figure 2.9.3 Changes in the vehicle Angle of Attack and Air-Speed due to the Wind-Gust

68

2.10 Load-Torques

The linear and angular accelerations of the vehicle generate disturbance torques at the engine gimbals or at the hinges of the aerosurfaces. The actuator device, which is either hydraulic or electro-mechanical position control servo, must have the control torque capability to overcome friction, load inertia and to react against the externally generated load-torques in order to position the engine or aerosurface at the angle commanded by the flight control system. This external loading on the actuator, in launch vehicles is referred to as "*Actuator Load-Torque*" or sometimes "*Dog-Wags-Tail*". In aircraft it is called "*Hinge Moments*".

The vehicle accelerations at the hinges consist of both: rigid body and flex components due to local vibrations. For preliminary control analysis we do not include tail-wags-dog and load-torque dynamics in the vehicle model, often because the information is not yet available. In Flixan we set the effector flags in the vehicle input data to "NO TWD". Later on, when the design matures, we can turn on the TWD/ Load-Torque option by setting the flag to "WITH TWD" in the effector data. When the flag is set to "With TWD/load-torque", the vehicle model includes the required inputs and outputs that enable it to be properly combined with the actuator models. It includes gimbal rates and acceleration inputs in addition to gimbal deflections for each engine and aerosurface that enable the implementation of the tail-wag-dog dynamics in the vehicle model. It also provides load-torque outputs for each effector that is fed back to the corresponding actuator for the implementation of the load-torque feedback loop, as shown in Figure 2.8.1. Otherwise, if the flag is set to "NO TWD" those additional inputs and outputs are not included in the dynamic model and in this case a simple transfer function is sufficient for modeling the actuator.

2.10.1 Load Torques at the Nozzle Gimbal

We will examine the load-torques for the engine nozzles and for the control surfaces separately, beginning with the load-torques at an engine gimbal. We will consider two methods of implementing flexibility in the load-torque equations, similar to the approach taken in the equations modeling the structural flexibility. That is, a simple method that does not require h-parameters and a more refined approach that includes the h-parameters. In the first case we assume that the engines are rigid and they are dynamically coupled with a flexible vehicle that does not include the engines in the structural model. In the second case the engines are included in the finite elements model rigidly attached at the gimbals and the reaction load torques are calculated via the pitch and yaw inertial coupling coefficients: $h_{ye}(k,j)$ and $h_{ze}(k,j)$.

Rigid Engine Coupling with Flexible Vehicle

The first implementation is shown in equation 2.10.1a, where: $T_{LYe(k)}$, $T_{LZe(k)}$ are the load torques due to vehicle motion in pitch and yaw axes at the gimbal of the kth engine.

$$
\begin{aligned}
T_{LYe(k)} &= m_{ek}\, l_{ek} \left[V \cos\alpha\, \dot\gamma - a_{Zek} \cos\Delta_{Yek} - a_{Xek} \sin\Delta_{Yek} \right] - I_{ek}\left[\dot q + \sum_{j=1}^{Nm} \sigma_{Ye(k,j)} \ddot\eta_j \right] \\
\\
T_{LZe(k)} &= m_{ek}\, l_{ek} \left[a_{Yek} \cos\Delta_{Zek} - a_{Xek} \sin\Delta_{Zek} \right] \quad - I_{ek}\left[\dot r + \sum_{j=1}^{Nm} \sigma_{Ze(k,j)} \ddot\eta_j \right]
\end{aligned}
$$

(2.10.1a)

For small variations about trim conditions the load-torque equations become:

$$T_{LYe}(k) = m_{ek} l_{ek} \begin{bmatrix} V_0 \cos\alpha_0 (q - \dot{\alpha}) - a_{zek} \cos\Delta_{Ek} - a_{xek} \sin\Delta_{Ek} \cos\Delta_{Zk} \\ + A_Z \sin\Delta_{Ek}\delta_{yek} + A_X \left(\sin\Delta_{Ek} \sin\Delta_{Zk}\delta_{zek} - \cos\Delta_{Ek} \cos\Delta_{Zk}\delta_{yek} \right) \end{bmatrix}$$

$$- I_{ek} \left[\dot{q} + \sum_{j=1}^{N\,\text{mod}} \sigma_{ye}(k,j)\ddot{\eta}(j) \right]$$

$$T_{LZe}(k) = m_{ek} l_{ek} \left[a_{yek} \cos\Delta_{Zk} - a_{xek} \sin\Delta_{Zk} - \left(A_X \cos\Delta_{Zk} + A_Y \sin\Delta_{Zk} \right)\delta_{zek} \right]$$

$$- I_{ek} \left[\dot{r} + \sum_{j=1}^{N\,\text{mod}} \sigma_{ze}(k,j)\ddot{\eta}(j) \right]$$

Equation 2.10.1 Variations in Pitch and Yaw Load-Torques at Engine (k) Gimbal

Where:

a_{xek}, a_{yek}, a_{zek}	are the vehicle accelerations at k^{th} gimbal along x, y, z, including flexibility
Δ_{Ek} and Δ_{Zk}	are the pitch and yaw trim angles of kth engine as defined in Figure 2.4.4
I_{ek}, m_{ek}	are the kth engine mass and engine moment of inertia about the gimbal
L_{ek}	is the moment arm between the kth engine gimbal and engine CG
$\sigma_{ye(k,j)}$, $\sigma_{ze(k,j)}$	are the pitch and yaw modal slopes of mode j at the kth engine

$$a_{xe}(k) = \ddot{x}_{CG} + l_{Zek}\dot{q} - l_{Yek}\dot{r} + \sum_{j=1}^{Nm} \phi_{xe}(k,j)\ddot{\eta}(j)$$

$$a_{ye}(k) = \ddot{y}_{CG} + l_{Xek}\dot{r} - l_{Zek}\dot{p} + \sum_{j=1}^{Nm} \phi_{ye}(k,j)\ddot{\eta}(j)$$

$$a_{ze}(k) = \ddot{z}_{CG} + l_{Yek}\dot{p} - l_{Xek}\dot{q} + \sum_{j=1}^{Nm} \phi_{ze}(k,j)\ddot{\eta}(j)$$

Vehicle Accelerations at the gimbal

- The first term in the pitch equations 2.10.1 is the load torque on the actuator due to changes in the flight path angle, caused by the centripetal force: $mV\dot{\gamma}$. It's negative because $\dot{\gamma}$ is negative and it becomes significant towards the end of second stage because V is high.
- The second set of terms is the torque generated by the coupling of vehicle translational accelerations A_X and A_Z and the pitch and yaw engine deflections δ_{yek} and δ_{zek} from the trim angles Δ_{Ek} and Δ_{Zk}, see equations 2.4.2. The deflections consist of rigid rotation plus rotational bending at the gimbal.
- The last set of terms in equations 2.10.1 is the reaction torque generated by the rotational acceleration of the vehicle at the gimbal. The nozzle inertia produces a reaction torque against the actuator (minus sign). The acceleration is a combination of rigid rotation plus rotational bending at the gimbal.

Figure 2.8.1 shows the load-torque feedback loop for a vehicle with three aerosurfaces. This is a mechanical loop from the control surface hinge moments outputs generated by the vehicle model to the actuator load-torque inputs.

- Each actuator has two inputs: the first input (δ_{comd}) comes from the TVC mixing logic which converts the roll, pitch, and yaw flight control system demands to actuator deflection commands, and the second input is the load-torque that receives the hinge moment feedback from the vehicle model.
- Each actuator has three outputs: engine deflections in (rad), engine rates in (rad/sec), and engine accelerations in (rad/sec^2). The actuator outputs connect to the inputs to the vehicle model. One actuator per aerosurface or two actuators per TVC engine (pitch and yaw).

The engine accelerations are important for the implementation of TWD dynamics. The rates provide aero damping forces in the control surfaces. The positions generate the aerodynamic forces. Detail actuator models are described in Section 4.

Engine Load-Torque using Inertial Coupling Coefficients

When the pitch and yaw inertial coupling coefficients $h_{ye}(k,j)$ and $h_{ze}(k,j)$ for the engine nozzles are available, the load-torque equations are modified as shown in Equation 2.10.2. In this case the torque due to flexibility at the gimbal is captured by the inertial coupling coefficients and this is a more accurate representation than Equation 2.10.1, where the rigid aerosurfaces is coupled via the modal slopes at the support structure.

$$
\begin{aligned}
T_{LYe}(k) = m_{ek}\, l_{ek} &\left[\begin{array}{l} V_0 \cos\alpha_0 (q-\dot\alpha) - a_{ze(k)} \cos\Delta_{Ek} - a_{xe(k)} \sin\Delta_{Ek}\cos\Delta_{Zk} \\ + A_Z \sin\Delta_{Ek}\delta_{ye(k)} + A_X\left(\sin\Delta_{Ek}\sin\Delta_{Zk}\delta_{ze(k)} - \cos\Delta_{Ek}\cos\Delta_{Zk}\delta_{ye(k)} \right) \end{array} \right] \\
&- I_{ek}\,\dot q - \sum_{j=1}^{N\,\mathrm{mod}} h_{ye}(k,j)\,\ddot\eta(j) \\
T_{LZe}(k) = m_{ek}\, l_{ek} &\left[a_{ye(k)} \cos\Delta_{Zk} - a_{xe(k)} \sin\Delta_{Zk} - \left(A_X \cos\Delta_{Zk} + A_Y \sin\Delta_{Zk} \right)\delta_{ze(k)} \right] \\
&- I_{ek}\,\dot r - \sum_{j=1}^{N\,\mathrm{mod}} h_{ze}(k,j)\,\ddot\eta(j)
\end{aligned}
$$

Equation 2.10.2 Pitch and Yaw Load-Torque Variations Using Inertial Coupling Coefficients (h$_{ye}$)

The dynamic coupling between structure and load-torque in this case is included in the h-parameters and the FEM. The linear accelerations at the gimbals, therefore, should not include flexibility:

$$
\begin{aligned}
a_{xe}(k) &= \ddot x_{CG} + l_{Zek}\,\dot q - l_{Yek}\,\dot r \\
a_{ye}(k) &= \ddot y_{CG} + l_{Xek}\,\dot r - l_{Zek}\,\dot p \\
a_{ze}(k) &= \ddot z_{CG} + l_{Yek}\,\dot p - l_{Xek}\,\dot q
\end{aligned}
$$

Accelerations at the Engine Gimbals without Flex

2.10.2 Hinge Moments at the Aerosurfaces

The moment generated at the hinge of a control surface as a result of actuator and vehicle motion is similar in nature to load-torque at the engine gimbal. In the Flixan program the hinge moments are implemented using two different approaches: a simple method and a more complex one that requires h-parameters and GAFD data. In the first approach we assume that the aerosurfaces are rigid panels that interact with a flexible vehicle by the aerodynamic and reaction forces generated at the hinges. The second method is more efficient because it is based on a finite elements model that includes the aerosurfaces with the hinges locked. It uses inertial coupling coefficients to calculate the inertial moments due to aerosurface slewing and hinge moment coefficients obtained from a GAFD model.

Rigid Surfaces Coupled with a Flex Vehicle

The first method assumes that each aerosurface is rigid and it is attached to the corresponding node of the flexible structure and flexibility at the attachment is captured by the modal slope (σ_{hsk}) at the hinge. Their mass properties must not be included in the vehicle mass properties and in the structural models. The moment at the hinge of the control surface is produced by the vehicle translational and rotational accelerations at the hinge, including flexibility. There are also contributions due to variations in the angles of attack and sideslip and their rates. It is also affected by the aerosurface deflection and rate, as shown in Equation 2.10.3.

$$
\begin{aligned}
M_{hs}(k) = {} & m_{sk} l_{hsk} \cos\left(\Delta_{sk}\right)\left[a_{Ns}(k) - \dot{V}_o \delta_{fcs}(k)\right] - m_{sk} l_{hsk} a_{Xs}(k) \sin\left(\Delta_{sk}\right) \\
& + m_{sk} l_{hsk} V_0\left(q - \dot{\alpha}\right) - I_{hsk} \dot{W}_{sk} - \sum_{j=1}^{N\,\text{mod}}\left[I_{hcsk}\sigma_{hs}(k,j)\ddot{\eta}(j)\right] \\
& + \overline{Q} S_{sk} \overline{c}_{sk}\left\{C_{h\alpha k}\alpha_w + C_{h\beta k}\beta_w + C_{h\delta k}\delta_{fcs(k)} + \left(\frac{l_{ch}}{2V_0}\right)C_{h\dot{\alpha}k}\dot{\alpha}_w + \left(\frac{l_{sp}}{2V_0}\right)C_{h\dot{\beta}k}\dot{\beta}_w + \left(\frac{\overline{c}_{sk}}{2V_0}\right)C_{h\dot{\delta}k}\dot{\delta}_{fcs(k)}\right\}
\end{aligned}
$$

Equation (2.10.3) Hinge Moment Variations at a Control Surface Hinge

Where:

W_{sk}	is the vehicle rate resolved parallel to the hinge vector of control surface (k).
$a_{Ns(k)}$	is the vehicle acceleration at the hinge line perpendicular to the control surface (k), as defined in equation 2.10.4.
S_{sk}, c_{sk}	are the aero-surface reference area in (ft^2) and its reference length in (ft). They are defined in the aero data and are used to normalize the hinge moment coefficients.
$\phi_{hsk}, \lambda_{hsk}$	are the kth aerosurface hinge vector bank and sweep angles.

$$
\begin{aligned}
\dot{W}_{sk} &= \left[\cos\phi_{hsk}\dot{q} + \sin\phi_{hsk}\dot{r}\right]\cos\lambda_{hsk} + \dot{p}\sin\lambda_{hsk} \\
a_{Ns}(k) &= a_{Ys}(k)\sin\phi_{hsk} - a_{Zs}(k)\cos\phi_{hsk}
\end{aligned}
\qquad (2.10.4)
$$

- The first three terms on the right hand side of the hinge moment equation are reaction moments at the hinge of the kth control surface due to vehicle linear acceleration at the hinge.
- The fourth term represents the moment generated by the centripetal force due to the variation in flight path angle (γ).
- The fifth term is a reaction moment due to the vehicle angular acceleration $\dot{W}_{sk}$ resolved about the kth hinge vector.
- The sixth term is also a reaction moment due to vehicle rotational bending at the hinge of the control surface.
- The last term represents variations in aerodynamic loading at the hinge due to variations in the angles of attack and sideslip (relative to the wind), the aerosurface deflection, and the rates of those variables.
- The surface deflections $\delta_{fcs}(k)$ include also structural flexibility components as defined in equation 2.5.6.

The modal slope (σ_{hsk}) about the hinge vector of a control surface (k) is defined as a function of the hinge orientation angles and the modal slopes about x, y, z, as in equation 2.10.5

$$\sigma_{hsk} = \left(\cos\phi_{hsk}\,\sigma_{ysk} + \sin\phi_{hsk}\,\sigma_{zsk}\right)\cos\lambda_{hsk} + \sin\lambda_{hsk}\,\sigma_{xsk} \tag{2.10.5}$$

The vehicle acceleration along x, y, and z, at the mid-point of the kth hinge line is defined by equation 2.10.6. The accelerations include structural accelerations.

$$
\begin{aligned}
a_{xcs}(k) &= \ddot{x}_{CG} + l_{Zsk}\,\dot{q} - l_{Ysk}\,\dot{r} + \sum_{j=1}^{Nm}\phi_{xcs}(k,j)\,\ddot{\eta}(j) \\[2mm]
a_{ycs}(k) &= \ddot{y}_{CG} + l_{Xsk}\,\dot{r} - l_{Zsk}\,\dot{p} + \sum_{j=1}^{Nm}\phi_{ycs}(k,j)\,\ddot{\eta}(j) \\[2mm]
a_{zcs}(k) &= \ddot{z}_{CG} + l_{Ysk}\,\dot{p} - l_{Xsk}\,\dot{q} + \sum_{j=1}^{Nm}\phi_{zcs}(k,j)\,\ddot{\eta}(j)
\end{aligned}
\tag{2.10.6}
$$

The moment arms between the hinge line of an aerosurface (k) and the vehicle CG are defined in the following equations:

$$l_{XSk} = X_{Sk} - X_{CG} \qquad l_{YSk} = Y_{Sk} - Y_{CG} \qquad l_{ZSk} = Z_{Sk} - Z_{CG} \tag{2.10.7}$$

Using GAFD and Inertial Coupling Coefficients

A more accurate representation of the hinge moments can be obtained when the inertial coupling coefficients and hinge moments coefficients are available from GAFD data, as shown in equation 2.10.8. The mass properties and finite elements model include the aerosurfaces in this case, and the hinge moments due to aerosurfaces slewing is calculated by the inertial coupling coefficients $h_{s(k,j)}$.

The hinge moment coefficients are obtained from the GAFD model and they include terms due to the angles of attack and sideslip variations relative to the airflow, including rates. There are also hinge moment contributions due to the vehicle angular rates and accelerations, surface deflections and rate of deflections, and terms due to flex mode excitations (η_j) and rates.

$$
\begin{aligned}
M_{hs}(k) =\ & m_{sk}l_{hsk}\cos(\Delta_{sk})\left(a_{Ns}(k) - \dot{V}_o\delta_{cs}(k)\right) - m_{sk}l_{hsk}a_{Xs}(k)\sin(\Delta_{sk}) \\
& + m_{sk}l_{hsk}V_0(q - \dot{\alpha}) - I_{hsk}\dot{W}_{sk} - \sum_{j=1}^{N\,\mathrm{mod}}\left[h_s(k,j)\ddot{\eta}(j)\right] \\
& + \overline{Q}S_{sk}\overline{c}_{sk}\left[C_{h\alpha k}\alpha_w + C_{h\beta k}\beta_w + \left(\frac{l_{ch}^*}{2V_0}C_{h\dot{\alpha}k}\dot{\alpha}_w + \frac{l_{sp}^*}{2V_0}C_{h\dot{\beta}k}\dot{\beta}_w\right)\right] \\
& + \overline{Q}S_{sk}\overline{c}_{sk}\left[\left(\frac{l_{ch}^*}{2V_0}C_{hkq}q + \frac{l_{sp}^*}{2V_0}(C_{hkp}p + C_{hkr}r)\right) + \left(\left(\frac{l_{ch}^*}{2V_0}\right)^2 C_{hk\dot{q}}\dot{q} + \left(\frac{l_{sp}^*}{2V_0}\right)^2(C_{hk\dot{p}}\dot{p} + C_{hk\dot{r}}\dot{r})\right)\right] \\
& + \overline{Q}S_{sk}\overline{c}_{sk}\sum_{l=1}^{NSurf}\left[C_{h\delta(k,l)}\delta_{cs}(l) + \left(\frac{\overline{c}_{s(l)}}{2V_0}\right)C_{h\dot{\delta}(k,l)}\dot{\delta}_{cs}(l)\right] \\
& + \overline{Q}S_{sk}\overline{c}_{sk}\sum_{j=1}^{NMode}\left[C_{h\eta(k,j)}\eta(j) + \left(\frac{C_{h\dot{\eta}(k,j)}}{V_0}\right)\dot{\eta}(j)\right]
\end{aligned}
$$

Equation (2.10.8) Hinge Moments at the Control Surfaces, using GAFD derived Hinge Moment and Inertial Coupling Coefficients

Where:

S_{sk} is the reference area in (ft^2) of a control surface (k), used to normalize the GAFD data.

c_{sk} is the reference length of a control surface (k) in (ft), used to normalize the GAFD.

δ_{csk} is the clockwise rotation of the control surface (k) about the hinge vector. It does not include structural flexibility at the hinge.

$l_{sp}\ l_{ch}$ are the reference lengths in (feet) used to normalize the GAFD data. They are normally equal to the vehicle span (l_{sp}) and mean aero chord (l_{ch}) used in the aero equations.

$h_{s(k,j)}$ is the inertial coupling coefficient that couples the flex mode (j) generalized acceleration to the hinge moment at surface (k). In matrix form it is the transpose of the h-parameters matrix used in equation (3.9.4).

W_{sk} is the vehicle rate resolved parallel to the hinge vector of control surface (k).

$a_{Ns(k)}$ is the vehicle acceleration at the hinge line perpendicular to the control surface (k), as defined in equation (2.10.4).

74

The angles {ϕ_{hsk} and λ_{hsk}) are the bank and sweep angles that define the orientation of the control surface hinge vector with respect to the vehicle axes, as shown in Figure 2.5.3.

$$\begin{array}{|l|}\hline \dot{W}_{sk} = \left[\cos\phi_{hsk}\dot{q} + \sin\phi_{hsk}\dot{r}\right]\cos\lambda_{hsk} + \dot{p}\sin\lambda_{hsk} \\ a_{Ns}(k) = a_{Ys}(k)\sin\phi_{hsk} - a_{Zs}(k)\cos\phi_{hsk} \\ \hline \end{array}$$
(2.10.9)

The vehicle accelerations along x, y, and z, at the mid-point of the kth hinge line is defined by equation 2.10.10. Notice that the linear accelerations do not include the flex contributions because the flexibility coupling at the hinge moments is captured by the inertial coupling coefficients $h_s(k,j)$. Also the control surface deflections and rates {$\delta_{cs}(k), \dot{\delta}_{cs}(k)$} in this case are relative to the hinge and they do not include deformation at the hinge because it is already included in the flex implementation.

$$\begin{array}{|l|}\hline a_{xcs}(k) = \ddot{x}_{CG} + l_{Zsk}\dot{q} - l_{Ysk}\dot{r} \\ a_{ycs}(k) = \ddot{y}_{CG} + l_{Xsk}\dot{r} - l_{Zsk}\dot{p} \\ a_{zcs}(k) = \ddot{z}_{CG} + l_{Ysk}\dot{p} - l_{Xsk}\dot{q} \\ \hline \end{array}$$
(2.10.10)

References

- Subsonic GAFD Theory, The Doublet Lattice Method, Subsonic Unsteady Aero For General Configurations, by Giesing, Kalman and Rodden. Computer Program N5KA. Technical Report: AFFDL-TR-71-5, Part II, Vol II, April 1972.
- Supersonic GAFD Theory. The Piston Element Method. Second Order Theory of Ashley and Zartarian. AIAA Journal, Vol 23, No 12, Dec 1956.
- User's Guide, MSC/Nastran Aeroelastic Analysis – Version 68, by William P. Rodden and Erwin H. Johnson, October 1994.
- Rodden, W. P. and Giesing, J. P. "Application of Oscillatory Aerodynamic Theory to estimation of Dynamic Stability Derivatives", AIAA Journal of Aircraft Engineering Notes, Vol. 7, No.3, May-June 1970 pages 272 to 275.
- H. Norman Abramson "The Dynamic Behavior of Liquids in Moving Containers with Applications to Space Vehicle Technology", NASA SP-106

2.11 Output Variables

The output variables represent vehicle sensor measurements. They are functions of the dynamic model states, including structural flexibility. They are used for modeling sensor characteristics, implementing guidance and control laws in simulations, and also in dynamic models for control analysis and design. They consist of Euler angle attitude measurements, rate gyros, accelerometers, altitude and velocity sensors, cross-range velocity, and angles of attack and sideslip, (α_w & β_w) sensors relative to the airflow. The following equations describe the sensor measurements as a function of vehicle states.

2.11.1 Vehicle Attitude, Euler Angles

The Euler angles (Φ, Θ, Ψ) are used to define the orientation of the vehicle body axes relative to an earth bounded reference axes or to a local-vertical-local-horizontal (LVLH) frame. They are calculated by integrating a set of kinematic differential equations, which are functions of the body rates, and used in 6-DOF simulations. There are 12 sets of kinematic equations that can be used to calculate the Euler angles by integrating functions of the body rates. Their derivation depends on the chosen rotational sequence. The Euler angles, however, are not suitable for large angle maneuver simulations because they are vulnerable to singularities. Quaternions are a better choice for modeling attitude, because they do not have singularities, but quaternions are beyond our scope. The analyst must choose a set of Euler equations that will prevent singularities in the range of attitudes of a particular application.

$$1-2-3 \; Rotation$$
$$\dot{\Phi} = P + \tan\Theta \left(Q\sin\Phi + R\cos\Phi \right)$$
$$\dot{\Theta} = Q\cos\Phi - R\sin\Phi \qquad \dot{\Psi} = \frac{Q\sin\Phi + R\cos\Phi}{\cos\Theta}$$

$$3-2-1 \; Rotation$$
$$\dot{\Phi} = P\cos\Theta + R\sin\Theta$$
$$\dot{\Theta} = Q + \tan\Phi \left(P\sin\Theta - R\cos\Theta \right) \qquad \dot{\Psi} = \frac{R\cos\Theta - P\sin\Theta}{\cos\Phi}$$

$$1-3-2 \; Rotation$$
$$\dot{\Phi} = P + \tan\Psi \left(R\sin\Phi - Q\cos\Phi \right)$$
$$\dot{\Theta} = \frac{Q\cos\Phi - R\sin\Phi}{\cos\Psi} \qquad \dot{\Psi} = Q\sin\Phi + R\cos\Phi$$

Equation (2.11.1) Attitude Propagation as a function of body rates

Equations 2.11.1 include three commonly used sets of differential equation for propagating the Euler angles, as a function of body rates (P, Q, R). They must be initialized at some initial attitude values. The angle Θ is measured between the vehicle x axis and the local horizontal plane. The angle Φ is the angle between the vehicle y axis and the horizontal plane. The angle Ψ is between an arbitrary reference line in the horizontal plane and the projection of the vehicle x axis in that plane.

Equations 2.11.2 are obtained by linearizing equations 2.11.1. They calculate variations in roll, pitch, and yaw Euler angles (φ, θ, ψ), measured with respect to the trim Euler angles (Φ_0, Θ_0, Ψ_0). They represent variations from the steady-state attitude measurements (Φ_o, Θ_o, Ψ_o) as seen by the flight vehicle attitude sensors. They are included in dynamic models used for linear control analysis.

$1-2-3$ *Rotation*

$$\dot{\phi} = p + \tan\Theta_o \left[q\sin\Phi_o + r\cos\Phi_o + (Q_o\cos\Phi_o - R_o\sin\Phi_o)\phi \right] + \left(\frac{Q_o\sin\Phi_o + R_o\cos\Phi_o}{\cos^2\Theta_o} \right)\theta$$

$$\dot{\theta} = q\cos\Phi_o - r\sin\Phi_o - (R_o\cos\Phi_o + Q_o\sin\Phi_o)\phi$$

$$\dot{\psi} = \frac{(R_o\cos\Phi_o + Q_o\sin\Phi_o)\tan\Theta_o\theta + r\cos\Phi_o + q\sin\Phi_o + (Q_o\cos\Phi_o - R_o\sin\Phi_o)\phi}{\cos\Theta_o}$$

$3-2-1$ *Rotation*

$$\dot{\phi} = p\cos\Theta_o + r\sin\Theta_o + (R_o\cos\Theta_o - P_o\sin\Theta_o)\theta$$

$$\dot{\theta} = q + \tan\Phi_o \left[p\sin\Theta_o - r\cos\Theta_o + (P_o\cos\Theta_o + R_o\sin\Theta_o)\theta \right] + \left(\frac{P_o\sin\Theta_o - R_o\cos\Theta_o}{\cos^2\Phi_o} \right)\phi$$

$$\dot{\psi} = \frac{(R_o\cos\Theta_o - P_o\sin\Theta_o)\tan\Phi_o\phi + (P_o\cos\Theta_o + R_o\sin\Theta_o)\theta}{\cos\Phi_o}$$

$1-3-2$ *Rotation*

$$\dot{\phi} = p + (Q_o\sin\Phi_o + R_o\cos\Phi_o)\phi + \tan\Psi_o \left[r\sin\Phi_o - q\cos\Phi_o \right] + \left(\frac{R_o\sin\Phi_o - Q_o\cos\Phi_o}{\cos^2\Psi_o} \right)\psi$$

$$\dot{\theta} = \frac{(Q_o\cos\Phi_o - R_o\sin\Phi_o)\tan\Psi_o\psi + q\cos\Phi_o - r\sin\Phi_o - (R_o\cos\Phi_o + Q_o\sin\Phi_o)\phi}{\cos\Psi_o}$$

$$\dot{\psi} = r\cos\Phi_o + q\sin\Phi_o + (Q_o\cos\Phi_o - R_o\sin\Phi_o)\phi$$

Equation (2.11.2) Attitude Propagation as a function of Body Rates for Small Variations

2.11.2 Vehicle Altitude (h)

The rate of change in vehicle altitude ($\dot{h}$) is related to the velocity and flight path angle (γ) by the following equation: $\dot{h} = V_0 \sin \gamma$. We can also prove that the rate of change in altitude with respect to ground can be expressed in this form.

$$\dot{h} = V_0 \left(\sin \Theta \cos \Phi \cos \alpha \cos \beta - \sin \Phi \sin \beta - \cos \Theta \cos \Phi \sin \alpha \cos \beta \right) \qquad (2.11.3)$$

This equation can be linearized by replacing γ with a nominal (γ_o) plus a variation ($\delta\gamma$) as follows:

$$\dot{h} = V_0 \sin(\gamma_0 + \delta\gamma)$$

Where: $\gamma_0 = \Theta_0 - \alpha_0$ and $\delta\gamma = \theta - \alpha$

γ_o is the nominal flight path angle
$\delta\gamma$ is the small perturbation about (γ_o), and
V_0 is the nominal vehicle speed along the velocity vector.

After linearization, we can calculate variations in vehicle altitude (δh) relative to trim altitude (h_o) by using equation 2.11.4, as a function of variations in (δV, α, β, θ, ϕ).

$$\begin{aligned}
\delta\dot{h} = & \left(\cos\alpha_0 \sin\Theta_0 - \beta_0 \cos\Theta_0 \sin\Phi_0 - \sin\alpha_0 \cos\Theta_0 \cos\Phi_0 \right) \delta V \\
& - V_0 \left(\cos\alpha_0 \cos\Theta_0 \cos\Phi_0 + \sin\alpha_0 \sin\Theta_0 \right) \alpha \\
& - V_0 \left(\beta_0 \cos\alpha_0 \sin\Theta_0 + \cos\Theta_0 \sin\Phi_0 - \beta_0 \sin\alpha_0 \cos\Theta_0 \cos\Phi_0 \right) \beta \\
& + V_0 \left(\cos\alpha_0 \cos\Theta_0 + \beta_0 \sin\Theta_0 \sin\Phi_0 + \sin\alpha_0 \sin\Theta_0 \cos\Phi_0 \right) \theta \\
& - V_0 \left(\beta_0 \cos\Theta_0 \cos\Phi_0 - \sin\alpha_0 \cos\Theta_0 \sin\Phi_0 \right) \phi
\end{aligned}$$

Equation (2.11.4) Rate of Change in Vehicle Altitude

The cross-range velocity in the lateral direction V_{CR} is a function of velocity and heading direction, as shown below.

$$V_{CR} = V_0 \cos(\gamma) \sin(\beta + \Psi) \qquad (2.11.5)$$

After linearization, the variation in cross-range velocity is as follows:

$$\delta V_{cr} = V_0 \cos(\gamma_0) \cos(\beta_0 + \Psi_0) \left[\beta + \psi \right] \qquad (2.11.6)$$

2.11.3 Gyros or Rate Gyros

The roll, pitch and yaw signals measured by a gyro or a rate gyro located on the vehicle consists of two components: a rigid-body motion ($\mathbf{p_b}$, $\mathbf{q_b}$, $\mathbf{r_b}$), plus an elastic component that represents the local flexibility of the structure at the rate gyro. The generalized displacements $\eta_{j(t)}$ generated by the flex modes are not directly measurable and they do not represent any physical quantity but they do affect the measurements via the mode shapes at the sensors. A gyro sensor measures not only rigid-body motion but also a linear combination/ superposition from all modal displacements η_j, that is, modes detectable at the gyro node as shown in equation 2.11.7. The rigid-body roll, pitch and yaw rates are shown in equation 2.2.2.

$$
\begin{aligned}
p_g &= p_b + \sum_{j=1}^{N\,\text{mod}} \sigma_{xg}(k,j)\,\dot{\eta}(j) \\
q_g &= q_b + \sum_{j=1}^{N\,\text{mod}} \sigma_{yg}(k,j)\,\dot{\eta}(j) \\
r_g &= r_b + \sum_{j=1}^{N\,\text{mod}} \sigma_{zg}(k,j)\,\dot{\eta}(j)
\end{aligned}
\qquad (2.11.7)
$$

Where:

p_g q_g r_g are the rates sensed by the gyro.
N_{mod} is the number of bending modes.
σ_{xg} σ_{yg} σ_{zg} are the modal slopes of the jth mode at the kth gyro location in (rad/foot).
$\eta(j)$ is the generalized modal displacement for the jth mode

Vehicle Rates with Respect to the Stability Axes

When the flight vehicle is operating at high angles of attack, roll maneuvering is usually performed by rotating about the velocity vector V_0 instead of the x-axis. This minimizes the sideslip transients and the undesirable side loads. The vehicle, therefore, is commanded to rotate about both: roll and yaw body axes (P_b & R_b) simultaneously in order to minimize sideslip transients. We often need to create, therefore, vehicle models that include roll and yaw output rates with respect to the stability axes rather than the body axis which is most commonly used. The following equations calculate the roll and yaw rates (P_s and R_s) in the stability axes as a function of nominal body rates and the angle of attack.

$$
\begin{aligned}
P_s &= P_b \cos\alpha + R_b \sin\alpha \\
R_s &= R_b \cos\alpha - P_b \sin\alpha
\end{aligned}
$$

This measurement is relative to the velocity vector V_0 instead of the body x-axis. The stability axes roll rate P_s represents rotations about the velocity vector. The stability axes yaw rate R_s is orthogonal to the roll and pitch axes. The pitch rate in stability axis is the same as in the body axes.

The variations in stability rates (p_s and r_s) are obtained from equations 2.11.8 by linearizing the previous equations relative to trim (α_0) and the nominal body rates (P_0 and R_0). They are related to the variations in the body rates (p_b and r_b) and in the angle of attack (α).

$$p_s = p_b \cos\alpha_o + r_b \sin\alpha_o + \left(R_o \cos\alpha_0 - P_o \sin\alpha_o\right)\alpha$$

$$r_s = r_b \cos\alpha_o - p_b \sin\alpha_o - \left(R_o \sin\alpha_0 + P_o \cos\alpha_o\right)\alpha$$

Equation (2.11.8) Body to Stability axes transformation for small variations

This transformation is useful in developing dynamic models at high angles of attack, where roll rotations are commanded about the velocity vector rather than the x axis. Stability axis models are often used for flight control design at high angles of attack. Guidance commands are calculated in stability axes rather than in the body axes and the control gains "assume" a stability axes rate feedback, which is transformed to body axes roll and yaw commands that simultaneously rotate the aileron and the rudder to rotate the vehicle about the velocity vector. This implementation minimizes the angle of sideslip and hence lateral loading. For more details read the Space Shuttle reentry example where the vehicle is commanded to rotate about the velocity vector.

Turn Coordination

In a coordinated turn the vehicle is experiencing zero lateral acceleration at the cg. It banks at an angle Φ and allows a small gravity component to counteract the centripetal force due to turning. It maintains the same pitch and roll attitude but its heading is changing at constant rate. Turn coordination is desirable for passenger comfort and also the pilot functions more effectively. It minimizes sideslip and undesirable aero loading and maximizes aerodynamic efficiency. To perform coordinated stability-axis rolls, both roll and yaw controllers are used to maintain zero sideslip. At low angles-of-attack there is usually adequate rudder power to obtain the desired motion. However, as the angle-of-attack increases, the demand on rudder authority increases rapidly.

In level flight with small sideslip, the yaw rate R required to produce a coordinated turn at a constant bank angle (Φ) and an air speed (V_0) is:

$$R = \frac{g \cos\Theta \tan\Phi}{V_0} \approx \frac{g \sin\Phi}{V_0}$$

(2.11.9)

The circle radius (r_c) of the coordinated turn is: $r_c = \dfrac{V_0^2}{g \cos\gamma \tan\Phi}$

(2.11.9b)

When the flight control system receives a roll rate command in stability axes, a coordinated turn system applies a feedback signal from bank angle (Φ) and the velocity (V_0) to the yaw rate (R) as defined in equation (2.11.9). This loop allows the vehicle to achieve its commanded roll rate, otherwise, without the turn coordination feedback it would result in a non-zero steady-state roll rate error.

If we know ahead of time that the vehicle will be using a turn coordination feed-forward loop it may be convenient, for modeling and control design purposes, to include this feed-forward loop in the dynamic model instead of including it in the flight control system. After linearization, the perturbations in the stability rates as a function of the body rates plus other parameter variations become:

$$
p_s = p_b \cos\alpha_o + r' \sin\alpha_o + (R_o \cos\alpha - P_o \sin\alpha_o)\alpha
$$
$$
r_s = r' \cos\alpha_o - p_b \sin\alpha_o - (R_o \sin\alpha + P_o \cos\alpha_o)\alpha
$$
where:
$$
r' = r_b + \left[\frac{g \sin\Phi_0 \sin\Theta_0}{V_0} \right]\theta - \left[\frac{g \cos\Phi_0 \cos\Theta_0}{V_0} \right]\phi + \left[\frac{g \sin\Phi_0 \cos\Theta_0}{V_0^2} \right]\delta V
$$

Equation (2.11.10) Body to Stability Transformation that Includes Turn Coordination

By including the turn coordination terms of equation (2.11.10) in the control design model and then using this model to design feedback gains, the gains "assume" that the vehicle control system has a turn-coordination loop already implemented. It separates the two control issues: turn-coordination and state-feedback design. This feature is useful for designing gains when the vehicle is at a steady bank angle (Φ_0).

In Flixan vehicle modeling program the "*stability axes output*" and the "*turn-coordination logic*" are options that can be selected in the input data. When the "*stability axes*" option is turned on, and the "*turn-coordination*" is not included, the term (r') in equation (2.11.10) becomes equal to (r_b), of equation (2.11.8). The analyst must be careful to avoid double-booking of the turn-coordination logic, both in the vehicle model and in the flight control. We typically include these options in the vehicle model during control analysis and design, but not in simulations. In simulations we use body axis models and include the body to stability transformations plus the turn coordination logic in separate blocks, as shown in the examples.

2.11.4 Acceleration Sensed by an Accelerometer

Normal, lateral and axial accelerometers are used to measure the vehicle translational accelerations along the z, y, and x axes respectively. Accelerometer feedback is used by the flight control system to regulate speed and to provide load-relief in order to protect the vehicle structure from excessive aerodynamic loading. It is also used to control the angles of attack and sideslip, and the rate of descent in a reentry vehicle. Excessive aero-loading due to alpha and beta may be catastrophic especially at high dynamic pressures. The aero loads are measured in terms of Qα= (Qbar * α). Typically, normal and lateral loads should not exceed 3000 to 3500 (psf-deg). In launch vehicles during high dynamic pressures, a load relief feedback loop is included in parallel with the attitude control loop in order to alleviate structural loading. When the load-relief system is operating the flight control system steers the vehicle in a direction that trades-off a certain amount of directional controllability in order to gain reduction in normal and lateral loading. The control gains in the load-relief feedback loop are usually phased in-and-out, proportionally with the dynamic pressure.

The acceleration measured by an accelerometer consists of three components:

- A term due to rigid-body acceleration at the CG
- Terms due to angular acceleration multiplied with the accelerometer distance from the vehicle CG, and
- Terms that introduce structural flexibility at the accelerometer node

The non-linear equation below describes the accelerometer measurement in 6-DOF simulations.

$$A_{Yaccel} = A_{YCG} + l_{Xacc}\left(\dot{R} + PQ\right) - l_{Zacc}\left(\dot{P} - QR\right) - l_{Yacc}\left(P^2 + R^2\right) + \sum_{j=1}^{N\,\mathrm{mod}} \phi_{Yacc}(j)\ddot{\eta}(j)$$

$$A_{Zaccel} = A_{ZCG} - l_{Xacc}\left(\dot{Q} - PR\right) - l_{Yacc}\left(\dot{P} + QR\right) - l_{Zacc}\left(P^2 + Q^2\right) + \sum_{j=1}^{N\,\mathrm{mod}} \phi_{Zacc}(j)\ddot{\eta}(j)$$

Equation (2.11.11) Accelerometer Measurement in Large Angle Non-Linear Simulation

After linearization, the variations in the accelerometer measurements along the x, y, and z axes from steady-state accelerations become:

$$a_{Xaccel} = a_{XCG} + l_{Zacc}\dot{q} - l_{Yacc}\dot{r} + \sum_{j=1}^{N\,\mathrm{mod}} \varphi_{Xacc}(j)\ddot{\eta}(j) - A_Z \sum_{j=1}^{N\,\mathrm{mod}} \sigma_{Yacc}(j)\eta(j)$$

$$a_{Yaccel} = a_{YCG} + l_{Xacc}\dot{r} - l_{Zacc}\dot{p} + \sum_{j=1}^{N\,\mathrm{mod}} \varphi_{Yacc}(j)\ddot{\eta}(j) - A_X \sum_{j=1}^{N\,\mathrm{mod}} \sigma_{Zacc}(j)\eta(j)$$

$$a_{Zaccel} = a_{ZCG} - l_{Xacc}\dot{q} + l_{Yacc}\dot{p} + \sum_{j=1}^{N\,\mathrm{mod}} \varphi_{Zacc}(j)\ddot{\eta}(j) + A_X \sum_{j=1}^{N\,\mathrm{mod}} \sigma_{Yacc}(j)\eta(j)$$

$$where: l_{Xacc} = X_{accel} - X_{CG}; l_{Yacc} = Y_{accel} - Y_{CG}; l_{Zacc} = Z_{accel} - Z_{CG}$$

Equation (2.11.12) Accelerometer Measurement for Small Variations Simulation

Where:

$\varphi_{xacc}, \varphi_{zacc}, \varphi_{yacc}$	Mode shapes of an elastic mode (j) at the accelerometer in (ft/ft), along x, z and y axes respectively.
$\sigma_{Yacc}, \sigma_{Zacc}$	Modal slopes of an elastic mode (j) at the accelerometer in (rad/foot), in the pitch and yaw directions.
a_{xcg} a_{ycg} a_{zcg}	Accelerations at the vehicle CG due to the external forces (no gravity).

The flex terms consist of two components: a term due to the modal accelerations ($\ddot{\eta}_j$), and a term due to rotational structural bending coupling with the vehicle acceleration A_X.

2.11.5 Angle of Attack and Sideslip Sensors

Vane sensors measure the angles of attack and sideslip relative to the airflow, and also the relative wind velocity V_0. This device is generally a probe sticking out in front of the aircraft. Sometimes it consists of tiny holes measuring pressure in different locations near the nose, and from the pressure difference a processor estimates the alpha and beta angles. These measurements are often used in aircraft as flight control inputs to control the aerodynamic angles (α and β). In launch vehicles they can be used instead of accelerometers to provide aerodynamic load-relief at high dynamic pressures.

The measured angles of attack and sideslip (α_s and β_s), however, are different from the actual rigid-body angles relative to the airflow (α_w and β_w), because the measurements are corrupted by vehicle rotations, and structural flexibility at the sensor location. The angles of attack and sideslip measured by a vane sensor are defined in equations 2.11.13 and the right hand side of the equation consists of the following terms:

- The first terms are the actual angles of attack and sideslip (α_w and β_w) relative to the airflow, as defined in section 2.9.
- The second terms represents measurement errors produced by the body rates and the moment arm distance from the vehicle CG.
- The last two terms introduce errors due to structural flexibility at the sensor. That includes local structural bending and translational velocity at the vane node.

$$\alpha_s = \alpha_w - \left(\frac{l_{xv} q - l_{yv} p}{V_0} \right) + \sum_{j=1}^{N\,\text{mod}} \sigma_{YV}(j)\, \eta(j) + \left(\frac{1}{V_0} \right) \sum_{j=1}^{N\,\text{mod}} \phi_{ZV}(j)\, \dot{\eta}(j)$$

$$\beta_s = \beta_w + \left(\frac{l_{xv} r - l_{zv} p}{V_0} \right) - \sum_{j=1}^{N\,\text{mod}} \sigma_{ZV}(j)\, \eta(j) + \left(\frac{1}{V_0} \right) \sum_{j=1}^{N\,\text{mod}} \phi_{YV}(j)\, \dot{\eta}(j)$$

Equation (2.11.13) Angle of Attack and Sideslip Measurement at a Vane Sensor

where:

φ_{zv}, φ_{yv}	are the mode shapes along Z and Y of the vehicle at the vane sensor in (ft/ft)
$\sigma_{y\alpha}$, $\sigma_{z\beta}$	are the pitch and yaw modal slopes at the vane sensor in (radians/ft)
η_j	is the modal displacement of mode (j), in (feet)
$l_{xv}\ l_{yv}\ l_{zv}$	are the distances along x, y, and z, between the vane sensor located in front of the vehicle, and the vehicle CG, ($l_{xv}=X_v - X_{cg}$).